**Deltares**

Enabling Delta Life

# The Coastal Genesis II Terschelling - Ameland inlet (CGII-TA) model

**Model setup, calibration and validation of a hydrodynamic-wave model**

# The Coastal Genesis II Terschelling - Ameland inlet (CGII-TA) model

**Model setup, calibration and validation of a hydrodynamic-wave model**

1220339-008

# Deltares

**Title**
The Coastal Genesis II Terschelling - Ameland inlet (CGII-TA) model

| **Project** | **Attribute** | **Pages** |
|---|---|---|
| 1220339-008 | 1220339-008-ZKS-0004 | 88 |

**Keywords**
Kustgenese 2.0; Coastal Genesis II; Terschelling; Ameland; hydrodynamic modelling; wave modelling; Delft3D-FLOW; SWAN

**Summary**
In the framework of the Coastal Genesis II Program (GCII, or Kustgenese 2.0) a coupled hydrodynamic-wave model has been setup, calibrated and validated in and around Ameland Inlet. The model will be used as basis for modelling sand transport at the lower shoreface and sediment exchange through the Ameland inlet in a next phase of the project.

This report presents the setup, calibration and validation of the model. Calibration and validation shows that the model is well capable of representing the water levels, currents and waves in and near the Ameland inlet. Hence, the model is considered well suitable as a base for sediment transport modelling in the next phases of the project.

An extensive summary (in Dutch) of the main findings and their contribution to answering the KG2 research questions is presented hereafter.

| Version | Date | Author | Initials | Review | Initials | Approval | Initials |
|---|---|---|---|---|---|---|---|
| 1.0 | 11-01-2019 | ir. C.M. Nederhoff | | Drs. R.F. de Graaff | | Drs. F.M.J. Hoozemans | |
| | | Drs. R. Schrijvershof | | | | | |
| | | ir. P.K. Tonnon | | | | | |
| | | Dr. ir. J.J. van der Werf | | | | | |
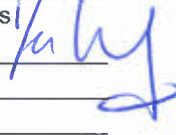
**Status**
final

# Deltares

# Samenvatting

**Achtergrond**
Het Nederlandse kustbeleid streeft naar een structureel veilige, economisch sterke en aantrekkelijke kust. Dit wordt bereikt door het onderhouden van het gedeelte van de kust dat deze functies mogelijk maakt; het Kustfundament. Dit gebeurt door middel van zandsuppleties; het suppletievolume is ongeveer 12 miljoen m$^3$/jaar sinds 2000.

In 2020 neemt het Ministerie van Infrastructuur en Milieu een beslissing over een eventuele aanpassing van het suppletievolume. Het Kustgenese 2.0 programma heeft als doel hiervoor de kennis en onderbouwing te leveren. Deltares richt zich in opdracht van Rijkswaterstaat binnen Kustgenese 2.0 op de volgende drie hoofdvragen:
1. Is er een andere zeewaartse begrenzing mogelijk voor het kustfundament?
2. Wat is het benodigde suppletievolume om het kustfundament te laten meegroeien met zeespiegelstijging?
3. Wat zijn de mogelijkheden voor (en effecten van) toepassing van suppleties rond zeegaten?

Het deelproject 'Diepere Vooroever' draagt bij aan het beantwoorden van de eerste twee hoofdvragen. Het deelproject 'Systeemkennis Zeegaten' draagt bij aan het beantwoorden van de tweede en de derde hoofdvraag van het project Kustgenese 2.0. Beide deelprojecten maken voor de beantwoording gebruik van een combinatie van literatuurstudie, analyse van (veld)data en modelstudies.

De hoofdvragen van Kustgenese 2.0 zijn vertaald in meerdere onderzoeksvragen (Tabel 1.1). Deelproject 'Diepere Vooroever' richt zich op onderzoeksvragen KFGR-01 tot en met KGFR-03 en SVOL-01 tot en met SVOL-03. Deelproject 'Systeemkennis Zeegaten' richt zich op onderzoeksvragen SVOL-07 tot en met SVOL-10 en INGR-01 en ING-02.

*Tabel 1.1    Overzicht van de onderzoeksvragen van de Kustgenese 2.0 deelprojecten 'Diepere Vooroever' (KFGR-01 t/m KGFR-03, SVOL-01 t/m SVOL-03) en 'Systeemkennis Zeegaten' (VOL-07 t/m SVOL-10, INGR-01 en ING-02). De laatste kolom geeft aan of het voorliggende rapport (indirect) bijdraagt aan de betreffende onderzoeksvraag.*

| Code | Onderzoeksvraag | Bijdrage |
|---|---|---|
| KFGR-01 | Wat is de opbouw van de kust, in termen van bodemvormen, sedimentaire structuren, bodemopbouw en korrelgrootteverdelingen? | NEE |
| KFGR-02 | Wat zijn de maatgevende processen voor de uitwisseling van sediment tussen de vooroever en de diepere vooroever, en wat is hun frequentie van optreden en hun bijdrage? | JA |
| KFGR-03 | Hoe groot zijn de dwars- en langstransporten (bruto / netto), en hoe variëren deze over het kustprofiel, per deelgebied, en wat is de trend voor de komende 50 jaar met een doorkijk tot 200 jaar? | JA |
| KFGR-04 | In welke deelgebieden (of zones) kan het kustprofiel opgedeeld worden, waarbij sprake is van een vergelijkbaar (stabiel) profiel, opbouw en dynamiek? | JA |

**Title**
The Coastal Genesis II Terschelling - Ameland inlet (CGII-TA) model

| **Project** | **Attribute** | **Pages** |
|---|---|---|
| 1220339-008 | 1220339-008-ZKS-0004 | 88 |

| | | |
|---|---|---|
| KFGR-05 | Wat is een goed criterium of wat zijn goede criteria voor een zeewaartse begrenzing, en ten opzichte van welke referentievlak zou deze moeten worden uitgedrukt (NAP, MSL, GLW?) | JA |
| SVOL-01 | Hoe groot is de totale netto uitwisseling van zand over de zeewaartse grens van het KF? | JA |
| SVOL-02 | Hoe groot is de onzekerheid in deze netto uitwisseling, als gevolg van de (on)nauwkeurigheid in de dwarstransporten over de zeewaartse grens? | JA |
| SVOL-03 | Is het nodig en is het mogelijk om deze uitwisseling mee te nemen bij het bepalen van het suppletievolume? | JA |
| SVOL-07 | Wat zijn de drijvende (dominante) sedimenttransportprocessen en -mechanismen en welke bijdrage leveren ze aan de netto import of export van het bekken? | JA |
| SVOL-08 | Hoe beïnvloeden de morfologische veranderingen in het bekken en op de buitendelta de processen en mechanismen die het netto transport door een zeegat bepalen?<br>Hoe zetten deze veranderingen door in de toekomst, rekening houdend met verschillende scenario's voor ZSS? | NEE |
| SVOL-09 | Wordt de grootte van de netto import of export beïnvloed door het aanbod van extra sediment in de kustzone of de buitendelta? | JA |
| SVOL-10 | Wat zijn de afzonderlijke bijdragen van zand en slib aan de sedimentatie in de Waddenzee, als gevolg van de ingrepen en ZSS? En wat betekent dat voor het suppletievolume? | NEE |
| INGR-01 | Hoe beïnvloeden de ontwikkelingen van een buitendelta (inclusief de verandering van omvang) de sedimentuitwisselingen tussen buitendelta, bekken en aangrenzende kusten en welke consequenties en/of randvoorwaarden levert dat voor een suppletieontwerp? | JA |
| INGR-02 | Is het, op basis van beschikbare kennis van het morfologisch systeem, zinvol om grootschalige suppleties op buitendelta's te overwegen? | JA |

**Relatie Terschelling-Ameland model en de onderzoeksvragen**
Dit rapport beschrijft de opzet, kalibratie en validatie van een dieptegemiddeld, gekoppeld golf- en stromingsmodel van Terschelling en Ameland, inclusief de tussengelegen buitendelta en het zeegat. In een later stadium van het KG2 project zal dit model gebruikt worden om de dynamiek en de zandtransporten op de diepe vooroever van Terschelling en Ameland en in het zeegat van Ameland te kunnen bestuderen onder verschillende condities. Als zodanig beantwoordt dit rapport niet *direct* de onderzoeksvragen van Kustgenese 2.0, maar draagt het *indirect* wel bij aan de beantwoording van de meeste onderzoeksvragen, zoals aangegeven in Tabel 1.1.

**Opzet, kalibratie en validatie en het Terschelling-Ameland model**
De resolutie van het gebruikte rekenrooster varieert van 50 m in het zeegat tot 350 m bij de zeerand. Het model wordt aangestuurd met berekende wind- en luchtdrukgegevens uit het HIRLAM model, met berekende waterstanden uit het DCSMv4ZUNOv6 model en met gemeten golfspectra voor golfboeien Eierlandse gat en Schiermonnikoog Noord. De

# Deltares

bodemligging is gebaseerd op vaklodingen voor de periode 2012 tot en met 2017, aangevuld met Jarkus en Lidar data.

Het model is gekalibreerd met gemeten waterstandsdata voor 2017 en met gemeten stroomsnelheden, debieten en golven van de Kustgenese 2.0 meetcampagne van najaar 2017. Het gekalibreerde model reproduceert waterstandsdata met een gemiddelde kwadratische fout (RMSE; Root Mean Square Error) van ca. 0,10 m, het gemeten debiet door de keel van het zeegat van Ameland met een gemiddelde absolute fout (MAE; Mean Absolute Error) van ca 10 M $m^3$ ofwel 2% en gemeten snelheden met een RMSE van 0,15 m/s in het zeegat en 0,10 m/s op de wantijen. Golfhoogte, perioden en richtingen buitengaats worden gereproduceerd met respectievelijk een RMSE kleiner dan 0,20 m, 0.5 s en 20 graden, in het bekken nemen deze fouten toe tot respectievelijk 0,20 m, 1.0 s en 40 graden.

Het gekalibreerd model, met vaste model- en parameterinstellingen, is gevalideerd met meetdata uit 2008, 2011 en drie opeenvolgende meetcampagnes ten behoeve van Kustgenese 2 in november 2017, januari 2018 en maart 2018. Het model reproduceert de waterstandsdata voor deze perioden met een RMSE fout kleiner dan 0,10 m. Deze fout is vooral gerelateerd aan de grootschalige stormopzet en andere fluctuaties. Gemeten stroomsnelheden worden gereproduceerd met een RMSE fout van 0,10 – 0,15 m/s, waarbij de Scatter Index (SCI) gemiddeld genomen kleiner dan 20 tot 25% is. Gemeten golfhoogte, -periode en richtingen worden geproduceerd met een RMSE fout kleiner dan 0,20 m, 1.0 s en 35 graden, respectievelijk. De modelnauwkeurigheid voor de validatieperioden is vergelijkbaar met die voor de kalibratieperiode en van dezelfde orde-grootte als de nauwkeurigheid van gevalideerde modellen uit eerdere modelstudies (Deltares, 2009a; Zijl et al., 2013).

## Eindconclusies Terschelling-Ameland model
- Het model presteert goed in termen van berekende waterstanden, debieten, stroomsnelheden en golfhoogte, -periode en –richting. De berekende fout in de waterstanden is vooral gerelateerd aan de grootschalige stormopzet en waterstandsfluctuaties.
- De modelinstellingen zijn gebaseerd op een goede, algemene reproductie van waterstanden, debieten, stroomsnelheden en golven. De reproductie van stroomsnelheden op het wantij kan verbeterd worden met aangepaste modelinstellingen (meteo, ruwheid), wat wel ten koste gaat van de reproductie elders in het interessegebied.
- Het model laat zien dat er een aanzienlijke stroming (> 1 m/s) staat over het wantij van Terschelling en in iets mindere mate ook over het wantij van Ameland gedurende stormen uit het westen.
- De varende KG2 ADCP metingen in het Amelander Zeegat zijn uitgewerkt naar watervolumes. De eb- en vloedvolumes variëren tussen de 330 en 506 M $m^3$, afhankelijk van het moment in de springtij-doodtij-cyclus.
- De rekentijd op 2 Xeon E3-1276v3 processoren bedraagt ca. 3 dagen voor een volledig jaar zonder golven en ca. 26 dagen voor een volledig jaar inclusief golven.

- Het model is hiermee geschikt om de meetgegevens uit de Kustgenese 2.0 meetcampagnes ruimtelijk en temporeel te interpreteren en een goed startpunt om de dynamiek en de zandtransporten op de diepe vooroever van Terschelling en Ameland en in het zeegat van Ameland te bestuderen.

# Contents

**Deltares**

# 1 Introduction

## 1.1 Background

The Dutch coastal policy aims for a safe, economically strong and attractive coast (Deltaprogramma, 2015). This is achieved by maintaining the part of the coast that supports these functions: i.e. keep the coastal foundation in sustainable balance with sea level rise. The coastal foundation is the area between the NAP -20 m depth contour and the landward edge of the dune area (closed coast) and the tidal inlets (open coast). The offshore boundary of the coastal foundation near Ameland inlet is illustrated in Figure 1.1 . In particular, the coastal foundation is maintained by means of sand nourishments. The total nourishment volume for the Netherlands is approximately 12 million $m^3$/year since 2000. The Wadden Sea basin and Western Scheldt are not part of the coastal foundation, but are taken into account within the computation of the total nourishment volume needed.

In 2020, the Dutch Ministry of Infrastructure and Environment will make a decision about the nourishment volume. The Coastal Genesis II program (GCII, or Kustgenese 2.0) is aimed to deliver knowledge to enable this decision making. Within the scope of the CGII program, Rijkswaterstaat (RWS WVL) commissioned two projects to Deltares 'Diepe Vooroever' and 'Systeemkennis Zeegaten', to address the following main (policy) questions:

1 What are the possibilities for an alternative offshore boundary of the coastal foundation?
2 How much sediment is required for the coastal foundation to keep up with sea level rise and how much sediment is lost in the Wadden Sea basin and Western Scheldt?
3 What are the possibilities and effects of applying large-scale nourishments in the ebb tidal deltas?

Project 'Diepe Vooroever' ('Lower Shoreface'; i.e. the area between 20-12 meter water depths) addresses the first and second question and project 'Systeemkennis Zeegaten' ('System Knowledge Tidal Inlets') addresses the second and third question.

As part of CGII, a large measurement campaign was carried out in and around Ameland Inlet in September and November 2017 and north of Terschelling in January and March 2018 (see Figure 1.1). Measurements were obtained on the lower shoreface, in the inlet and in the Wadden Sea basin. The measurements are used to develop knowledge of the relevant processes of long-term morphodynamics and are considered the area and time period of interest for this study.

## 1.2 Objective

The objective of this study is to set-up, calibrate and validate a model of the area of interest near Terschelling and Ameland (Figure 1.1), that can be used as base model to (1) study the sand transport on the lower shoreface (within the CGII 'Diepe Vooroever' project), to (2) study the sand exchange through Ameland inlet and (3) serve as a basis for a morphodynamic model of Ameland inlet (both within the CGII 'Systeemkennis Zeegaten' project). The model needs to reproduce CGII measurements well.

The model applications for sediment transport modeling in the next project phases require:

1 A hydrodynamic model with an online coupled wave model having a relatively high resolution in the Ameland inlet (+/- 50 m) and sufficient resolution in the rest of the model domain);

2    The inclusion of the adjacent inlets of Ameland (i.e. Terschelling and Schiermonnikoog) in order to resolve the identified issues by Deltares (2017a) of an imbalance between the offshore directed tidal component and the onshore direction wave-driven component in the existing (morphodynamic) Ameland inlet model (Teske, 2013)

3    Feasible computational times (2-3 days computation for 1 month of simulation);

4    Similar or better representation of hydrodynamics (i.e. water levels & currents) and waves in the area of interest compared to previous modeling efforts (Deltares, 2009a; Deltares, 2010; Zijl et al., 2013; Deltares, 2014).
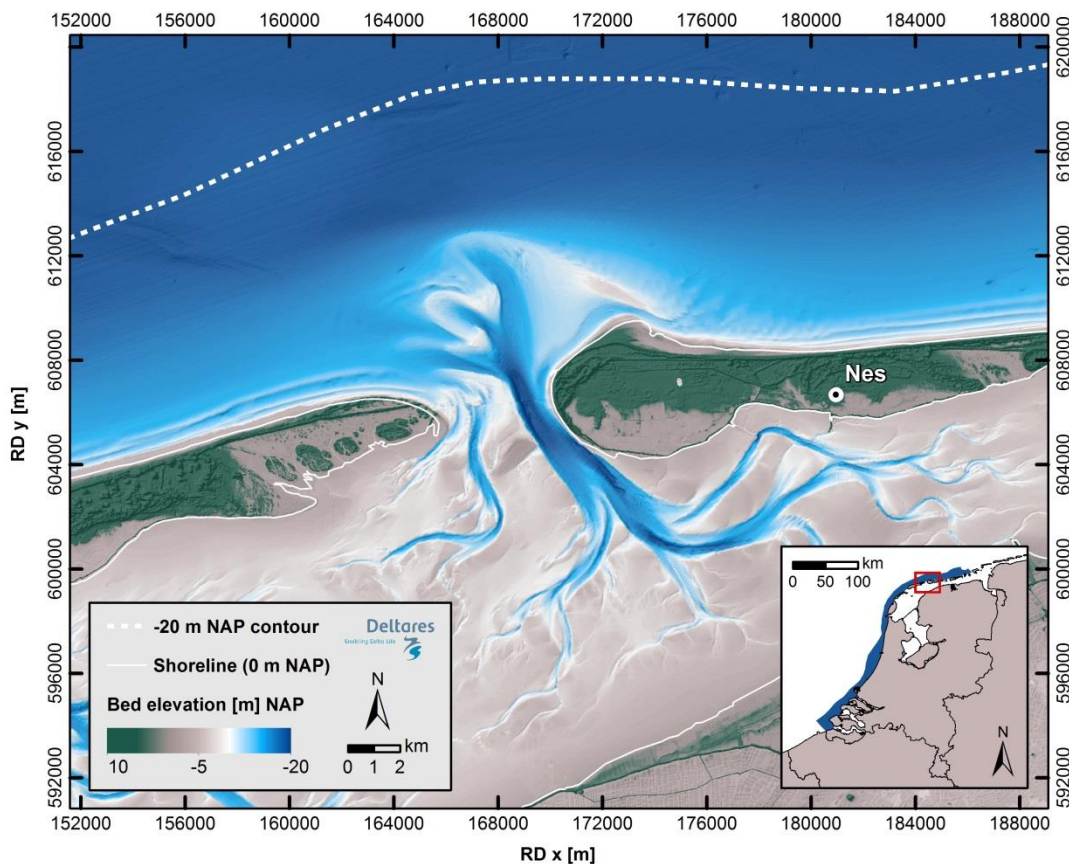


*Figure 1.1    the The area of interest around Ameland Inlet and lower shoreface of Terschelling and Ameland (large map). The area of interest and the coastal foundation illustrated as respectively red box and blue polygon on the map of the Netherlands.*

## 1.3    Model strategy

There is a hydrodynamic model available that covers the Wadden Sea basin (WadSea; Deltares, 2009a). This Wadsea model is a well-calibrated 2DH hydrodynamic Delft3D model focused on the reproduction of water levels and flow velocities. However, the model does not include waves and has an arguably too coarse resolution with a 200-250 m grid cell resolution at Ameland Inlet. Locally refining the Wadsea model and including waves is an option to set up an appropriate model. However, this approach will most likely result in a large number of computational cells and is therefore not considered suitable for the intended application of the model.

Therefore, in order to meet the objectives, a new coupled Delft3D-FLOW (Lesser et al., 2004) & SWAN (Booij et al., 1999) model was created. The model has a relatively fine grid

resolution in the inlet (+/- 50 m) and covers the tidal inlets of Terschelling, Ameland, and Schiermonnikoog to account for the hydrodynamics on the watershed of Ameland within the model domain. Similar to Deltares (2009), the model domain starts at ±25 m water depth and has a maximum coarse resolution of 250 m. Moreover, by nesting the model within a large-scale hydrodynamic model, it accounts for tidal and meteorological (wind + atmospheric pressure) forces.

In first instance a 2DH (depth-averaged) model instead of a 3D model was created in order to achieve reasonable computational times whilst still being able to compute sand transport and morphodynamics. Besides, it is expected that a 2DH model around Ameland Inlet, which assumes a logarithmic vertical velocity profile and therefore neglects the vertical distribution of the offshore-directed undertow and density-driven currents, accounts for most of the important sand transport processes.

### 1.4 Study approach
In order to achieve the defined objectives according to the described model strategy the following actions are carried out:
1  **Data collection**, analysis and quality review;
2  **Model set-up** by creating a numerical model grid and matching bathymetry for a Delft3D-FLOW & SWAN model for several time periods (2008, 2011, 2017 and 2018). The second step was to derive boundary conditions. This was partly based on observations (e.g. observed spectral wave information) and partly on numerical models (e.g. water levels and wind speeds);
3  **Model calibration** by adjusting various relevant model parameters and comparison against water levels, currents and waves. The year 2017 was used as model calibration period to include the data from the extensive field campaign in the Ameland Inlet in the calibration exercise;
4  **Model validation** with data from the years 2008, 2011, November 2017 and January and March 2018 due to the availability of data from field campaigns in these time periods.

### 1.5 Outline report
This report is outlined as follows: Chapter 2 describes the data applied for the study. The model setup is discussed in Chapter 3. The model calibration is described in Chapter 4, and the model validation in Chapter 5. Chapter 6 discusses the setup, calibration and validation of the model. The conclusions and recommendations are presented in Chapter 7.

# 2 Applied data

## 2.1 Introduction

This Chapter describes all the data that was used in the setup (Section 2.2), calibration (Section 2.3) and validation (Section 2.4) of the model. Figure 2.1 presents the locations of the measurement instruments. The symbols indicate different types of instruments and/or recording periods

## 2.2 Model setup/forcing

### 2.2.1 Bathymetry

Information on the bed level in the Wadden Sea was derived from the following sources:
- Rijkswaterstaat 'Vaklodingen'. Every year Rijkswaterstaat measures part of Dutch coastal zone between the dunes/beach till a water depth of approximately 25 m. These datasets can be used to create temporal varying bathymetries. See Deltares (2017b) for an overview of available datasets.
- Additional Rijkswaterstaat 'Vaklodingen' data gathered at the Ameland Inlet in 2017
- Digital Elevation Model of the Netherlands (AHN). A static dataset available only for land (i.e. topography or height above mean sea level)
- Bathymetry information from the Hydrographic Service of the Royal Netherlands Navy. A static dataset available only for the sea (i.e. bathymetry or height below mean sea level). This dataset is used for areas where no Vaklodingen data is available.

### 2.2.2 Water levels

Water levels at the model boundary for the hydrodynamic model were derived from the DCSMv6ZUNOv4 model (Zijl et al., 2013). The DSCMv6ZUNOv4 model includes tide-generating forces, ERA-interim meteorological forcing and has a good reproduction of water levels with RMSEs less than 10 cm, see Appendix C for the details.

### 2.2.3 Waves

Time series of measured wave spectral information was requested at Rijkswaterstaat Servicedesk Water for Schiermonnikoog-Noord (SON) and Eierlandse Gat (EIR) and used as boundary conditions for the wave model. For details of the records, one is referred to Table 2.1.

*Table 2.1    Wave buoy locations from which spectra measurements are used as forcing.*

| Full name | Short | RDx [m] | RDy [m] | Depth [m] |
|---|---|---|---|---|
| Eierlandse Gat | ELD | 106601 | 616004 | 19 |
| Schiermonnikoog Noord | SON | 206610 | 617304 | 22 |
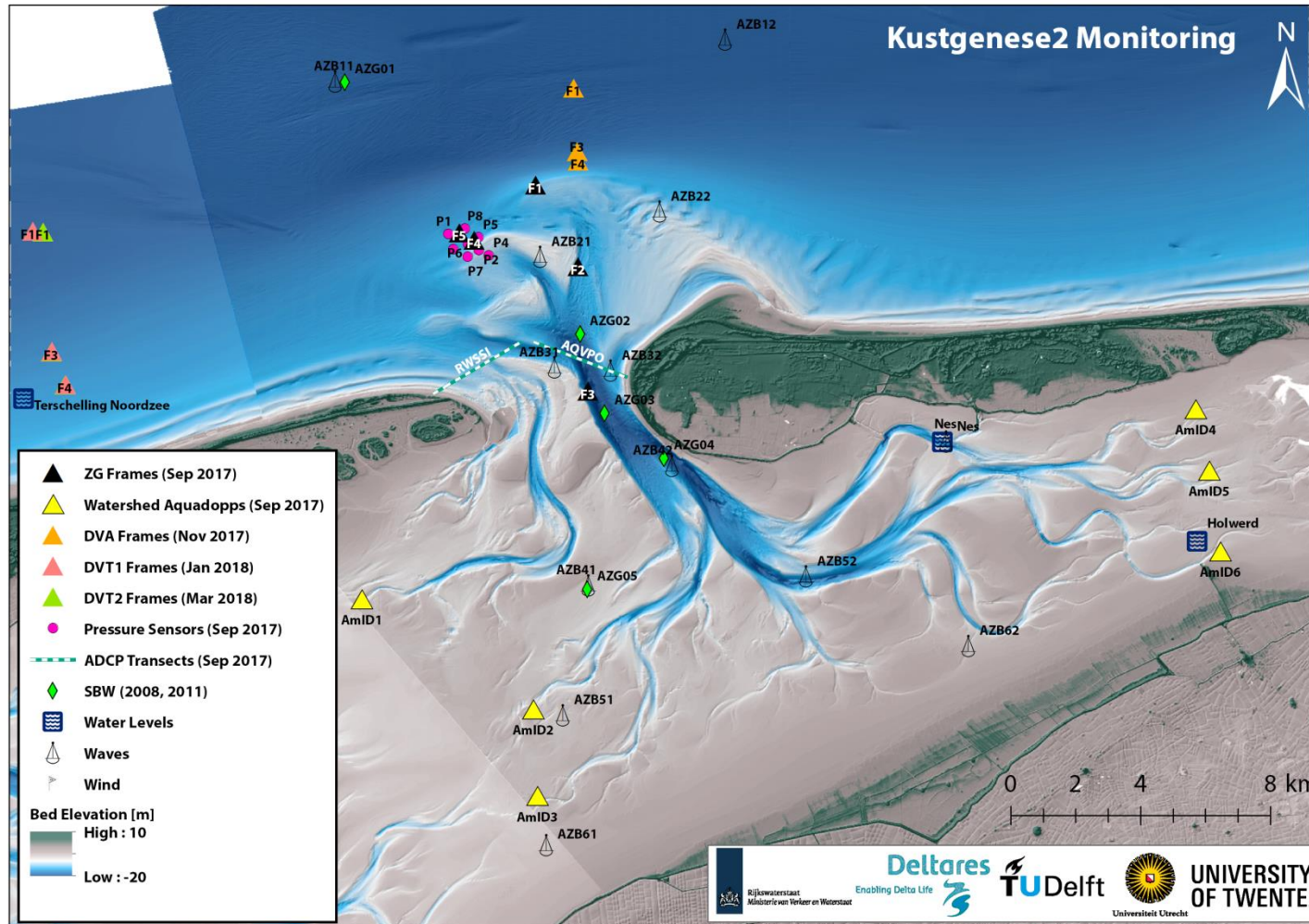
*Figure 2.1 Locations of the measurement instruments during the Coastal Genesis II campaigns.*

### 2.2.4 Wind and pressure

Besides observations, several weather models exist that hindcast the status of the atmosphere. The advantage of using weather models over measurements is that the spatial variability in wind and pressure conditions can be used to force the hydrodynamic models. Two of the known global atmospheric reanalysis models are ERA-Interim (Dee et al., 211) and NCEP (Kalnay et al., 1996). A meteorological reanalysis is a meteorological data assimilation project which aims to assimilate historical observational data spanning an extended period. HIRLAM is another local atmospheric reanalysis model operated by the Royal Dutch Meteorological Institute (KNMI). Every three hours model output of winds and pressure computed by ERA-interim and NCEP for the period 2000-2017 were collected. For HIRLAM every hour model output is available. The ERA-interim has a resolution of 80 km and NCEP data has a resolution of approximately 30 km. The HIRLAM data has a resolution of 3 to 16 km.

## 2.3 Model calibration

### 2.3.1 Water levels

Time-series of measured water levels were downloaded from the Waterbase & MATROOS database for a total of 4 stations in the Wadden Sea (Table 2.2, Figure 2.2). Moreover, harmonic constituents for these stations were determined with the Matlab t_tide toolbox (Pawlowicz et al., 2002) to allow for comparisons with the model results in the frequency domain.

The spatial extent of the numerical domain of the CGII-TA model covers the stations Terschelling Noordzee, Wierumergronden, Nes and Holwerd. The stations Schiermonnikoog, Vlieland Haven, West-Terschelling and Harlingen are located in the model domain as well, however, these locations are not in the area of interest and will not be included in the calibration/validation.

*Table 2.2    Water level measurement names, location, depth and periods*

| Name | RDx [m] | RDy [m] | Depth [m] |
|------|---------|---------|-----------|
| Terschelling Noordzee | 151400 | 606249 | 11 |
| Wierumgronden | 192881 | 614561 | 12 |
| Nes | 179706 | 604915 | 8 |
| Holwerd | 187549 | 601849 | 5 |

**Deltares**
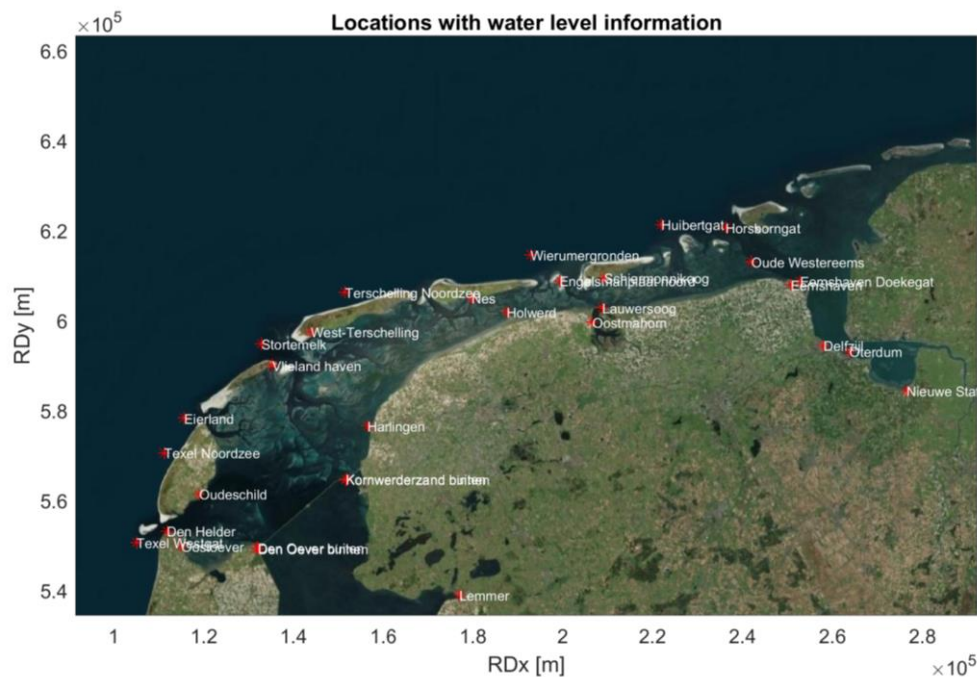


*Figure 2.2    Overview stations water levels Wadden Sea*

All the water level measurements for 2017 were inspected and deemed suitable for the calibration of the hydrodynamic model.

2.3.2    Wave height, period and direction
Time series of measured wave height, wave period, and wave direction were downloaded from the Waterbase & MATROOS database for the wave buoys in the Ameland Inlet. These data are applied for model calibration and validation (Table 2.3). NB: not all wave buoys record wave period and/or direction.

All the wave information for 2017 were inspected and deemed suitable for the calibration of the wave model. The data does, however, not include continuous time series for the complete periods analyzed (i.e. there are periods with missing data, see Table 2.3. These periods are usually concentrated at the summer months (May – August) because the wave buoys are removed during these months for maintenance.

*Table 2.3    Wave buoy stations with names, locations, depth and indication if period and direction are measured.*

| Full name | Short | RDx [m] | RDy [m] | Depth [m] | Period / Direction |
|-----------|-------|---------|---------|-----------|--------------------|
| Amelander Zeegat - Boei 1-1 | AZB11 | 161006 | 616004 | 19 | Y / Y |
| Amelander Zeegat - Boei 1-2 | AZB12 | 173011 | 617304 | 22 | Y / Y |
| Amelander Zeegat - Boei 2-1 | AZB21 | 167307 | 610978 | 4 | Y / Y |
| Amelander Zeegat - Boei 2-2 | AZB22 | 170688 | 611040 | 5 | Y / N |
| Amelander Zeegat - Boei 3-1 | AZB31 | 168318 | 606745 | 4 | Y / Y |
| Amelander Zeegat - Boei 3-2 | AZB32 | 169349 | 607115 | 7 | Y / Y |
| Amelander Zeegat - Boei 4-1 | AZB41 | 168792 | 600501 | 2 | Y  / Y |
| Amelander Zeegat - Boei 4-2 | AZB42 | 171319 | 604249 | 13 | Y /  Y |
| Amelander Zeegat - Boei 5-1 | AZB51 | 167963 | 596444 | 2 | Y / N |
| Amelander Zeegat - Boei 5-2 | AZB52 | 175490 | 600699 | 10 | Y / Y |
| Amelander Zeegat - Boei 6-1 | AZB61 | 167500 | 592500 | 1 | N / N |
| Amelander Zeegat - Boei 6-2 | AZB62 | 180506 | 598604 | 1 | N / N |

2.3.3    Current (Coastal Genesis 2.0 campaign)

2.3.3.1    *13-hour ship-mounted ADCP measurements*

During the Coastal Genesis 2.0 measurement campaign in the Ameland Inlet (September 2017) velocities were measured in the tidal inlet. Vertical velocity profiles were measured using ADCP instruments that were mounted on the hull of two vessels that sailed across the inlet simultaneously. The ships sailed back and forth along a predefined navigation route for approximately 13 hours, covering a complete tidal cycle. The routes sailed by the ships were chosen in such a way that a one-way trip along the route could be completed in approximately 20 minutes. The measurements were executed at three (non-consecutive) days during the September campaign. An overview of the time frames in which the measurements were executed is given in Table 2.4

*Table 2.4    Time frame of the CGII ship-mounted ADCP measurements across the Ameland inlet.*

| Day | Ship | Start | End | Duration |
|-----|------|-------|-----|----------|
| 1 September 2017 | AQVPO | 05:10:13 | 18:08:26 | 12 h 58 min |
| | RWSSI | 05:10:30 | 18:08:17 | 12 h 57 min |
| 5 September 2017 | AQVPO | 05:30:07 | 18:32:43 | 13 h 2 min |
| | RWSSI | 05:29:48 | 18:28:04 | 12 h 58 min |
| 19 September 2017 | AQVPO | 04:50:26 | 18:06:40 | 13 h 16 min |
| | RWSSI | 04:50:15 | 18:01:46 | 13 h 11 min |

The measurements were processed to calculate the instantaneous discharge through the tidal inlet. For this purpose, the measurements were projected on a (manually defined) track route which best fitted the scattered locations of the measurements (Figure 2.3). For each measurement location, a discharge of unit width ($m^3$/m/s) was determined by integrating the flow velocity over the depth. It is assumed that there is no flow at the base of the profile ($U_{z0}$ = 0 m/s) and that the flow at the surface is equal to the measurement closest to the surface. The blanking distance under the water surface is 1.5 – 2 meters till 1-1.5 meter above the sea surface. The discharge through the tidal inlet is calculated by integrating the discharge over the width of the defined track routes. For this purpose two assumptions were made:

1. The flow does not change substantially during the 20-minute time frame in which the measurements are executed;
2. There is no flow at the landward outer ends of the defined tracks.
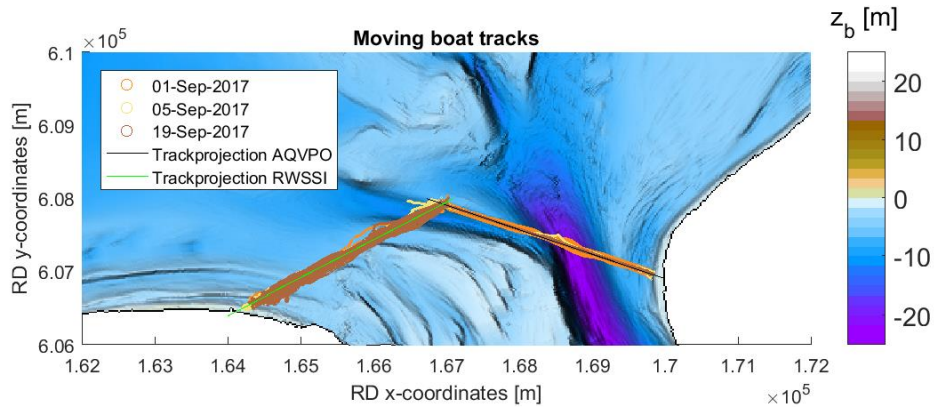


*Figure 2.3   Tracks of the ADCP measurements in the Ameland tidal inlet, simultaneously executed by the survey vessels Rijkswaterstaat Siege (RWSSI) and Aquavision Potvis (AQVPO). At every location water depth and flow velocity was recorded is plotted (circles).*

The transect-integrated discharge ($m^3$/s) for the two separate tracks is visualized in Figure 2.4. Summation of the discharge measured by each vessel gives the total discharge through the tidal inlet (yellow line). The time-integrated discharge volume is indicated in the figure, with the background color indicating the ebb and flood phases. The measurements show that the total ebb or flood volume through the tidal inlet varies between approximately $330 * 10^6$ $m^3$ and $506 * 10^6$ $m^3$, mainly depending on the moment within the spring-neap tidal cycle (indicated in the caption). Note that only full-time periods of ebb and/or flood can be used to compute the total ebb or flood volume and that ebb and flood volume per tidal cycle does not have to result in exactly the same net in- and outflow due to water flow over the watersheds.

Time-integrated discharge volumes per ebb and flood phase ($m^3$) were inspected and deemed suitable for the calibration of the hydrodynamic model.
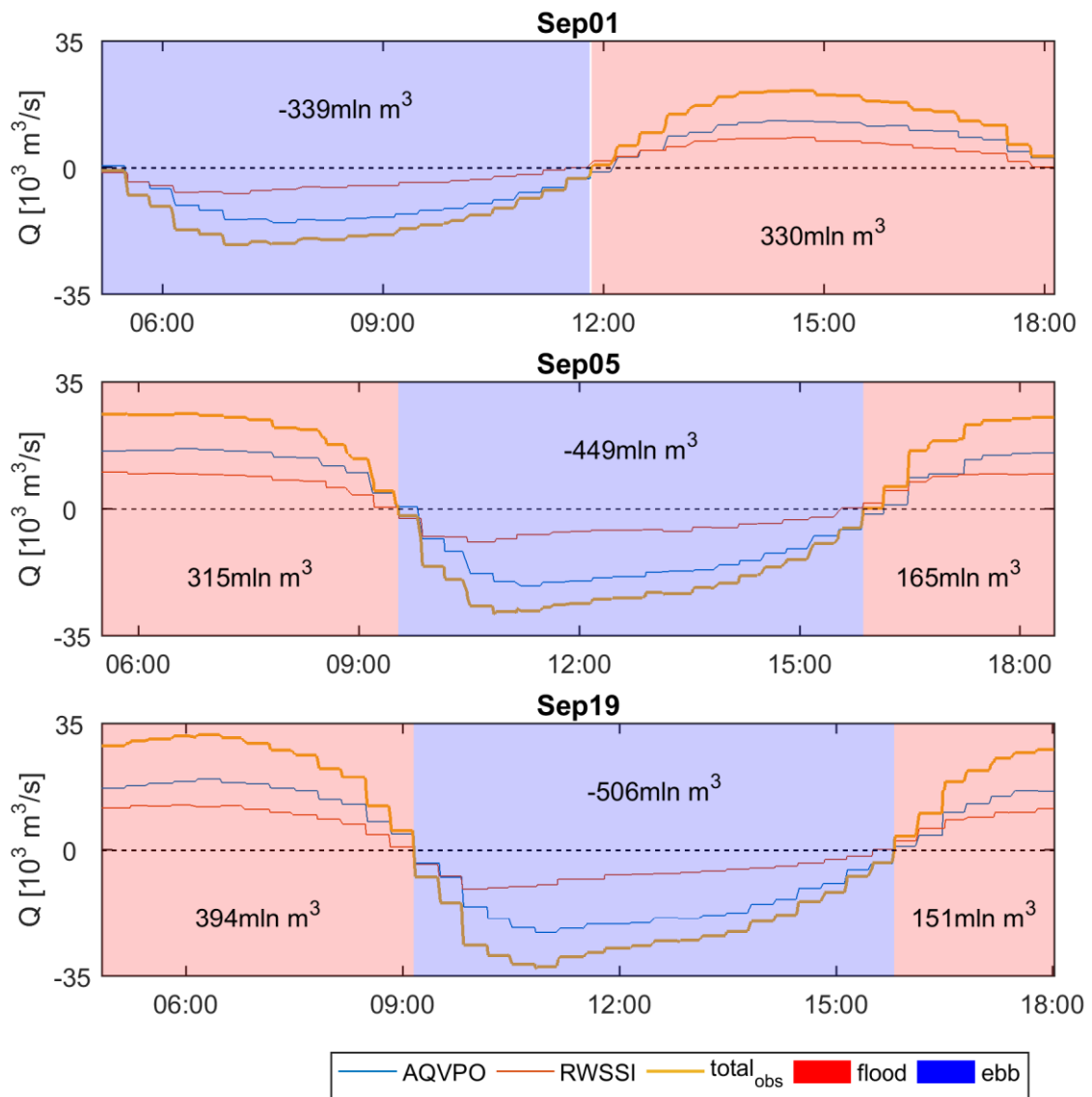
Figure 2.4   Discharge determined from the ship mounted ADCP measurements for the two separate vessels
AQVPO (blue) and RWSSI (red) and the total discharge through the tidal inlet (yellow). Positive values are
flood discharges, i.e. into the Wadden Sea. Data is gathered at 1 Sep. (near neap tide), 5 Sep. (in between
neap and spring tide), and at 19 Sep. (near spring tide).

2.3.3.2   *Frames*

During the Coastal Genesis 2.0 campaigns (September and November 2017 at Ameland, January and March 2018 at Terschelling) stationary frames were deployed with, among other instruments, upward-looking ADCP instruments to measure velocity profiles. The bed level, locations and the time periods of operation are indicated in Table 2.5   for each frame used for model calibration.

During the September 2017 campaign, a total of five frames were deployed in the Ameland Inlet and on the seaward part of the ebb tidal delta (Figure 2.1, black triangles). One of these frames could not be retrieved at the end of the measurement campaign (F2) and the data of another frame (F5) was not available during model calibration. The data of the other three frames is used for the model calibration (Table 2.5      ; Figure 2.5).

*Table 2.5    Bed level, coordinates and time period of operation of the measurement frames used for model calibration (September 2017; AZG).*

| Frame | RDx [m] | RDy [m] | Depth [m] | Start | End |
|--------|---------|---------|-----------|--------|--------|
| AZG-F1 | 167169 | 612748 | 8 | 30-Aug | 9-Oct |
| AZG-F3 | 168783 | 606398 | 20 | 30-Aug | 10-Oct |
| AZG-F4 | 165276 | 611043 | 5 | 29-Aug | 9-Oct |
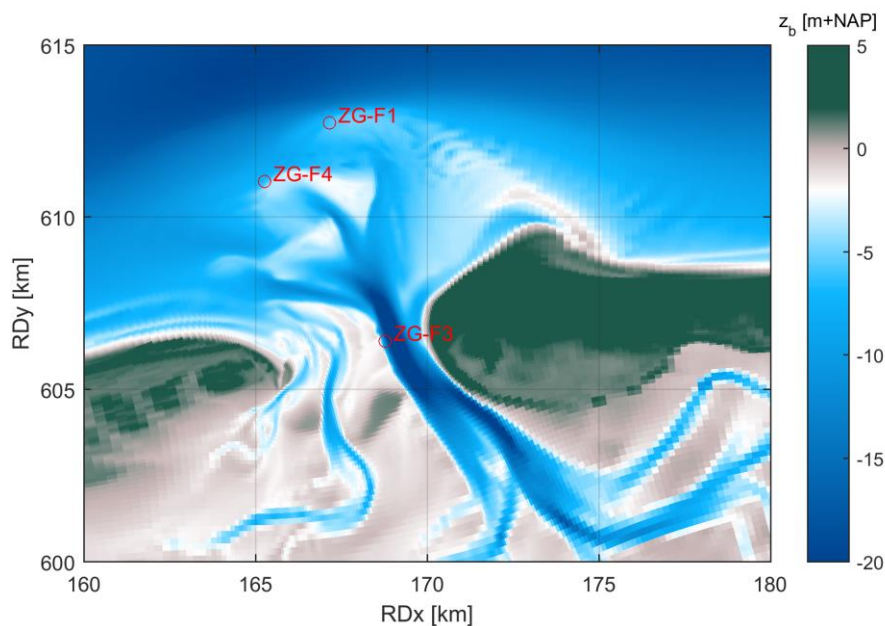


*Figure 2.5   Locations of the current measurements in the inlet during the CGII campaign.*

The methods of processing the raw-data signal is described in the data report (Deltares, 2018). After raw data processing the ADCP measurements were processed into 10-minute averaged and depth-averaged values for model comparison. This processing step is described in the data report as well; yet, a concise summary of the processing method is given below.

The data of each measurement bin is averaged on 10-minute intervals (profiles were recorded every second) by averaging over all the data available in the 5 minutes before and after the target time moment (600 samples). The ADCP instruments measured the first half of every hour. Measurements (bins) that are located above the water surface are ignored. For this step, the local water depth was determined using pressure measurements (after correction for atmospheric pressure fluctuations) from the ADCP instruments or from the pressure measurements of the Aquadopp instruments in case an ADCP did not measure pressure. The subsequent processing step (depth averaging) can be done in a number of different ways; the method described here is used for the datasets applied for model comparison. To process the data to depth averaged values a logarithmic profile was fitted to the velocity measurements over the vertical, to fill up the part of the water column for which the ADCP did not provide measurements (between the bed and the sensor height + blanking distance). The fit is based on the following equation:

$$u(z) = \frac{u_*}{\kappa} \ln\left(\frac{z}{z_0}\right)$$

With $u_*$ the shear velocity, $\kappa$ the Von Karmann constant (= 0.4), $z$ the height above the bed, and z0 the near-bed vertical level where the velocity is zero. Both the shear velocity as z0 follows from a fit to the data, while z0 was limited to 0.001 m to prevent unrealistic fits. Finally, the depth-averaged velocity estimate follows by averaging the velocity measurements of the ADCP combined with the fitted velocity profile outside the range of the ADCP instruments (below the sensor height + the blanking distance).

The depth-averaged values are rotated from eastward (u) and northward (v) components to a component stream wise to the main flow direction (major axis) and a component perpendicular to the stream wise direction (minor axis). The main flow direction is determined as the direction of the major axis of the ellips of the M2 tidal signal, which follow from a tidal analysis on the data. The rotation to streamwise direction is done following Boxel et al. (2004):

$$u_1 = u_0 \cos\theta + v_0 \sin\theta$$

$$v_1 = -u_0 \sin\theta + v_0 \cos\theta$$

Here $u_0$ and $v_0$ are the eastward and northward velocities, respectively, and $u_1$ and $v_1$ are the components in stream wise direction and perpendicular to that. The angle θ by which the flow is rotated follow from the tidal analysis.

The datasets of depth-averaged values were checked and it was concluded that the data is appropriate for model comparison. There is, however, probably an offset in the direction of the measurements due to compass errors. The cause and consequences of this offset is elaborated in Appendix E.

### 2.3.3.3 Watershed

Velocity profiles were recorded every minute with 10 cm bins at the watershed during the September 2017 campaign using Aquadopp instruments (Figure 2.1, yellow triangles). The water depth and coordinates of the instruments are listed in Table 2.6 . The signal was processed to 10-minute and depth-averaged values for model comparison. In contrast to the ADCP instruments, the depth-averaged velocity estimates for the watershed Aquadopp instruments were simply based on the average of the measured bins (below the water surface), as only a limited part of the water column was not measured (only 0.3 m was below the sensor height + blanking distance).

The accuracy of the depth averaged currents obtained during the CGII measurement campaign on the watershed is less than the accuracy of the measurements in the inlet due to the limited water depth. However, the measurements were deemed suitable for the calibration of the hydrodynamic model.

*Table 2.6    Frame current measurements at the watershed with names, locations, depth and time period used for model calibration (September 2017; AMID).*

| Name | RDx [m] | RDy [m] | Depth [m] | Start | End |
|------|---------|---------|-----------|-------|-----|
| AmID1 | 161815 | 600065 | 0.8 | 30-Aug | 01-Oct |
| AmID2 | 167105 | 596668 | 0.7 | 30-Aug | 17-Sep |
| AmID3 | 167233 | 594000 | 0.4 | 30-Aug | 01-Oct |
| AmID4 | 187515 | 605914 | 0.7 | 30-Aug | 02-Oct |
| AmID5 | 187191 | 603618 | 0.0 | 30-Aug | 02-Oct |
| AmID6 | 188278 | 601540 | 0.5 | 30-Aug | 02-Oct |
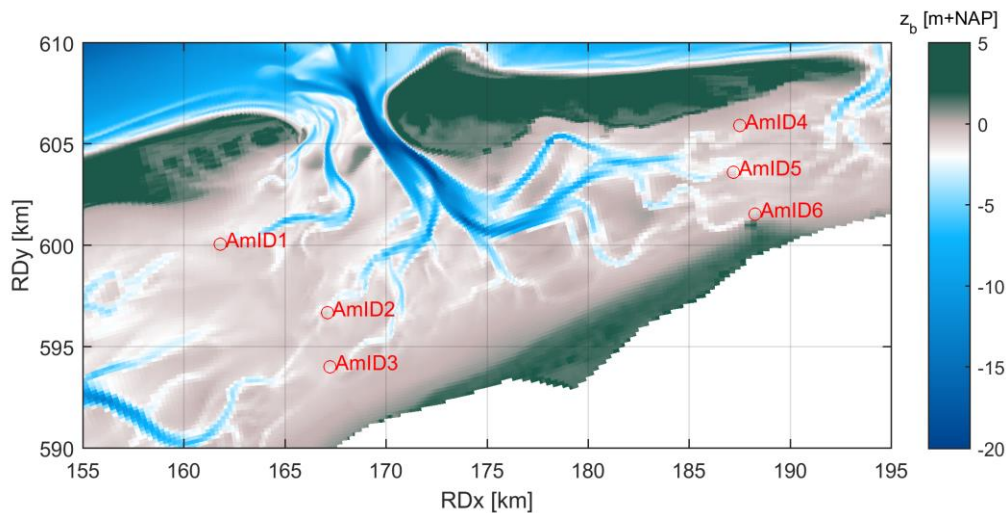


*Figure 2.6   Locations of the Aquadopps watershed measurements.*

## 2.4 Model validation

### 2.4.1 Water levels
Water level observations applied in the calibration and validation of the model is presented in Table 2.2. Observations for 2008 and 2011 were inspected and deemed suitable for the validation of the hydrodynamic model. Station Holwerd was, however, not recording for both these years.

### 2.4.2 Wave height, period and direction
Wave observations applied in the calibration and validation of the model is presented in Table 2.3. Observations for 2008 and 2011 were inspected and deemed suitable for the validation of the model. However, some data can be missing due to maintenance or because certain characteristics were not measured.

### 2.4.3 Velocities

#### 2.4.3.1 Coastal Genesis 2.0 campaign November 2017: DVA
During the November 2017 campaign, three frames were deployed in deeper water on the lower shoreface of the Amelander ebb tidal delta (Figure 2.1, orange triangles). The data were inspected and deemed suitable for the validation of the wave model.

*Table 2.7    Bed level, coordinates and time period of operation of the measurement frames used for model validation (November 2017; DVA).*

| Frame | RDx [m] | RDy [m] | Depth [m] | Start | End |
|-------|---------|---------|-----------|-------|-----|
| DVA-F1 | 168339 | 615736 | 20 | 8-Nov | 11-Dec |
| DVA-F3 | 168449 | 613779 | 16 | 8-Nov | 11-Dec |
| DVA-F4 | 168472 | 613485 | 10 | 8-Nov | 11-Dec |
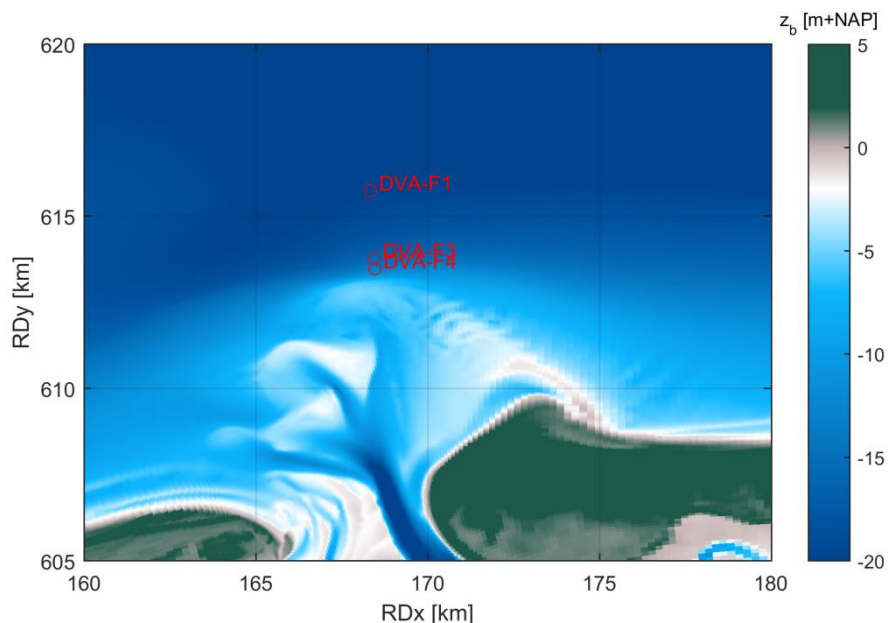


*Figure 2.7   Locations of the current measurements in the inlet performed during the CGII campaign in Nov'17*

In January and March 2018 three frames were placed on the lower shoreface of Terschelling. The locations of the frames for these two campaigns are indicated in Table 2.8        and Table 2.9        . In Figure 2.1 the locations are shown as red (January) and green (March) triangles. During the March 2018 campaign the upward looking ADCP did not operate properly at frame 3. Therefore, the data from this frame is not included in the data validation. The data gathered at the other frames was considered suitable for data validation. There are, however, doubts about the direction of the measurements (see Appendix E).

*Table 2.8    Bed level, coordinates and time period of operation of the measurement frames used for model validation (January 2018; DVT1).*

| Frame | RDx [m] | RDy [m] | Depth [m] | Start | End |
|-------|---------|---------|-----------|-------|-----|
| F1 | 151671 | 611326 | -20 | 11-Jan | 6-Feb |
| F3 | 152260 | 607627 | -14 | 11-Jan | 6-Feb |
| F4 | 152685 | 606596 | -10 | 11-Jan | 6-Feb |

*Table 2.9    Bed level, coordinates and time period of operation of the measurement frames used for model validation (March 2018; DVT2).*

| Frame | RDx [m] | RDy [m] | Depth [m] | Start | End |
|-------|---------|---------|-----------|-------|-----|
| F1 | 151993 | 611306 | -20 | 12-Mar | 26-Mar |
| F3 | 152249 | 607599 | -14 | 12-Mar | 26-Mar |

### 2.4.3.2    SBW measurements (2011 & 2008)

As part of the SBW project (in Dutch: *Sterkte en Belastingen Waterkingen*) ADCP measurements were carried out in the Ameland Inlet in 2008 and 2011 (Aqua Vision, 2008; Aqua Vision, 2012). The SBW project focusses on the influence of waves on flood safety during extreme conditions. Both the 2008 and 2011 measurement campaigns lasted for a period of approximately 6-8 weeks.
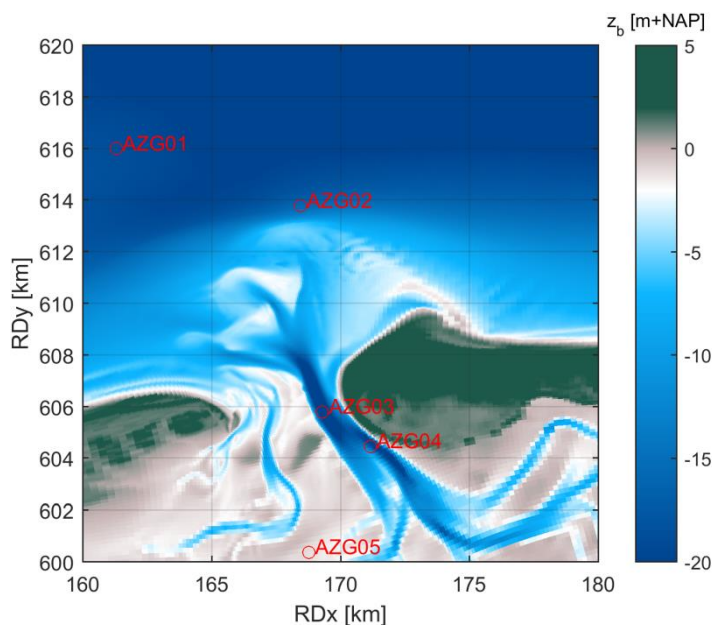


*Figure 2.8    Locations of the current measurements in the inlet performed during the SBW campaign 2011 & 2008*

### 2.4.3.2. *SBW measurements from 2011*

The measurements in 2011 were performed at two locations in the Ameland Inlet (Aqua Vision, 2012; see green diamonds in Figure 2.1 or Figure 2.8). Both locations are in relatively deep water. The exact location in Rijksdriehoek coordinates (RD), depth and measurement period can be found in Table 2.10     .

All the currents measurements from SBW 2011 was inspected and deemed suitable for the calibration of the hydrodynamic model.

*Table 2.10  Current measurements name, location, depth and periods for SBW 2011*

| Name | RDx [m] | RDy [m] | Depth [m] | Start date | End date |
|------|---------|---------|-----------|------------|----------|
| AZG02 | 168549 | 608245 | 15 | 26-10-2011 | 23-11-2011 |
| AZG03 | 169300 | 605800 | 26 | 26-10-2011 | 15-11-2011 |

### 2.4.3.2. *SBW measurements from 2008*

The measurements in 2008 were performed at three locations in and around the Ameland Inlet (Aqua Vision, 2008; see green diamonds in Figure 2.1 or Figure 2.8). Location 1 is near AZB11, about 12 km northeast of the inlet. Location 4 is near AZB42 in the Borndiep. Location 5 is near the watershed and close to AZB41 and about 5 km south of the inlet. The exact location in Rijksdriehoek coordinates (RD), depth and measurement period can be found in Table 2.11     .

All the ADCP measurements from SBW 2008 wwere inspected. AZG04 is of good quality during most parts of the measurement period. AZG05 is of poor quality. This is supported by Deltares (2009) that worked with the same data.

*Table 2.11  Current measurements name, location, depth and periods for SBW 2008*

| Name | RDx [m] | RDy [m] | Depth [m] | Start date | End date |
|------|---------|---------|-----------|------------|----------|
| AZG01 | 161300 | 616000 | 18 | 28-11-2007 | 29-01-2008 |
| AZG04 | 171157 | 604458 | 17 | 28-11-2007 | 08-01-2008 |
| AZG05 | 168769 | 600373 | 1 | 28-11-2007 | 09-01-2008 |

### 2.4.4 Wind and pressure

At 8 monitoring stations spread over the Wadden Sea area wind velocity, wind direction and atmospheric pressure were collected that are continuously being measured by the Royal Netherlands Meteorological Institute (KNMI) (Table 2.12     ). The collected wind data is the potential wind delivered by the KNMI (i.e. 10-minute averaged and extrapolated to 10 m above the surface).

All the wind and pressure measurements were inspected and deemed suitable for the validation of the weather models. Several weather models were validated for the Wadden Sea regarding wind speed, direction and pressure. The most accurate weather model will be used to force the hydrodynamic-wave model.

*Table 2.12   Wind and pressure measurements name, location, height*

| Name | RDx [m] | RDy [m] | Height [m+NAP] |
|------|---------|---------|----------------|
| De Kooij | 114244 | 549037 | 1.2 |
| Nieuw Beerta | 272762 | 580080 | -0.2 |
| Huibertgat | 221983 | 621345 | 0.0 |
| Groningen | 235172 | 571434 | 5.2 |
| Lauwersoog | 208989 | 603114 | 2.9 |
| Leeuwarden | 179336 | 581883 | 1.2 |
| Stavoren | 154749 | 545503 | -1.3 |
| Terschelling Hoorn | 152245 | 600549 | 0.7 |

# 3 Model set-up

## 3.1 Numerical grid

The computational domain of the numerical grid that is set-up covers the tidal inlets of Terschelling, Ameland, and Schiermonnikoog. The resolution of the Delft3D-FLOW grid varies between 50 and 350 m, with highest resolution in the Ameland Inlet (Figure 3.1). The SWAN grid has a larger spatial extent to avoid boundary issues within the FLOW computational domain (blue line in Figure 3.1). Furthermore, the resolution of the wave grid is a factor 2 coarser compared to the resolution of the FLOW grid. It is expected that a factor 2 coarsening of the SWAN domain still results in sufficient resolution while decreasing the computational demand. The Ameland Inlet is covered by a second, nested, SWAN domain (red line in Figure 3.1) having a resolution which is equal to the FLOW domain.
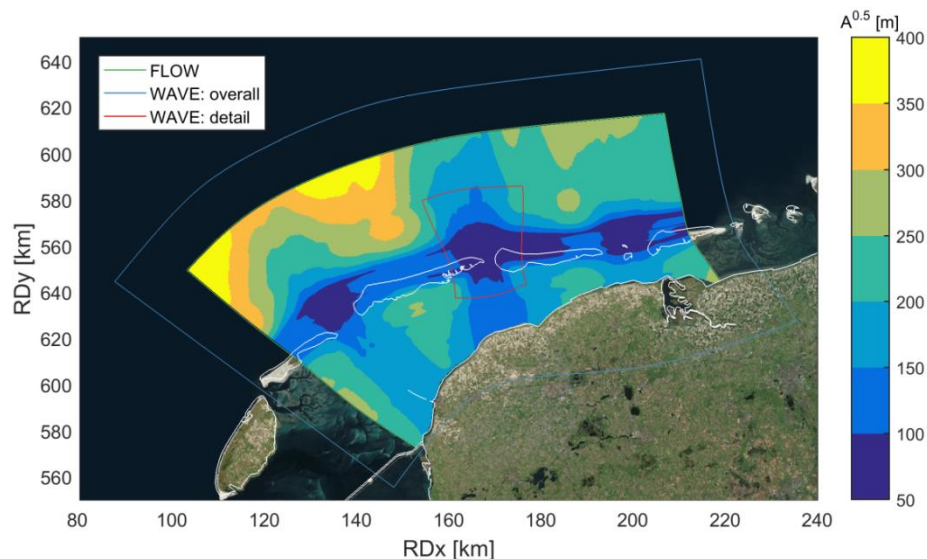


*Figure 3.1   Extent of the model grids with the resolution of the FLOW grid indicated as the length [in m] of the grid cells. In red the extent of the SWAN grid is presented.*

## 3.2 Boundary conditions

### 3.2.1 Meteorological forcing

Wind speed and direction and atmospheric pressure from HIRLAM were applied in all model simulations following a comparison with observations (refer to Appendix B). No calibration of the meteorological conditions was carried out in the present study. The HIRLAM model was selected over the NCEP and ERA-interim model based on the most accurate reproduction of wind speed and direction compared to observations in the area of interest. It was expected on forehand that HIRLAM will result in the most accurate reproduction of the meteorological forcing due to the high spatial resolution compared to global meteorological models. For a validation of the different meteorological models, see Appendix B.

### 3.2.2 Water levels

First, the mean water surface elevation applied at the oceanic boundary, a so-called A0 astronomic constituent, was adjusted to account for the offset between mean sea level (MSL)

and the model bathymetry datum NAP. Hence, the DSCMv4ZUNOv6 model has a vertical reference level of MSL and the CGII-TA model has a reference level of NAP. Next, a harmonic tidal analysis was performed on the simulated and observed water levels at the measurements locations over the analyzed time frame. This resulted in 56 tidal constituents (amplitudes and phases) and a non-tidal residual (NTR) signal at the boundary

The NTR is often also described as 'surge'. Splitting water levels into an astronomical and NTR component makes it possible to calibrate the tide in the frequency domain separately to improve the accuracy of the tidal water level reproduction.

Figure 3.2 shows the model boundary segments applied to force Delft3D-FLOW. Water level boundary conditions are defined along the deep water boundary of the model (blue color). In the surfzone and on the watershed a zero-gradient Neumann boundary is applied to give the model some freedom in the area where strong wave-driven currents can be present (red color).
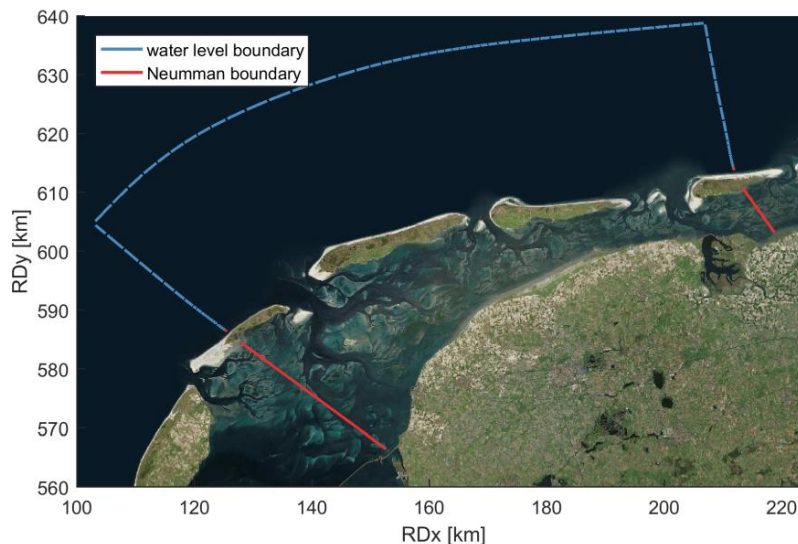


*Figure 3.2   Extent of the model grids in combination with the different types of boundary conditions given in blue (water level boundary) and red (zero-gradient Neumann)*

### 3.2.3   Waves
For the offshore (north), and lateral (west and east) wave model boundaries, measured wave spectra at EIR and SON were applied (similarly to Deltares, 2010). At the offshore boundary, an interpolation by the model, between EIR and SON was applied. The measured wave spectra were multiplied with a calibration factor of 1.1, which is in line with Deltares (2010).

### 3.3   **Bathymetry**
Bathymetric information was applied after relevance: first the Vaklodingen, then AHN and finally bathymetric information from the Hydrographic Service of the Royal Netherlands Navy. For the construction of the model bathymetry of a given year, Vaklodingen from the last ten years were taken into account (e.g. for the bathymetry of 2017, information of the period 2017-2008 was applied). These time windows were used, in order to cover all parts of the Wadden Sea. The datasets were combined by interpolating other data sources to the vaklodingen grid with a linear interpolation method. AHN and bathymetry from the Hydrographic Service are static, which means that for every year the same dataset was applied. The constructed bathymetric and seniority map of 2017 is presented in Figure 3.3.
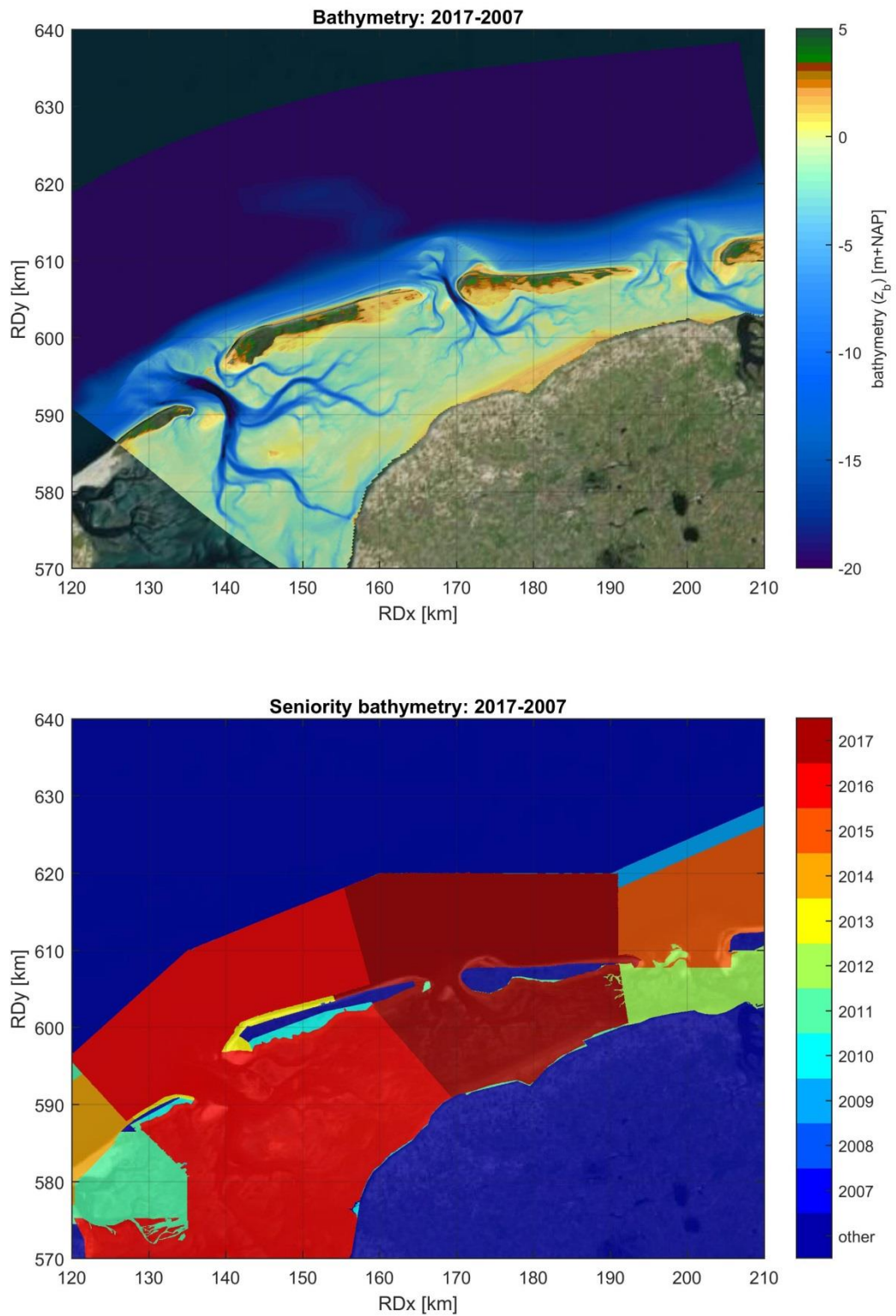
*Figure 3.3   Constructed bathymetry for 2017 (upper panel). Seniority map (Dutch: anciënniteitskaart; lower panel). Data without a time stamp is classified as 'other'.*

## 3.4 Other inputs

### 3.4.1 Thin dams

A thin dam is a virtual dam along the side of a grid cell across which no flow exchange is possible. This is needed to resolve processes substantially smaller than the computational grid. Thin dams were applied to represent the harbors of Harlingen and Vlieland.

## 3.5 Model settings

### 3.5.1 Delft3D-FLOW: water levels and currents

The Coastal Genesis II Terschelling - Ameland Inlet (CGII-TA) model was run with the Deltares hydrodynamic modeling program Delft3D (version 3.56.29165) in depth-averaged mode. The following model settings were applied:

- **Bed roughness**: The Van Rijn roughness predictor (Van Rijn, 2017) was applied. The roughness predictor of Van Rijn contains three contributions to the current-related roughness associated with the presence of ripples, mega-ripples and dunes. These contributions are scaled through user-defined coefficients. The advantage of a roughness predictor is that roughness can change over time. Calibration resulted in a coefficient for the contribution of ripples, mega-ripples and dunes to the roughness of respectively, 0.5, 0.5 and 0. During average flow conditions, this corresponds to a spatially varying Manning coefficient of 0.014 $s/m^{1/3}$ in the basin to 0.028 $s/m^{1/3}$ offshore and in the inlets.

- **Time step:** Sensitivity calculations showed that a computational time step of 0.25 min was required for stable results.

- **Time zone:** The model was run in GMT. This made it possible to directly use the water levels from the large-scale hydrodynamic model as boundary conditions.

- **Viscosity and diffusivity:** The model was run with a uniform horizontal eddy viscosity of 1 $m^2/s$ and a uniform horizontal eddy diffusivity of 10 $m^2/s$. These values are typically used for this grid resolution (e.g. Deltares, 2009a).

- **Drying and flooding**: The minimum drying/flooding procedure was applied with the criteria for drying and flooding of individual cells set to 0.02 m.

- **Wind stress formulation**: The wind stress formulation of Vatvani et al. (2012) was used (Table 3.1). In this formulation, the magnitude of the drag coefficient increases until a wind speed of about 30 m/s and then decreases with further increase of the wind speed since the stress above the air-sea interface starts to saturate. These Cd values correspond fairly well to a Charnock value of 0.032 that Deltares (2009b) recommends.

*Table 3.1  The wind stress formulation of Vatvani et al. (2012) in which wind speed with matching Cd coefficient is presented. Between the wind speed values a linear interpolation is used by Delft3D.*

| Wind speed [m/s] | Cd (10^-3) |
|---|---|
| 0 | 1 |
| 25 | 2.5 |
| 50 | 1.5 |

### 3.5.2 SWAN: wave height, period and direction

The CGII-TA model was run with spectral wave model SWAN (version 41.10). The following other model settings were applied

- **Communication time step:** stationary wave computations were performed every 30 minutes. We choose to apply stationary wave computations since this will also be done in the morphological simulations. Wave forces were computed based on radiation stresses and FLOW and SWAN communicate every 30 minutes. For the SWAN computations, water level, velocity and wind were taken and extended from the FLOW results. A communication time of 30 minutes is used since this will result in a maximum water level difference of less than 20 cm per sequential SWAN computation.

- SWAN was run in the **third-generation mode** with wind input, quadruplet interactions and whitecapping. Nonlinear saturation-based whitecapping combined with wind input of Yan (1987) was applied.
  - *GEN3 WESTH*

- **White-capping**: For the deep water physics, the combination of wind input and saturation-based whitecapping proposed by Van der Westhuysen (2007) was used.
  - *WCAP WESTH cds2=5.0E-5 br=1.75E-3 p0=4. cds3=0.000 QUAD*

- **Bed roughness**: A constant semi-empirical expression for JONSWAP results typical for sandy bottoms of 0.038 $m^2 s^{-3}$ was used.
  - *FRIC JON     0.0380*

- **Wave breaking**: The BKD formulation of Salmon & Holthuijsen (2011) was applied. This indicates that the breaker index scales with both the bottom slope (beta) and the dimensionless depth (kd). Default calibration coefficients were applied.
  - *BREAK BKD 1.0 0.54 7.59 -8.06 8.09*

- **Triad wave-wave** interactions were modeled using the LTA method. Calibration coefficients from Deltares (2010) were applied.
  - *TRIAD trfac=0.100 cutfr=2.500*

- The **numerical accuracy** was set to 2.5% for relative and absolute wave height differences. In which at least 98% of the wet grid cells should suffice. A frequency-dependent under-relaxation parameter (alpha) of 0.01 was used to improve convergence and a maximum amount of iterations was set to 50.
  - *NUM ACCUR     0.025   0.025   0.025   98.000   50 0.01*

## 3.6 Model simulations

For 2008, 2011, 2017 and 2018 both a model setup with only hydrodynamics and a coupled hydrodynamics + waves model were created. The model setup with only hydrodynamics runs for the entire year and was used to calibrate/validate the (tidal) water levels. The model setup with hydrodynamics + waves is used to analyze discharges, velocities and waves. An overview of the different simulations is provided in Table 3.2. All the simulations were carried out on the H6 Deltares UNIX bare-metal cluster. All simulations were run in parallel (2 nodes with 4 cores = 8 cores). Computational time for both the only FLOW as for the FLOW & SWAN models is on average 2,5 days (range 2 – 3 days).

*Table 3.2    Overview of the different simulations carried out.*

|  | # |  | Type | Period |
|---|---|---|---|---|
| Calibration | 1 | 2017 | Only FLOW | Full year |
|  | 2 | 2017/09 | FLOW+SWAN | 30-08-2017 – 08-10-2017 |
| Validation | 3 | 2008 | Only FLOW | Full year |
|  | 4 | 2008 | FLOW+SWAN | 05-01-2008 – 05-02-2008 |
|  | 5 | 2011 | Only FLOW | Full year |
|  | 6 | 2011 | FLOW+SWAN | 24-10-2011 – 24-11-2011 |
|  | 7 | 2017/11 | FLOW+ SWAN | 06-11-2017 – 13-12-2017 |
|  | 8 | 2018/01 | FLOW+ SWAN | 01-01-2018 – 15-02-2018 |
|  | 9 | 2018/03 | FLOW+ SWAN | 01-03-2018 – 15-04-2018 |

# 4 Calibration

## 4.1 Introduction

This chapter presents the results of the CGII-TA model calibration. In order to obtain the most accurate water levels (Section 4.2) and velocity reproductions (Section 4.3), the coefficient for the ripples, mega-ripples and dunes in the Van Rijn roughness predictor were varied between 0.1 and 1.0. First, however, the astronomical amplitudes and phases of the water levels defined at the open boundary of the model were calibrated based on two offshore observations (Terschelling Noordzee and Wierumergronden). Wave heights were calibrated by first increasing the measured energy density that is applied at the model boundary (Section 4.4.1). Secondly, the wave breaking coefficients were varied (Section 4.4.2).

Only data for 2017 was applied to calibrate the water levels, discharges, flow velocities and wave heights simulated. The main goal was to give the best reproduction of the measurements of the 2017 Coastal Genesis 2.0 campaign (see objective in Section 1.2). Calibration of the water levels was based on yearly simulations. Calibration of the velocities and waves were only based on results for the September 2017. The reproductive skill of the model for the other periods is presented in Chapter 5 (validation).

Regarding the variations in the Van Rijn roughness predictor, per measurement type first a table of all the simulations and their effect on the accuracy are presented. Secondly, the chosen coefficients for ripples, mega-ripples and dunes are presented and discussed in more detail. This is done to both present the optimal set of calibration coefficients for each dataset separately and to present the chosen values.

## 4.2 Water levels

### 4.2.1 Astronomical correction factors

Of the in total 58 tidal constituents, the 28 most important tidal constituents were corrected using measurements obtained at Terschelling Noordzee and Wierumergronden in a so-called astronomical correction factor file (*cor file). Changes in the amplitudes and phases were, generally speaking, in the order of a few centimeters for the amplitude and a few degrees for the phase. For example, the K2 amplitude was increased with 8.3% and the K2 phase was increased with 3.4 degrees. Larger changes were found for astronomical components with smaller amplitudes (e.g. MF or M8). For a full list of astronomical correction factors, one is referred to Table 4.1    .

Figure 4.1 presents the tide, NTR and total water level as observed and modeled at Terschelling Noordzee. Including the astronomical correction factors reduces the RMSE in the tidal reproduction at Terschelling Noordzee and Wierumergronden from 4 cm to less than 2 cm (Figure 4.1 – upper panel). The total RMSE in water levels decreases from 8 to 7 cm and is mainly related to the NTR (Figure 4.1 – middle and lower panel). The NTR was not calibrated. The error in (offshore) tidal amplitudes and phases is now very small (Figure 4.2 & Figure 4.3). The amplitudes and phases are reproduced with errors less than a few centimeters are degrees. This results in a vector difference (VD) of less than 1 cm. For an overview of the decrease in tidal error due to changing the astronomical correction factors, see Table 4.2.

*Table 4.1    Astronomical correction factors (amplitude and phase) at the model boundary based on water levels measured at Terschelling Noordzee. For each component the observed amplitude and phase are provided in order to place the corrections in perspective (e.g. MF x2.21 with an amplitude of 4 cm or M2 x1.014 with an amplitude of 90 cm). Note: the corrections are constant for the entire model domain.*

| Component | Amplitude correction [-] | Phase correction [deg] | Amplitude measured [m] | Phase measured [deg] |
|---|---|---|---|---|
| M2 | 1.014 | 0.1 | 0.901 | 204.0 |
| S2 | 1.030 | 0.2 | 0.259 | 264.0 |
| N2 | 1.010 | -0.5 | 0.150 | 182.9 |
| O1 | 1.000 | 2.3 | 0.094 | 190.9 |
| M4 | 0.963 | 2.6 | 0.089 | 269.5 |
| K2 | 1.083 | 3.4 | 0.077 | 263.9 |
| K1 | 1.072 | 3.3 | 0.073 | 345.6 |
| MU2 | 1.013 | 1.0 | 0.069 | 286.1 |
| 2MS6 | 1.256 | 28.1 | 0.067 | 35.2 |
| MM | 0.722 | -16.3 | 0.066 | 134.8 |
| MS4 | 1.081 | 3.9 | 0.063 | 337.5 |
| M6 | 0.804 | 19.7 | 0.056 | 342.4 |
| L2 | 0.998 | 3.2 | 0.049 | 210.0 |
| NU2 | 1.000 | 2.3 | 0.043 | 169.3 |
| MF | 2.206 | -6.8 | 0.040 | 118.4 |
| SSA | 1.392 | 23.3 | 0.037 | 274.6 |
| MN4 | 0.976 | 1.8 | 0.032 | 251.5 |
| 2MN6 | 1.059 | 18.6 | 0.032 | 311.5 |
| P1 | 0.935 | 2.2 | 0.030 | 348.1 |
| MSM | 0.533 | 31.6 | 0.029 | 12.3 |
| 2N2 | 0.998 | -8.9 | 0.029 | 118.3 |
| Q1 | 0.992 | 0.8 | 0.027 | 131.5 |
| MSF | 0.855 | 37.3 | 0.026 | 148.4 |
| MSN2 | 1.042 | -3.2 | 0.019 | 88.2 |
| MK4 | 1.147 | 7.6 | 0.018 | 347.1 |
| 2MK6 | 1.383 | 28.0 | 0.017 | 40.7 |
| 2Q1 | 0.914 | -17.4 | 0.012 | 106.6 |
| M8 | 0.849 | 19.1 | 0.007 | 95.1 |

*Table 4.2    RMSE in total water level reproduction in centimeters at 4 stations of interest near Ameland Inlet.*

| Locations | RMSE tide [cm] | | | RMSE total [cm] | | |
|---|---|---|---|---|---|---|
| | Before calibration tide | After | % | Before calibration tide | After | % |
| Terschelling Noordzee | 3.6 | 1.8 | 50% | 8.1 | 7.1 | 12% |
| Wierumergronden | 3.4 | 1.9 | 44% | 7.4 | 7.2 | 3% |
| Nes | 5.1 | 4.4 | 14% | 10.8 | 10.3 | 5% |
| Holwerd | 7.2 | 5.9 | 18% | 14.3 | 13.2 | 8% |
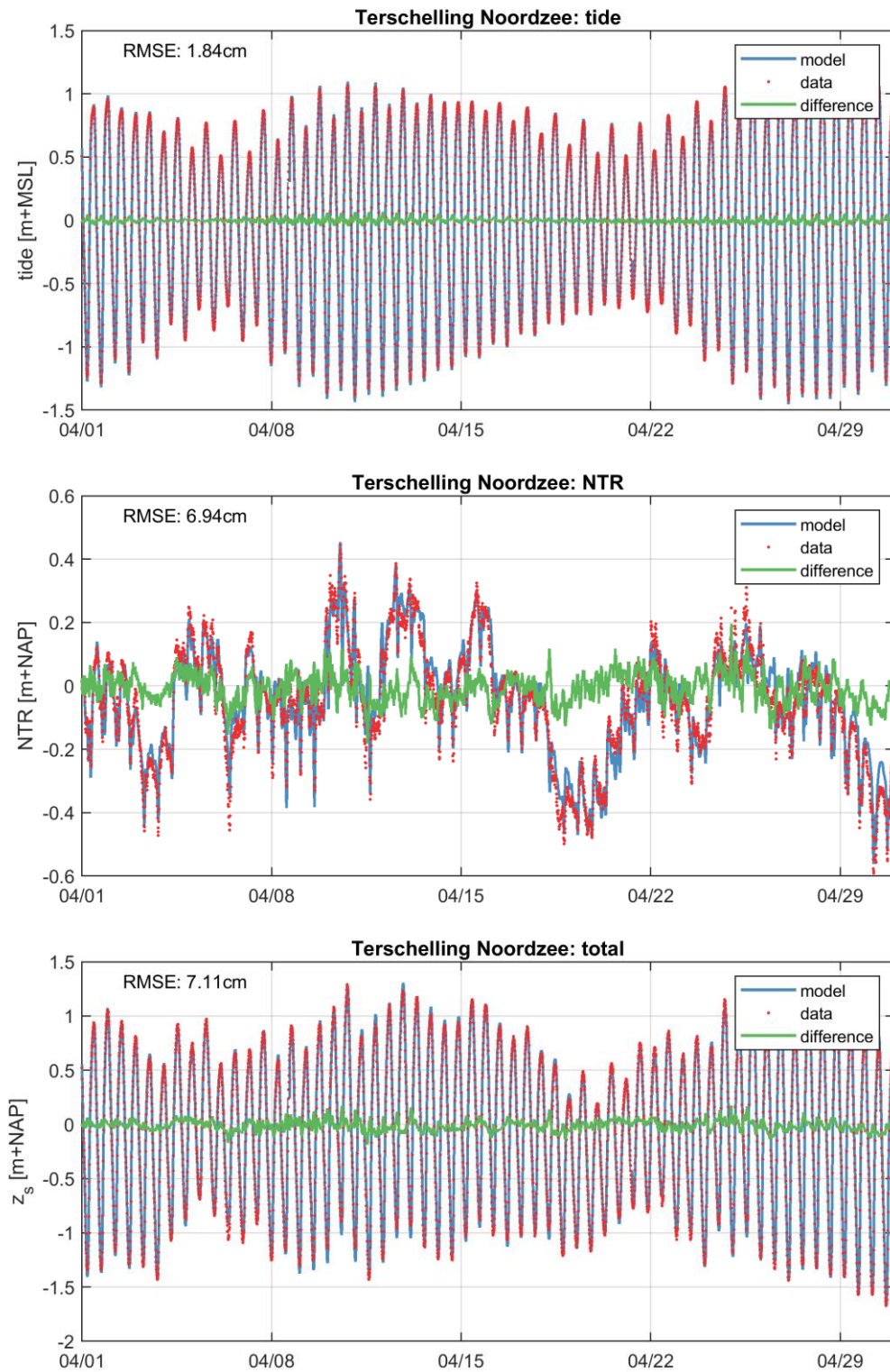
*Figure 4.1 Time series of the tide, NTR and total water level at Terschelling Noordzee as observed and modeled. Blue is modeled, red is data and green is the difference. Time series are after calibration with astronomical correction factors.*
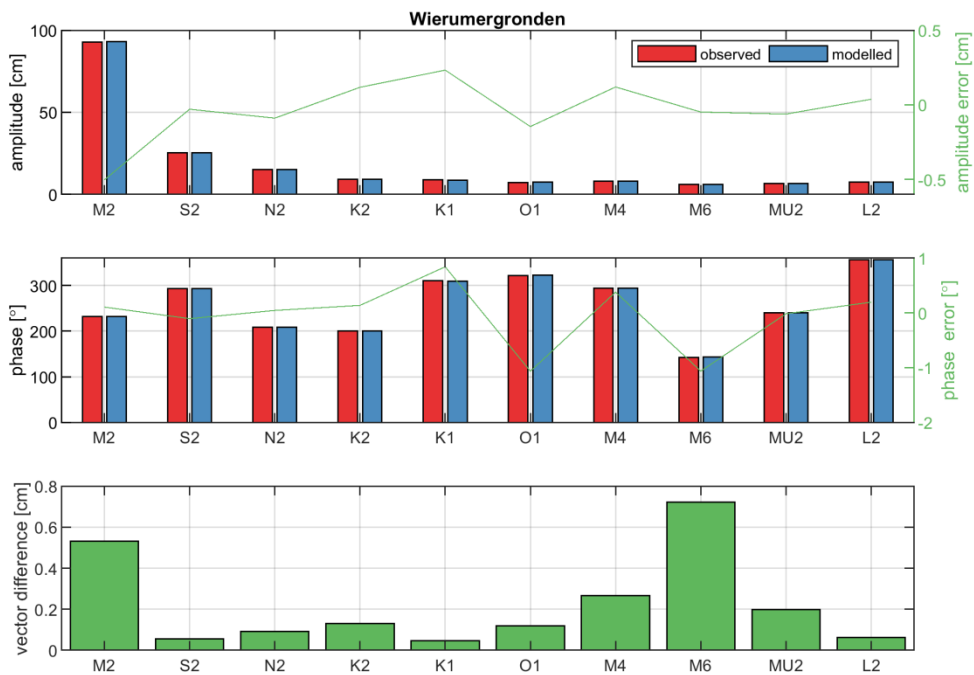
Figure 4.2 *The ten most important astronomical components at Wierumergronden, observed (red) and modeled (blue) after the astronomical boundary correction factors were applied.*
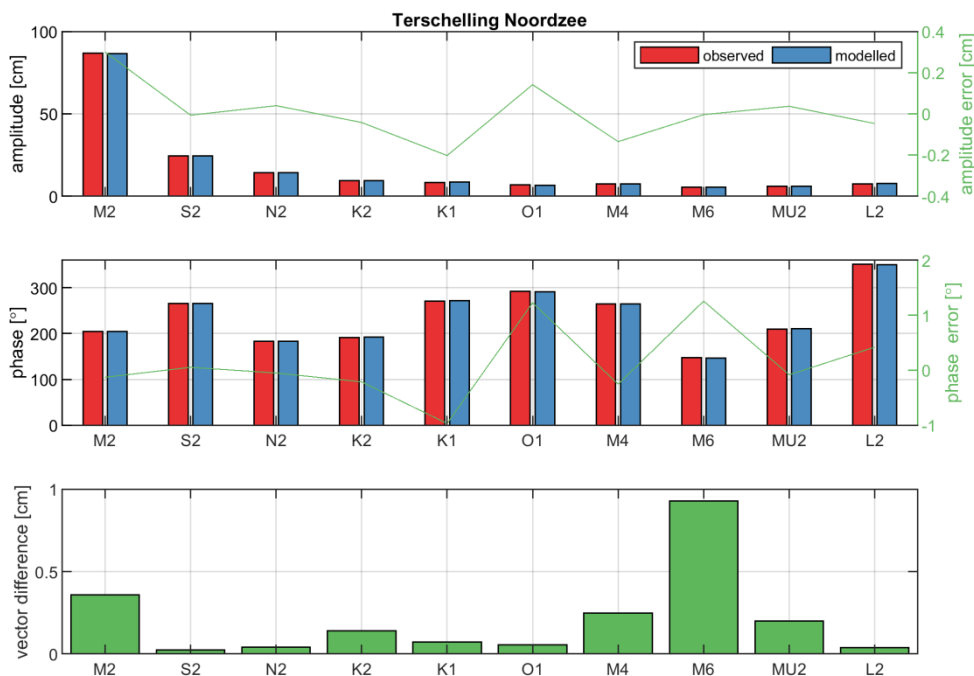


Figure 4.3 *The ten most important astronomical components at Terschelling Noordzee, observed (red) and modeled (blue) after the astronomical boundary correction factors were applied.*

### 4.2.2 Van Rijn roughness predictor

The coefficients for the ripples, mega-ripples and dunes in the Van Rijn roughness predictor were varied between 0.1 and 1.0. Previous experiences (e.g. Deltares, 2011) with the roughness predictor indicated that dunes should *not* be included. Therefore, the majority of the simulations were carried out without dunes. However, in order to verify the conclusion of previous studies, for the coefficients of 0.5 and 1.0 dunes were included. For the full range of calibration runs, one is referred to Table 4.3    .

*Table 4.3    Coefficient of the van Rijn roughness predictor*

| Name | Ripples | Mega-ripples | Dunes |
|---|---|---|---|
| 0.1 | 0.1 | 0.1 | 0 |
| 0.2 | 0.2 | 0.2 | 0 |
| 0.3 | 0.3 | 0.3 | 0 |
| 0.4 | 0.4 | 0.4 | 0 |
| 0.5 | 0.5 | 0.5 | 0 |
| 0.5_dunes | 0.5 | 0.5 | 0.5 |
| 0.6 | 0.6 | 0.6 | 0 |
| 0.7 | 0.7 | 0.7 | 0 |
| 0.8 | 0.8 | 0.8 | 0 |
| 0.9 | 0.9 | 0.9 | 0 |
| 1.0 | 1.0 | 1.0 | 0 |
| 1.0_dunes | 1.0 | 1.0 | 1.0 |

Model results indicate that a coefficient for the ripples, mega-ripples and dunes of respectively, 0.3, 0.3 and 0 gives the most accurate tidal and total water level reproduction (Table 4.4    ). Figure 4.4 presents the M2 amplitude and phase for a cross-shore transect from offshore to nearshore. Colored lines show different model simulations and the bars are the observed M2 amplitudes and phases. A decrease in coefficients in the roughness predictor results in a decrease in bottom friction and thus increases in tidal amplitude. Vice-versa is the case for an increase in coefficients in the roughness predictor. Especially the inclusion of dunes results in too much friction and consequently a decrease in M2 amplitude when the tidal wave propagates from offshore into the Wadden Sea basin.

However, we choose to apply not the optimal set of calibration coefficients for the water levels, but to use the calibrated CGII-TA model with 0.5 ripples, 0.5 mega-ripples and without dunes, which results in the most accurate results for all different measurements. The model reproduces the tide and total water levels fairly well (RMSE respectively between 2-5 cm for tide and 7-13 cm for total water level; Figure 4.6). Also, the spatial distribution of for example the M2 amplitude and phases is in line with observations (Figure 4.5). The error in water level reproduction does increase from offshore (e.g. Terschelling Noordzee and Wierumergronden) to the nearshore/basin (e.g. Nes and/or Holwerd). These errors in water level reproduction are in line with the accuracy of other numerical models. For example, Zijl et al. (2013) reproduced Terschelling Noordzee and Wierumgronden with a RMSE of 8.1 and 8.3 cm and Deltares (2009) computed the tidal water level within +/- 10 cm.

*Table 4.4    RMSE in total water level reproduction in centimeters at 4 stations of interest near Ameland Inlet.*

| Name | Terschelling Noordzee [cm] | Wierumergronden [cm] | Nes [cm] | Holwerd [cm] | Mean [cm] |
|---|---|---|---|---|---|
| 0.1 | 7.4 | 7.5 | 11.1 | 15.0 | 10.2 |
| 0.2 | 7.3 | 7.4 | 9.8 | 12.7 | 9.3 |
| 0.3 | 7.2 | 7.3 | 9.6 | 12.3 | 9.1 |
| 0.4 | 7.1 | 7.3 | 9.8 | 12.6 | 9.2 |
| 0.5 | 7.1 | 7.2 | 10.3 | 13.2 | 9.4 |
| 0.5_dunes | 7.0 | 7.1 | 19.7 | 23.4 | 14.3 |
| 0.6 | 7.1 | 7.2 | 10.7 | 13.9 | 9.7 |
| 0.7 | 7.1 | 7.2 | 11.2 | 14.7 | 10.1 |
| 0.8 | 7.0 | 7.2 | 11.8 | 15.5 | 10.4 |
| 0.9 | 7.0 | 7.1 | 12.3 | 16.3 | 10.7 |
| 1.0 | 7.0 | 7.1 | 12.8 | 17.1 | 11.0 |
| 1.0_dunes | 7.1 | 7.1 | 20.1 | 24.6 | 14.7 |
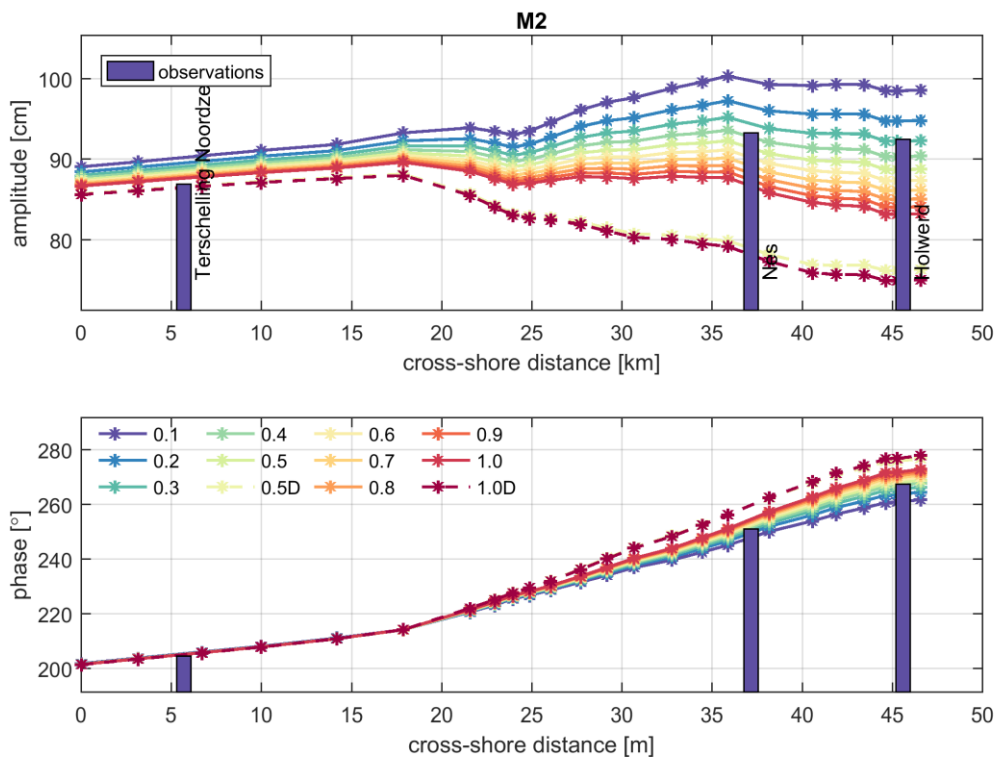


*Figure 4.4   Cross-shore distribution of M2 amplitude and phase as modeled (colored lines) and measured (vertical bars). Lines indicate the different simulations with various calibration coefficients for the Van Rijn roughness predictor. Blue is 0.1. Red is 1.0 with dunes (1.0D). One is referred to Figure 4.5 for the location of the cross-shore transect.*
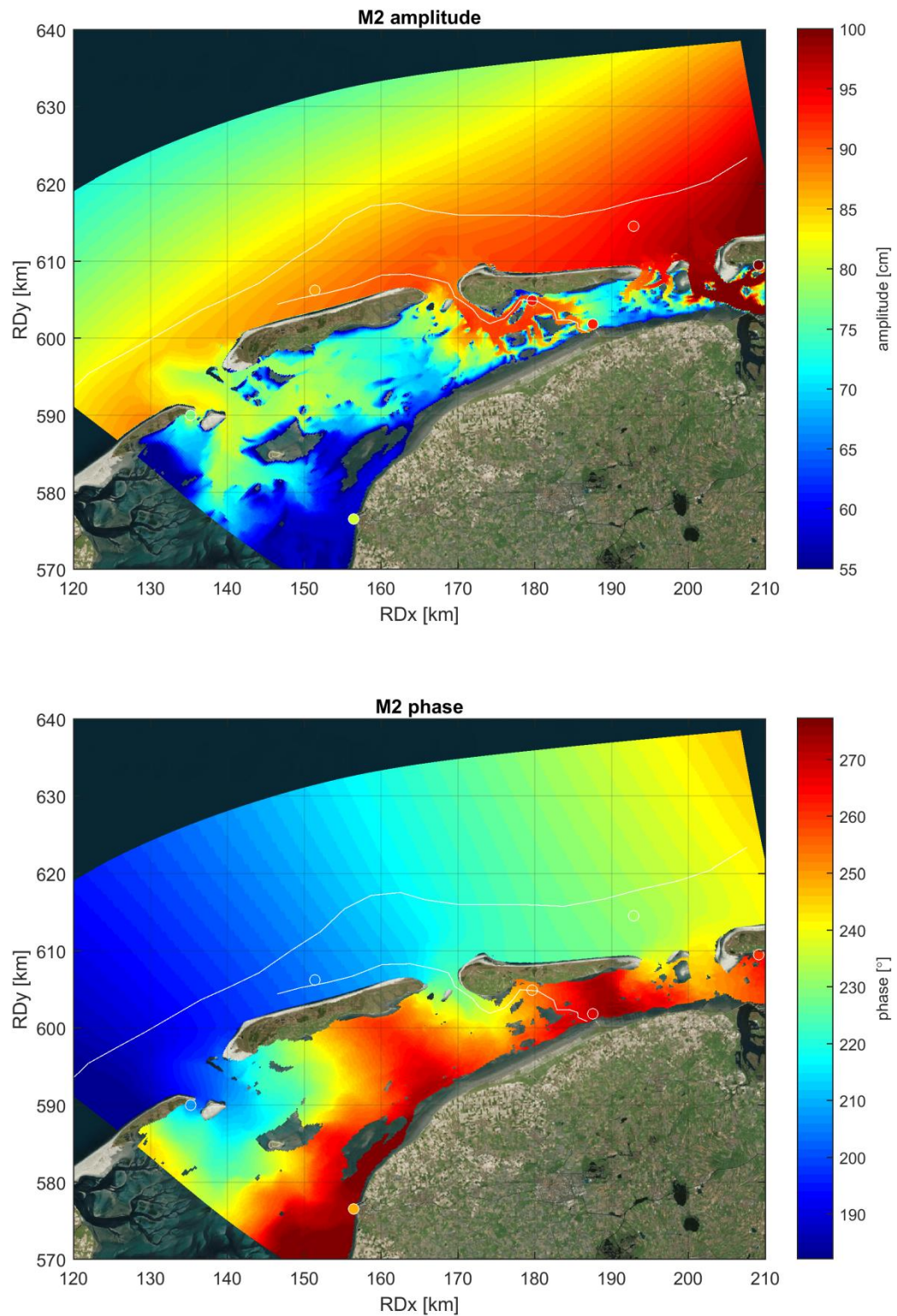
Figure 4.5   Observed and modeled M2 amplitude (upper panel) and phase (lower panel).  The heat map show the computed values and the circles are the observed values. White lines are two transects: longshore and cross-shore. The cross-shore transect is used to show M2 amplitude and phases in Figure 4.4.
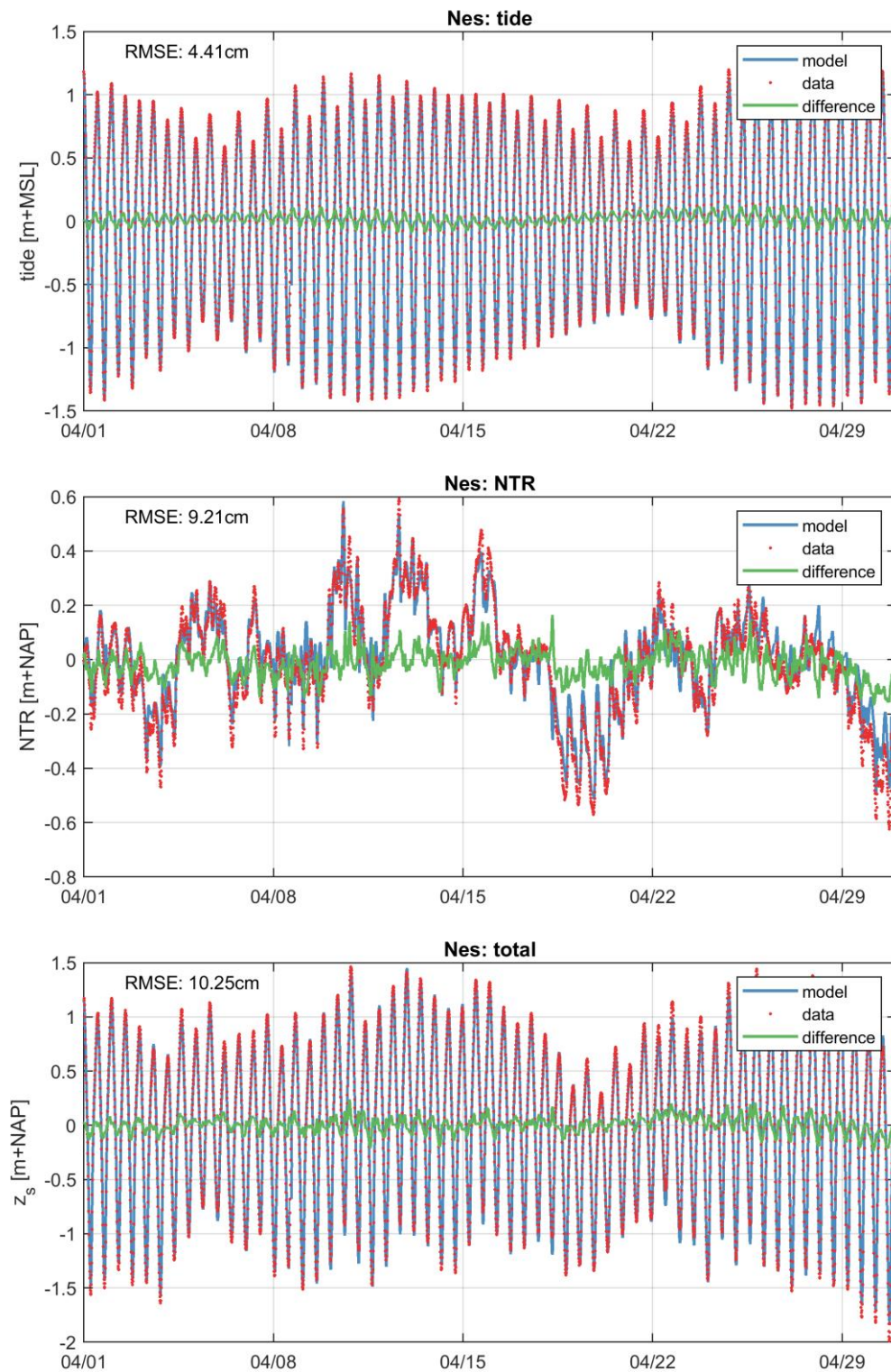
Figure 4.6   Time series of the tide, NTR and total water level at Nes as observed and modeled. Blue is model, blue is data and green is the difference.

### 4.2.3 Wave setup

One of the advantages of running Delft3D-FLOW with an online coupled wave module (SWAN) is that effects of waves on the hydrodynamics (and vice-versa) are included. This means for example that wave-driven setup and set-down can be simulated which are especially of importance during large wave conditions.

During the storm of September 13-14th 2017 offshore significant wave heights exceeded 5 m. Figure 4.7 presents time series of the total water level at Nes as observed (red), modelled without waves (green) and modelled with online waves (blue). Based on these results, it is estimated that the wave-driven setup in the Wadden Sea basin is +/- 10-15 cm. Moreover, model results are more in line with observations when waves are included. In particular, the RMSE decreases from 12.1 cm to 10.2 cm for respectively without and with online waves. This shows the advantage of a coupled hydrodynamic-wave model.
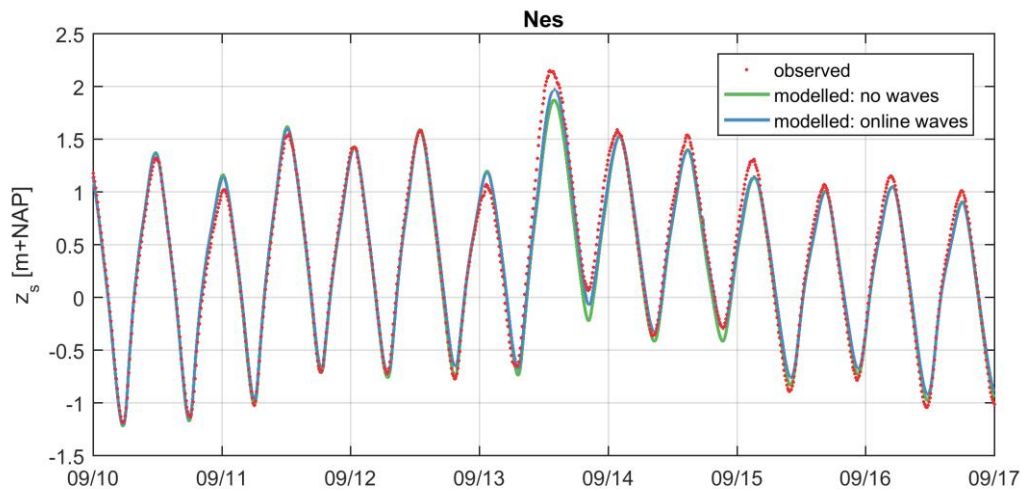


*Figure 4.7   Time series of the total water level at Nes as observed (red), modeled without waves (green), modelled with online waves (blue).*

### 4.3 Discharge and velocities

#### 4.3.1 Discharge

The discharge measurements in the inlet (Section 2.3.3.1) were used to calibrate the model. The performance of the model with different Van Rijn roughness calibration parameters is shown in Table 4.5     . Model results indicate that a coefficient for the ripples, mega-ripples of 0.7 without dunes gives the most accurate discharge volume (Table 4.6     ). However, the differences between 0.2 – 1.0 without dunes are minor. When dunes are included in the computation of the bottom friction, there is a sharp increase in the absolute difference between modeled and observed discharge volumes. Note: A mean-absolute error (MAE) of 10 M m$^3$ is about 2% of the observed tidal prism on 19th September.

Figure 4.8 presents the observed and modeled instantaneous discharge at Ameland Inlet. The modeled discharge is based on the CGII-TA model with coefficients 0.5, 0.5 and 0.0 for the Van Rijn roughness predictor. The time series of the observed and modeled instantaneous discharge compares rather well. However, there are small differences.

*Table 4.5    Modeled discharge volumes (10^6 m3) for variations in Van Rijn roughness calibration parameters.*

| Name | 1 Sep. | 5 Sep. | 19 Sep. | | |
|---|---|---|---|---|---|
| | Ebb | Flood | Ebb | Ebb | |
| **Measured** | **339** | **330** | **449** | **506** | **MAE** |
| 0.1 | 363 | 366 | 536 | 549 | 48 |
| 0.2 | 355 | 356 | 514 | 535 | 35 |
| 0.3 | 349 | 348 | 500 | 525 | 25 |
| 0.4 | 344 | 343 | 489 | 517 | 18 |
| 0.5 | 341 | 338 | 481 | 510 | 12 |
| 0.5_dunes | 316 | 312 | 427 | 446 | 32 |
| 0.6 | 337 | 334 | 474 | 504 | 9 |
| 0.7 | 335 | 330 | 467 | 499 | 8 |
| 0.8 | 332 | 327 | 462 | 495 | 9 |
| 0.9 | 330 | 324 | 456 | 490 | 10 |
| 1.0 | 327 | 321 | 452 | 486 | 12 |
| 1.0_dunes | 312 | 305 | 417 | 442 | 38 |
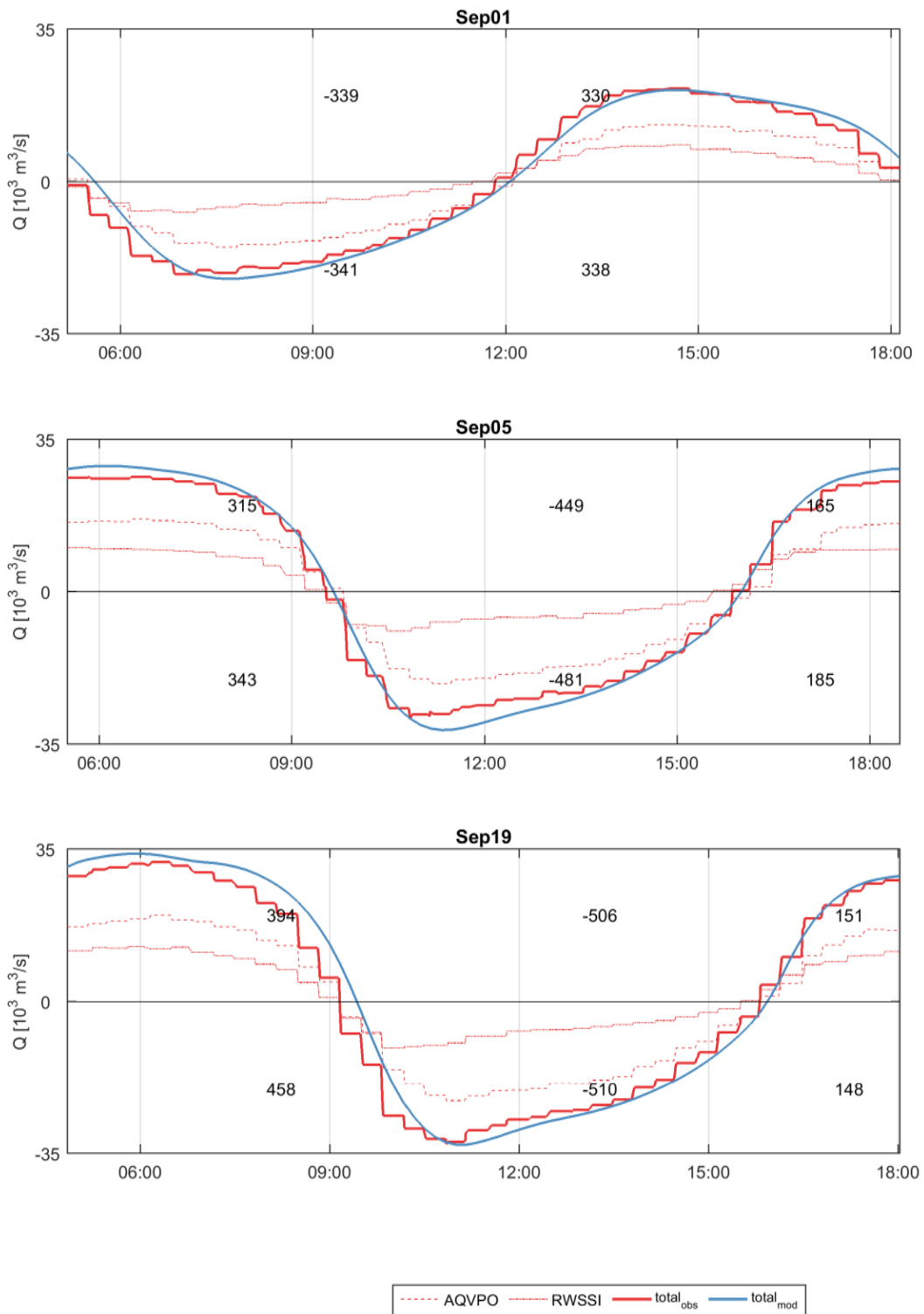
*Figure 4.8        Modeled and measured instantaneous discharge through the Ameland Inlet. Red lines are observed. The blue line is modeled with CGII-TA model while using a coefficient of 0.5, 0.5 and 0.0 for the ripple, mega-ripple and dune roughness in Van Rijn's (2007) predictor. Numbers represent integrated volumes. Upper numbers are based on measurements and lower are based on the model result. Negative values are ebb and positive values are flood*

### 4.3.2 Frames (ZG Sep'17)

The velocity measurements from frames located in the Ameland inlet and on the ebb delta (Section 2.3.3.2) were used to calibrate the model. The performance of the model with different Van Rijn roughness calibration parameters is shown in Table 4.6      .      From      this calibration exercise, it followed that a value of 0.4 or 0.5 for ripples and mega-ripples and no dunes give the most accurate representation of the depth-averaged flow magnitude in the inlet. However, the differences between 0.2 – 1.0 (without dune roughness) are minor. When dunes are included in the computation of the bottom friction, there is a sharp increase of the RMSE.

The calibrated CGII-TA model, with 0.5 ripples, 0.5 mega-ripples and without dunes, reproduces the depth-averaged flow velocities during the calibration period of 2017 fairly well (Figure 4.10 & Table 4.7       ). The different RMSE-values in flow velocity are in the order of 0.15 m/s. The storm of 13 September 2017 can be clearly seen in the observed and modeled time series of the magnitude of ZG-F1. However, the peak is underestimated by the model for ZG-F4. Moreover, the accuracy is in the same order than of other numerical models studies (e.g. Deltares, 2009)

Figure 4.9 presents the tidal ellipse of the M2 tidal signal, based on measurements and modeled values. The figure shows that the modeled ellipse aligns well with the orientation of the channel, which gives confidence in the modeled results. The tidal ellipse of the measurements, however, does not align well with the main direction of the channel. The deviation might be caused by local bathymetric variations that are not resolved well by the resolution of the model grid or by data processing. This will be further investigated by model-data comparison in the model validation chapter.

*Table 4.6    RMSE in flow velocity magnitude in m/s at 3 frames including a mean over the frames.*

| Name | ZG-F1 [m/s] | ZG-F3 [m/s] | ZG-F4 [m/s] | Mean [m/s] |
|---|---|---|---|---|
| 0.1 | 0.13 | 0.2 | 0.21 | 0.18 |
| 0.2 | 0.11 | 0.19 | 0.16 | 0.15 |
| 0.3 | 0.11 | 0.19 | 0.16 | 0.15 |
| 0.4 | 0.11 | 0.19 | 0.14 | 0.15 |
| 0.5 | 0.12 | 0.19 | 0.14 | 0.15 |
| 0.5_dunes | 0.17 | 0.19 | 0.16 | 0.18 |
| 0.6 | 0.12 | 0.19 | 0.14 | 0.15 |
| 0.7 | 0.11 | 0.18 | 0.12 | 0.14 |
| 0.8 | 0.12 | 0.19 | 0.14 | 0.15 |
| 0.9 | 0.13 | 0.19 | 0.14 | 0.15 |
| 1.0 | 0.13 | 0.19 | 0.14 | 0.15 |
| 1.0_dunes | 0.17 | 0.2 | 0.16 | 0.18 |

**Deltares**

*Table 4.7   ADCP-derived depth-averaged flow velocity reproduction for 2011 divided into RMSE (first number), bias (second number) and SCI (third number) of the major and minor axis, x and y-axis and total magnitude and tidal magnitude (only magnitude from tide). Values are in [m/s]. Major and minor axes are based on the computed M2 orientation. This means the orientation of the major and minor axis can be different for the observed and measured data.*

| Statistical methods | ZG-F1 | ZG-F3 | ZG-F4 |
|---|---|---|---|
| Major | 0.13 / 0.05 / 0.28 | 0.2 / -0.06 / 0.26 | 0.15 / 0.09 / 0.34 |
| Minor | 0.1 / 0.02 / 0.5 | 0.08 / 0 / 0.93 | 0.13 / 0.03 / 0.7 |
| x-axis | 0.16 / -0.07 / 0.35 | 0.22 / -0.02 / 2.38 | 0.17 / -0.1 / 0.36 |
| y-axis | 0.14 / 0.06 / 0.64 | 0.22 / -0.06 / 0.28 | 0.12 / -0.01 / 0.71 |
| total magnitude | 0.12 / 0 / 0.23 | 0.19 / -0.09 / 0.25 | 0.15 / -0.03 / 0.3 |
| tidal magnitude | 0.05 / 0.02 / 0.13 | 0.13 / -0.08 / 0.18 | 0.04 / 0 / 0.1 |
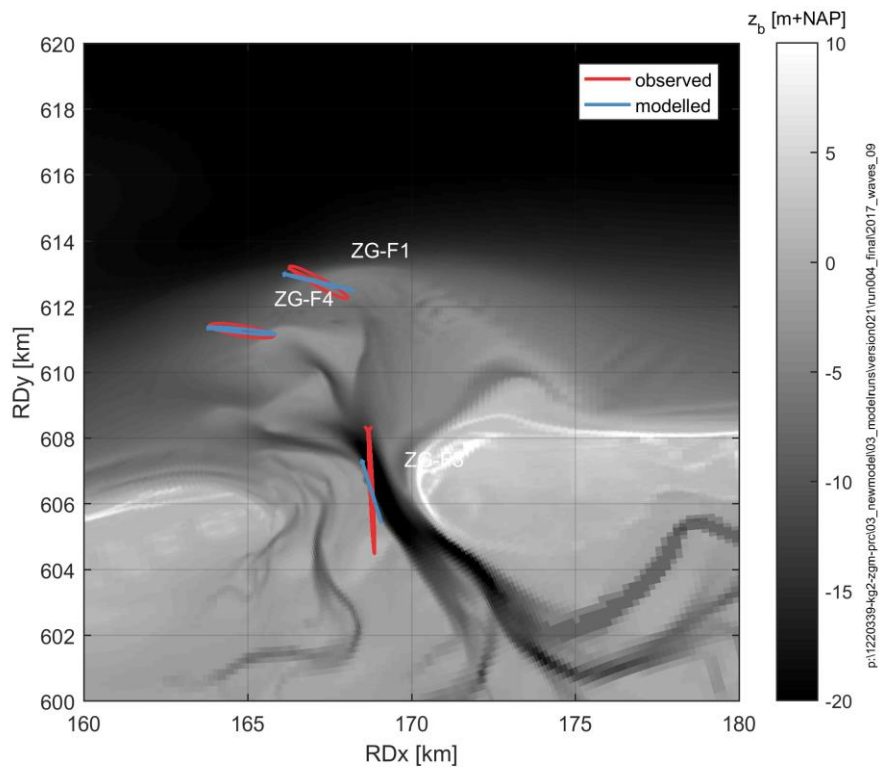


*Figure 4.9          Tidal ellipse of M2 as observed (red) and modeled (blue) plotted on top of that model bathymetry.*
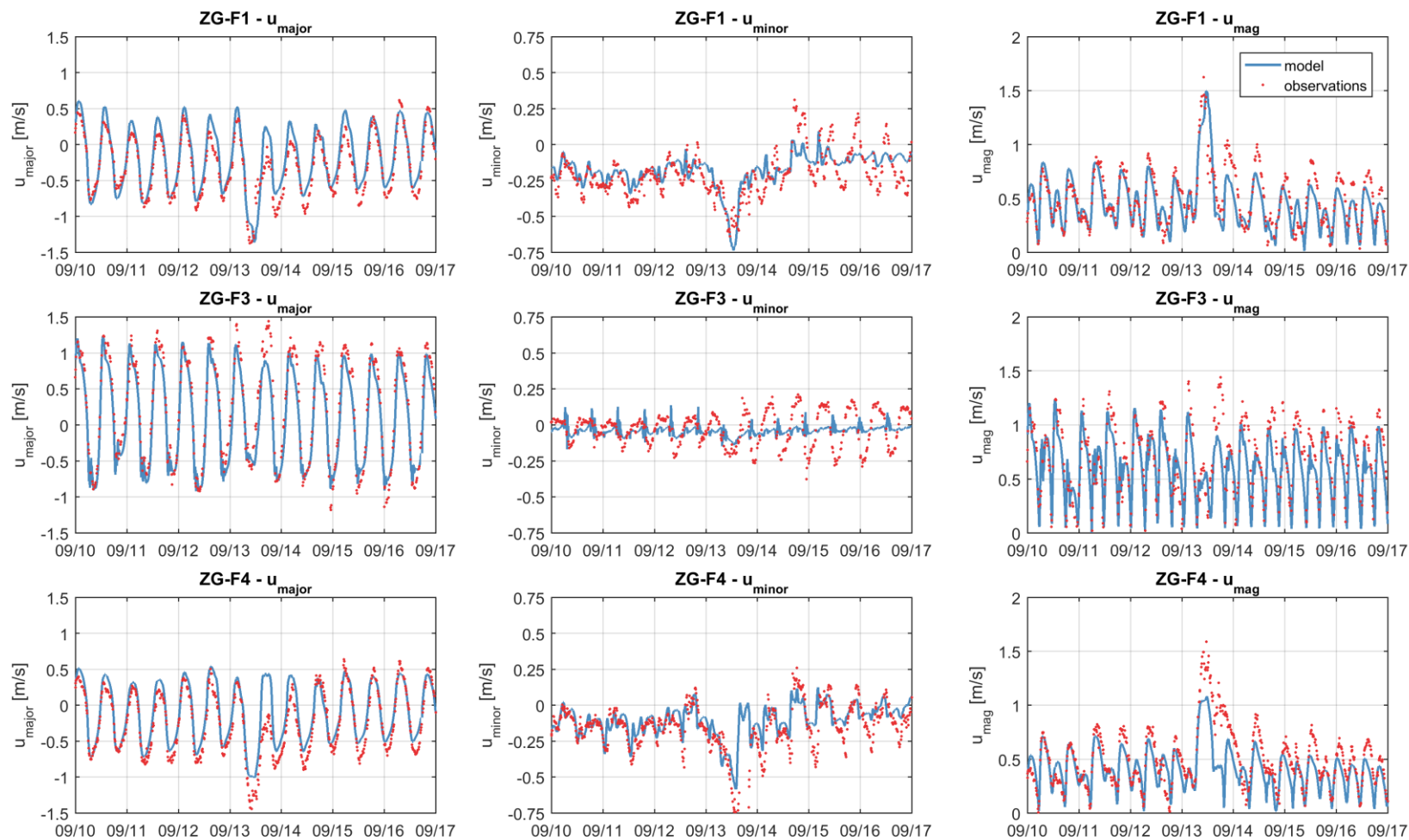
*Figure 4.10 Time series of flow velocities in m/s as observed (red) and modeled (blue) for the calibration period 2017 with coefficient 0.5, 0.5 and 0. Left panels are velocities in the major axis (determined by tidal analysis of M2). Middle panels are minor axis (again determined by tidal analysis of M2). The right panel is the depth-averaged flow velocity magnitude. Waves are included in these results.*

**Deltares**

4.3.3   Watershed Aquadopp

The velocity measurements at the watershed (Section 2.4.1.3) were used to calibrate the model. The performance of the model with different Van Rijn roughness calibration parameters is shown in Table 4.8        . From this calibration exercise followed that a value of 0.2, 0.3, or 0.4 for ripples and mega-ripples and no dunes gave the most accurate representation.

Figure 4.11 presents a time series of the measured and computed flow velocity and direction at AmID1 with calibration coefficients 0.5, 0.5 and 0.0. The observations and model results are in the same order. However, the model is not able to give an accurate reproduction of the peaks (especially during the large flow velocity of > 1 m/s during the storm on 13 September 2017; lower panel). Generally, the calibrated CGII-TA model reproduces the depth-averaged flow velocities at the watershed fairly well (RMSE of about 0.10 m/s).

In an effort to improve the model performance during the peaks, several sensitivity tests were carried out (see Appendix D). These tests include changes in 1) boundary conditions on the Wadden Sea open boundaries, 2) meteorological forcing, 3) wind stress formulations and 4) friction values. These tests showed that model performance can be improved by increasing the wind stress (either via an increase of the wind speed or wind-drag coefficient) or decreasing the bottom friction. Specifically, applying observed winds speed as observed at Huibertgat resulted in an improvement of the flow velocities on the watershed during the peak of the storm. However, the yearly discharge through the Ameland Inlet did not change whenever the model was forced with observed or HIRLAM winds. The water levels and flow velocities at the frames in the inlet were reproduced less well when observed winds were applied. Therefore, we choose to apply the HIRLAM wind fields and accept the underestimation of the flow velocity at the watershed during the peak of the storm. One is referred to Appendix D for these results.

Other possible reasons for the mismatch of the flow velocity (that were not tested) could be related to the correct representation of the model bathymetry (e.g. small channels in large grid cells), unresolved 3D effects or instrument-related issues (e.g. ADCP surface reflections at low water). All in all, the consequence for sediment transport modeling is expected to be minor since the yearly discharge through the Ameland Inlet is accurately reproduced.

*Table 4.8    Root-mean-squared-error (RMSE) of the magnitude in m/s of modeled velocity at the watershed. In green the friction coefficients that resulted in the lowest RMSE.*

| Name | AmID1 [m/s] | AmID2 [m/s] | AmID3 [m/s] | AmID4 [m/s] | AmID5 [m/s] | AmID6 [m/s] | Mean [m/s] |
|---|---|---|---|---|---|---|---|
| 0.1 | 0.13 | 0.18 | 0.09 | 0.06 | 0.09 | 0.10 | 0.11 |
| 0.2 | 0.12 | 0.16 | 0.10 | 0.06 | 0.09 | 0.11 | 0.10 |
| 0.3 | 0.11 | 0.14 | 0.10 | 0.06 | 0.10 | 0.12 | 0.10 |
| 0.4 | 0.11 | 0.14 | 0.10 | 0.07 | 0.10 | 0.12 | 0.11 |
| 0.5 | 0.11 | 0.13 | 0.11 | 0.07 | 0.10 | 0.13 | 0.11 |
| 0.5_dunes | 0.13 | 0.13 | 0.12 | 0.09 | 0.11 | 0.14 | 0.12 |
| 0.6 | 0.11 | 0.13 | 0.11 | 0.08 | 0.10 | 0.13 | 0.11 |
| 0.7 | 0.11 | 0.13 | 0.11 | 0.08 | 0.11 | 0.13 | 0.11 |
| 0.8 | 0.11 | 0.13 | 0.11 | 0.08 | 0.10 | 0.13 | 0.11 |
| 0.9 | 0.11 | 0.13 | 0.11 | 0.08 | 0.11 | 0.14 | 0.11 |
| 1.0 | 0.12 | 0.13 | 0.11 | 0.09 | 0.11 | 0.14 | 0.12 |
| 1.0_dunes | 0.13 | 0.13 | 0.12 | 0.10 | 0.12 | 0.15 | 0.12 |
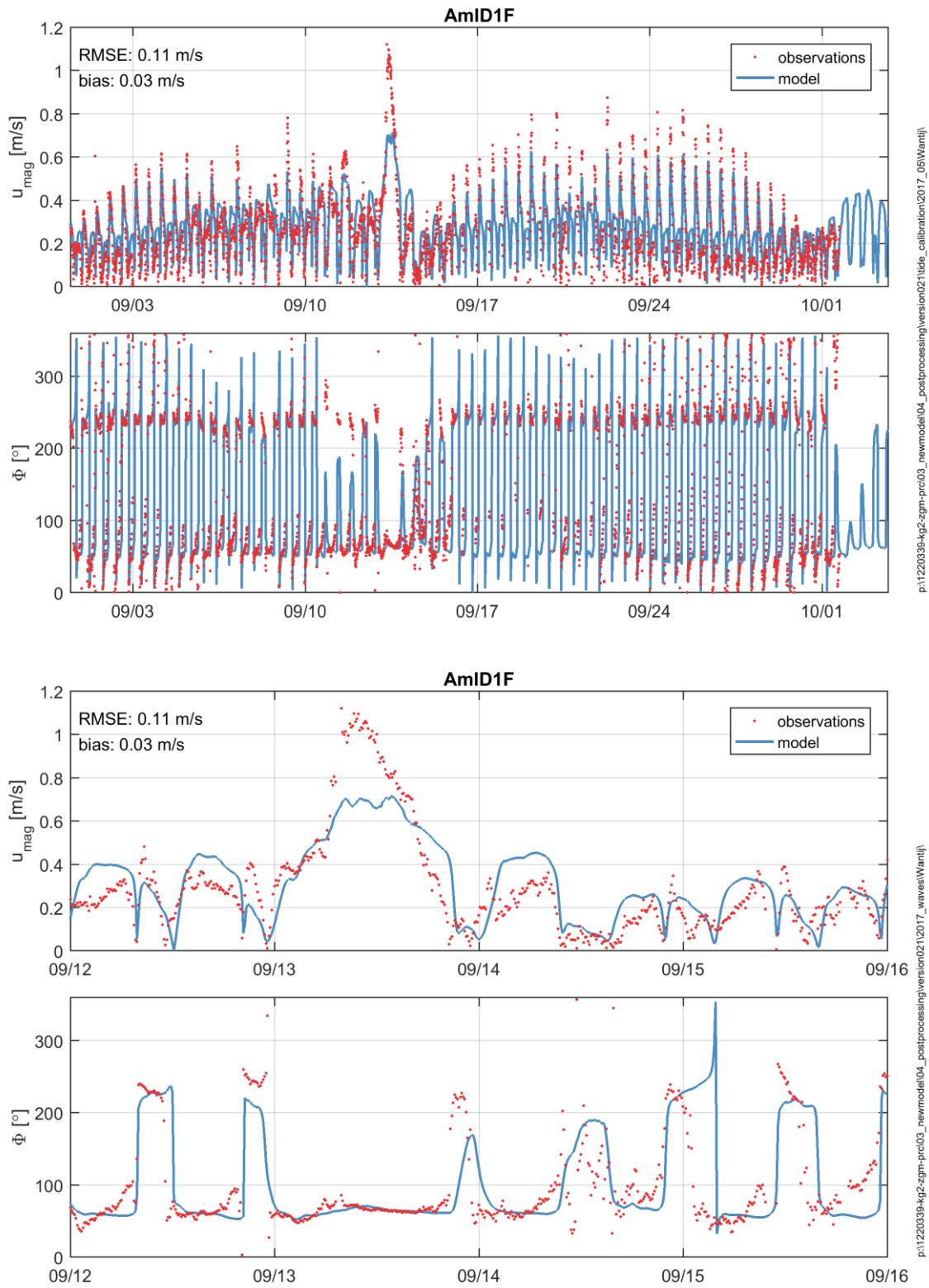
*Figure 4.11 Time series of modeled (blue) and measured (red) magnitude (top) and direction (bottom) at Aquadopp location AmID1 at the watershed*

## 4.4 Waves

### 4.4.1 Offshore wave height

Similar to Deltares (2010), the directional wave spectra measured at EIR and SON were applied as so-called "SP1-files" or "1.5D spectra" (i.e. energy, mean direction, directional spreading width for each frequency band) on the boundaries of the grid. However, the directional wave spectra were observed closer to shore than the locations of the model domain. In order to compensate dissipation (e.g. due to bottom friction) wave heights were calibrated by first increasing the measured energy density that is applied at the model boundary. In previous studies (e.g. Deltares, 2010) wave heights for a SWAN model were increased by 10% (or the measured energy density was multiplied by 1.21).

Based on the model results with the original (uncalibrated) directional wave spectra SWAN tends to underestimates the wave heights at AZB11 (Figure 4.12). However, this underestimation is not constant for each wave height and increases with the wave heights. In order to calibrate the wave heights at AZB11, the underestimation in wave height was binned in 0.5 m bins (i.e. 0-0.5 m, 0.5-1.0 m , etc.), the median computed, after which a linear fit (poly1) was determined based on the least squares fitting technique. This approach was preferred over a direct fit on the wave time series in order to account for a non-Gaussian distribution in wave heights (i.e. lower wave heights occur more frequent compared to high wave heights). The resulting fit is described with Equation (4.1) in which alpha and beta were found to be 1.0546 and 0.0539. This means an observed wave height of 1.0 meter at AZB11 results in an increase of 10% and a wave height of 5.0 m in an increase of almost 30%. Wave periods were not varied. This does, however, not result in a bias of the wave period at AZB11 (Table 4.10). Moreover, with the approach of directly applying the observed variance density spectra, it is not straightforward to scale the wave period without assuming a certain spectral shape (e.g. JONSWAP).

$$\frac{H_{s,observed}}{H_{s,\mathrm{mod}elled}} = \alpha + b \cdot H_{s,observed} \tag{4.1}$$
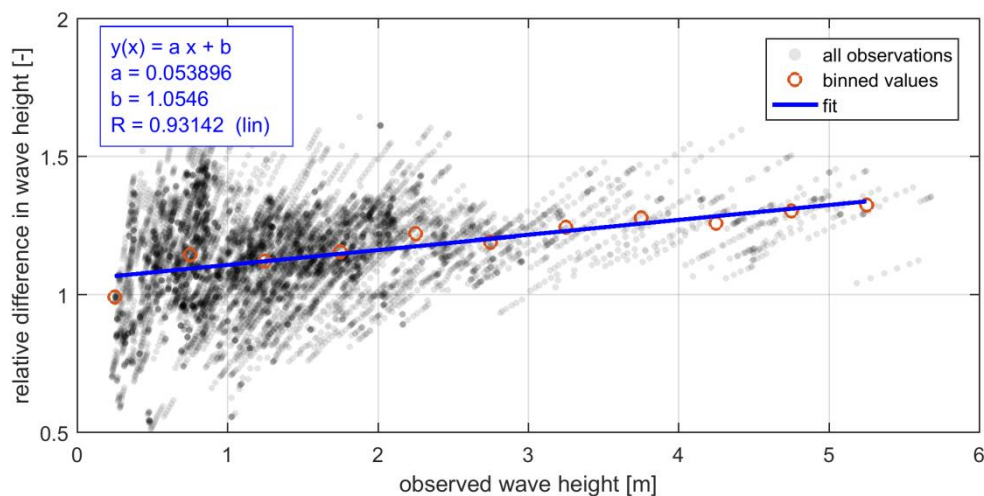


*Figure 4.12 Relative difference at AZB11 in wave height (observed/modeled) as a function of observed wave height. Grey dots are individual model realizations. More frequent realizations are shown as darker points. Red circles are binned values. The blue line is linear fit and applied as calibration.*

### 4.4.2 Wave breaking

The BKD formulation of Salmon & Holthuijsen (2011) was applied. This indicates that the breaker index scales with both the bottom slope (*beta*) and the dimensionless depth (*kd*), The BKD formulation has 4 coefficients which make it less trivial to calibrate wave breaking than a constant wave breaking formulation based on a single breaker index (i.e. ratio of the maximum individual wave height over depth). The formulation is presented in Equation 2.2 .

$$\gamma_{slope} = \gamma_0 + \alpha_1 \cdot \tan(slope)$$
$$\gamma_{kd} = \alpha_2 + a_3 \cdot kd \qquad (4.2)$$
$$\gamma_{bkd} = \frac{\gamma_{slope}}{\tanh(\gamma_{kd} / \gamma_{slope})}$$

Model results for AZB31 and AZB41 indicate that the default coefficient of the BKD formulation already gives accurate wave height reproduction. Varying $\gamma_0$, $\alpha_1$, $\alpha_2$ or $\alpha_3$ result in little improvements in the wave height reproduction at both stations. Therefore, we choose to apply the default values of $\gamma_0$ = 0.54, $\alpha_1$ = 7.59, $\alpha_2$ = -8.06 and $\alpha_3$ = 8.09.

The calibrated CGII-TA model reproduces the wave heights during the calibrated period of 2017 with reasonable accuracy (Table 4.9). Wave heights offshore are reproduced with an RMSE of 0.15-0.22 m. For offshore stations, EIR, SON, AZB11 and AZB12 the relative errors are the lowest (SCI of around 15%) and buoys in the inlet and the Wadden Sea basin have a larger absolute and relative error.  Wave periods are reproduced with an RMSE of 0.5-1.1 s ( ). The RMSE in wave direction is 15-20 degrees offshore and increases to 40 degrees at AZB41 (Table 4.11      ).

In previous studies a SCI of 20% and 10% for respectively the wave height and period was obtained (Deltares, 2010; Deltares, 2014). The wave direction had a mean RMSE of less than 20 degrees. However, a one-on-one comparison to the previous studies is not possible since these studies performed stationary SWAN simulations for 8 hindcast moments.  Moreover, the results were aggregated over all wave buoys into one statistical score.  Yet, the error statistics in wave height, period and direction are in the same order of magnitude as achieved in this wave modelling study.

Table 4.9    *Error statistics of wave heights (Hm0) in meters.*

| Stations | RMSE [s] | Bias [s] | SCI [-] |
|---|---|---|---|
| Eierlandse Gat boei | 0.22 | 0.04 | 0.13 |
| Schiermonnikoog noord boei | 0.19 | -0.08 | 0.16 |
| Amelander Zeegat - Boei 1-1 | 0.20 | -0.10 | 0.15 |
| Amelander Zeegat - Boei 2-1 | 0.19 | -0.02 | 0.24 |
| Amelander Zeegat - Boei 3-2 | 0.15 | -0.06 | 0.25 |

Table 4.10   *Error statistics of wave periods (Tm01) in seconds.*

| Stations | RMSE [s] | Bias [s] | SCI [-] |
|---|---|---|---|
| Amelander Zeegat - Boei 1-1 | 0.48 | -0.03 | 0.10 |
| Amelander Zeegat - Boei 2-1 | 0.83 | 0.39 | 0.23 |
| Amelander Zeegat - Boei 3-2 | 1.13 | -0.85 | 0.28 |

Table 4.11   *Error statistics of wave direction (dir) in degrees.*

| Stations | RMSE [degrees] | MAE [degrees] | Bias [degrees] |
|---|---|---|---|
| Eierlandse Gat boei | 16 | 10 | 1 |
| Schiermonnikoog noord boei | 18 | 13 | -9 |
| Amelander Zeegat - Boei 1-1 | 17 | 11 | -2 |
| Amelander Zeegat - Boei 2-1 | 37 | 29 | 21 |
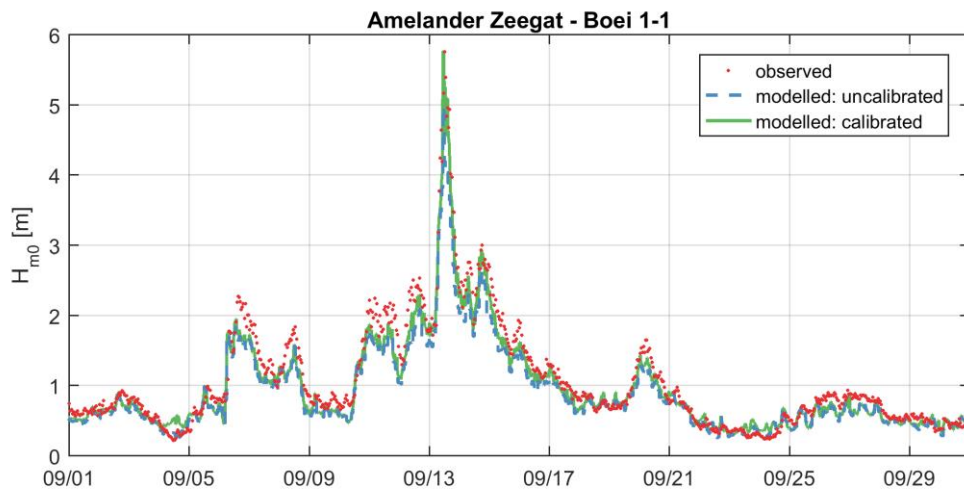
*Figure 4.13          Time series of observed, uncalibrated modeled and calibrated modeled wave heights at AZB11*
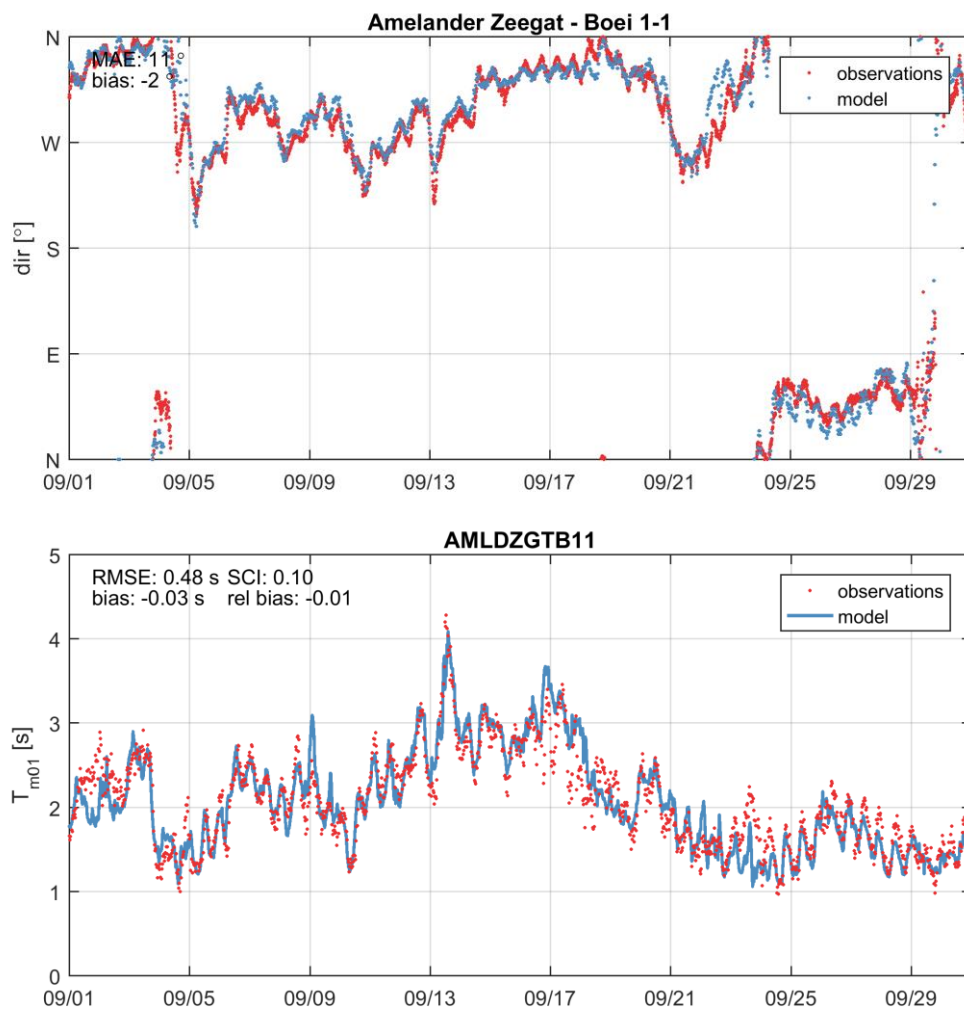


*Table 4.12  Wave direction (dir – upper panel) and wave period ($T_{m01}$) in seconds (lower panel) as observed (red)
         and computed (blue) for the calibration period in 2017 at AZB11*

## 4.5 Conclusions

The CGII-TA model was calibrated for an optimal reproduction of water levels, wave heights, discharges, and velocity measurements during the September 2017 Coastal Genesis II period.

First, the astronomical boundary conditions were calibrated by applying a correction file for amplitudes and phases based on the difference between the observed and computed astronomical tide at the offshore stations Terschelling Noordzee and Wierumergronden. This resulted in a decrease of the RMSE in the tidal water level from 4 to 2 cm. Second, the coefficients of the Van Rijn roughness predictor were calibrated. Based on water level reproduction, discharge measurements, velocity measurements on frames, and velocity measurements on the watershed, we chose to apply the following calibration coefficients for the Van Rijn roughness predictor: 0.5 for the ripple contribution, 0.5 for mega-ripple contribution and excluding the dune roughness. Including dunes resulted in a sharp decrease in the reproduction of the water level, discharge and velocities. The coefficient of 0.5 for ripples and mega-ripples is a trade-off between the water levels (optimal value 0.3), discharge measurements (optimal value 0.7), velocity on the watershed (optimal value 0.4) and velocity in the inlet (optimal value 0.5). The peak in velocities on the watershed during the storm of September 13th was not reproduced by the calibrated CGII-TA model.

Waves were calibrated by first increasing the measured energy density that is applied at the model boundary with 10-30% (depending on the observed wave height). Secondly, variations of the BKD wave breaking formulations were applied. We chose to stick to default values for the wave breaking formulations since there were little improvements in the reproductive skill of the model visible when we deviated from the default coefficients.

The calibrated model is able to reproduce the water levels with a RMSE of 10 cm, the integrated discharge volumes in the inlet with a MAE of 10 M $m^3$ or 2% of the tidal prism, the velocities in the inlet with a RMSE of 15 cm/s and the velocities on the watershed with a RMSE of 10 cm/s. Offshore, wave heights (AZB11) are reproduced with a RMSE of less than 20 cm, periods with 0.5 s and direction with 20 degrees. In the Wadden Sea basin (AZB21 & AZB32), these errors increase to 20 cm, 1.0 s and +/- 40 degrees.

In the next chapter, the validity of the settings derived by calibration is tested (validated) by comparison with other (independent) datasets at different locations and other time periods.

# 5 Validation

## 5.1 Introduction
This chapter shows the CGII-TA model validation against data from 2008, 2011, and the three consecutive Coastal Genesis II campaigns (November 2017, January and March 2018). In particular, full-year water level measurements from 4 locations in the area of interest of 2008 and 2011 were validated. Moreover, first, the modeled tidal prism was compared with values found in literature and second, the model results were compared with several velocity measurements in 2008, 2011, November 2017, and January and March 2018. On top of that, waves during the SBW velocity measurements from 2008 and 2011 were compared with the model results. The model settings as presented in Chapter 3.5 and derived in Chapter 4 were applied.

## 5.2 Water levels

### 5.2.1 Accuracy 2011
Again, the CGII-TA model reproduces the water levels during the full validation period of 2011 reasonably well (Figure 5.2 & Table 5.1). The RMSE of the total water level signal is around 10 cm. The error did increase compared to the calibration period due to an increase of the RMSE for the tide (an offshore increase from 2 to 3 cm). Apparently, part of the astronomical correction factors is not universal and dependent on the time period.

*Table 5.1    Water level reproduction for 2011 divided into total RMSE, tidal RMSE and NTR RMSE. Bias is determined for the total water level signal. There was no data recorded at Holwerd in 2011.*

| Error statistics | Terschelling Noordzee [cm] | Wierumergronden [cm] | Nes [cm] |
|---|---|---|---|
| RMSE (total) | 8.9 | 8.1 | 10.5 |
| RMSE (tide) | 3.2 | 3.2 | 3.4 |
| RMSE (NTR) | 8.3 | 7.5 | 10.0 |
| bias (total) | 4.6 | 1.5 | 3.9 |
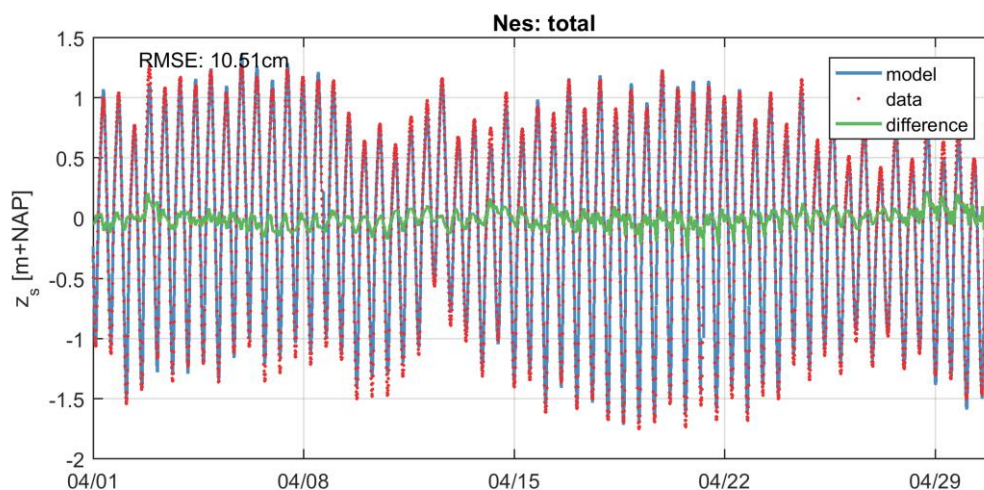


*Figure 5.1    Time series of total water levels in meter+ NAP at Nes (2008). Red is observed and blue is modeled. Error calculation is based on the yearly model results.*

5.2.2 Accuracy 2008

The CGII-TA model reproduces the water levels during the full validation period of 2008 reasonably well (Figure 5.1 & Table 5.3). The RMSE of the total water level signal is around 10 cm. The error did increase compared to the calibration period due to an increase of the RMSE for the tide (an offshore increase from 2 to 4 cm). Apparently, part of the astronomical correction factors is not universal and dependent on the time period. However, these errors in water level reproduction are in line with the accuracy of other numerical models. For example, Zijl et al. (2013) reproduced Terschelling Noordzee and Wierumgronden with a RMSE of 8.1 and 8.3 cm and Deltares (2009) computed the tidal water level within +/- 10 cm.

*Table 5.2    Water level reproduction for 2011 divided into total RMSE, tidal RMSE and NTR RMSE. Bias is determined for the total water level signal. There was no data recorded at Holwerd in 2008.*

| Error statistics | Terschelling Noordzee | Wierumergronden | Nes |
|---|---|---|---|
| RMSE (total) [cm] | 10.1 | 9.61 | 11.06 |
| RMSE (tide) [cm] | 4.11 | 4.21 | 4.91 |
| RMSE (NTR) [cm] | 9.20 | 8.62 | 9.92 |
| bias (total) [cm] | 4.68 | 2.79 | 0.66 |
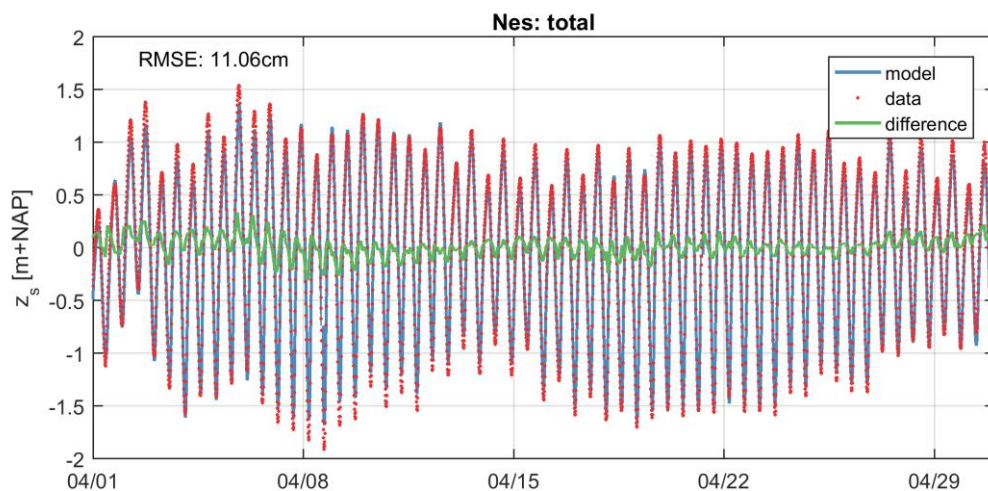


*Figure 5.2    Time series of total water levels in meter + NAP at Nes (2011). Red is observed and blue is modeled. Error calculation is based on the yearly model results.*

5.2.1 Spatial patterns

The calibrated CGII-TA model with astronomical correction factors  (calibration step 1) with the Van Rijn roughness predictor with coefficient 0.5, 0.5 and 0.0 (calibration step 2) result in the spatially-varying water levels of Figure 5.3 reflecting the westward tidal wave propagation. During low water, parts of the Wadden Sea basin become dry. Visually, the measurements (circles in Figure 5.3) are the same as the model output. Only for Harlingen there is a mismatch. This is related to the model boundary where a zero-gradient Neumann boundary is used.
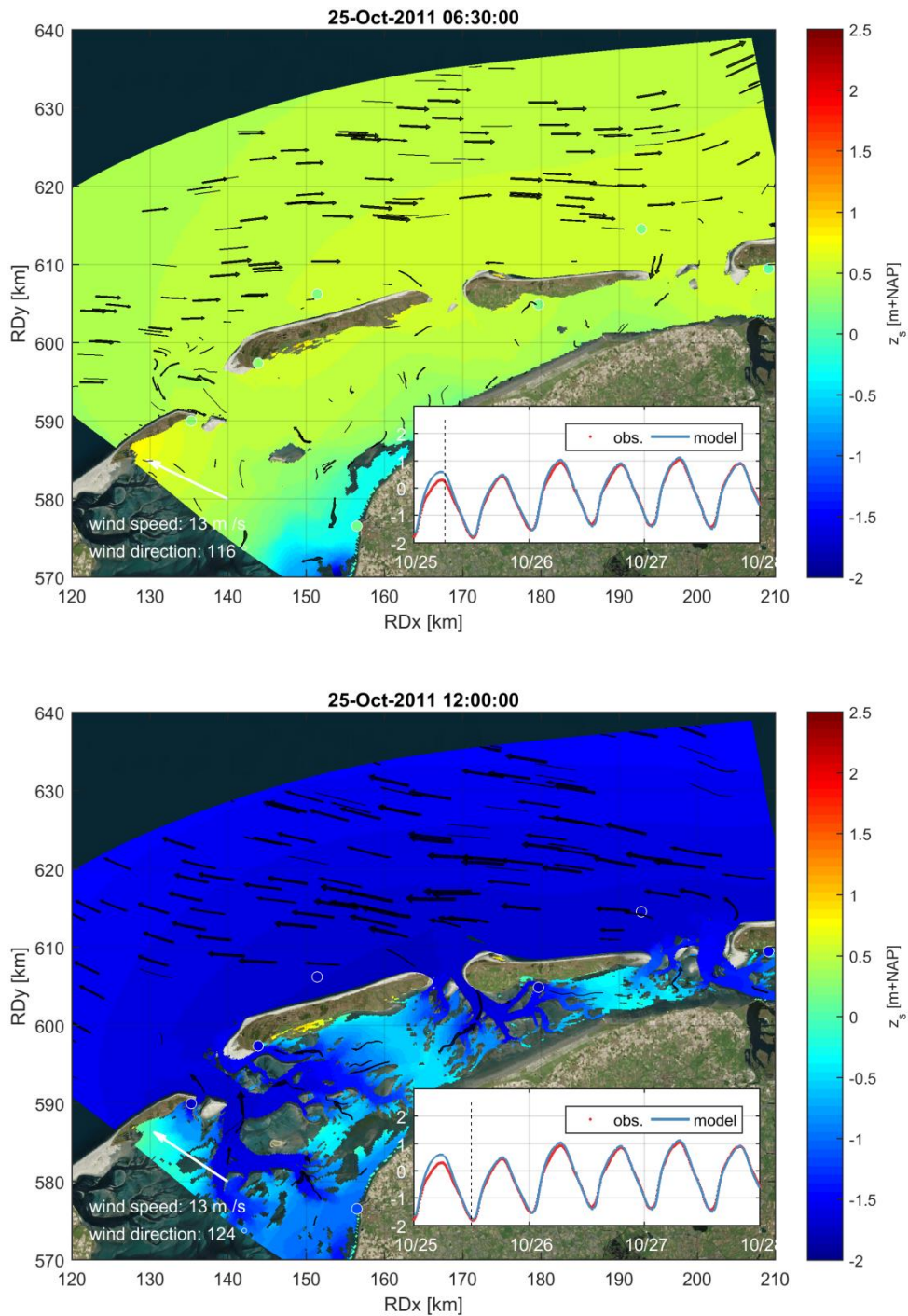
*Figure 5.3   Snapshot of the observed and computed water levels during the 2011 validation period. The heat map is the computed water levels. The circles are the observed water levels. Upper panel: high water. Lower panel: low water.*

## 5.3 Discharge and velocities

### 5.3.1 Tidal prism

The mean flood and ebb discharge volumes through the Ameland Inlet are known from measurements and are given by Deltares (2017a). The values given are recalculated to a mean tide, giving a proper representation of average conditions. Several sources indicate that the mean ebb and flood discharge volumes are somewhere between 400 to 540 $Mm^3$. Moreover, measurements from 1999 and 2001 indicate that small residual ebb dominance prevails of 11 to 38 $Mm^3$ (observed values of respectively mean flood and ebb 416 and 454 in 1999 and 407 to 418 $Mm^3$; 2-10% of tidal prism).

For a qualitative validation of 2011 of the modeled tidal prism, the annual mean ebb, flood and net discharges are shown in Table 5.3. The modeled flood and ebb discharge volumes compare well to the values given by Deltares (2017a).

*Table 5.3    Modeled ebb, flood and net discharge by the CGII-TA model for 2011.*

| | Mean discharge ($10^6$ $m^3$) | | |
|---|---|---|---|
| Year | Flood | Ebb | Net |
| 2011 | 446 | 464 | 18 E |

### 5.3.2 Velocities: 2008 (SBW; inlet)

The CGII-TA model reproduces the depth-averaged flow velocities during the validation period of 2008 reasonable (Table 5.4 & Figure 5.4). The major axis and magnitude for AZG04 are represented reasonable well (RMSE of 0.31 m/s and SCI of 36%. AZG05 is not reproduced well by the model. While the errors are around 0.20 m/s, the relative error (SCI) of the major axis is almost 100%. This is related to the quality of the measurement data (see also 2.4.3.2).

Overall, the different RMSE's in flow velocity are in the order of 0.25 m/s. This means the accuracy is less compared to the calibration period (Section 4.3.2) and previous modeling attempts (e.g. Deltares, 2009).

*Table 5.4    ADCP-derived depth-averaged flow velocity reproduction for 2008 divided into RMSE (first number), bias (second number) and SCI (third number) of the major and minor axis, x and y-axis and total magnitude and tidal magnitude (only magnitude from tide). Values are in [m/s]. Major and minor axes are based on the computed M2 orientation. This means the orientation of the major and minor axis can be different for the observed and measured data.*

| Statistical methods | AZG04 | AZG05 |
|---|---|---|
| Major | 0.32 / 0.06 / 0.38 | 0.23 / 0.05 / 1.01 |
| Minor | 0.04 / -0.01 / 1.01 | 0.13 / 0 / 1.08 |
| x-axis | 0.32 / -0.07 / 0.61 | 0.17 / 0.03 / 0.96 |
| y-axis | 0.19 / 0.01 / 0.29 | 0.21 / 0.04 / 1.08 |
| magnitude | 0.31 / 0.18 / 0.36 | 0.19 / 0.11 / 0.71 |
| tidal magnitude | 0.21 / 0.16 / 0.29 | 0.13 / 0.07 / 0.64 |
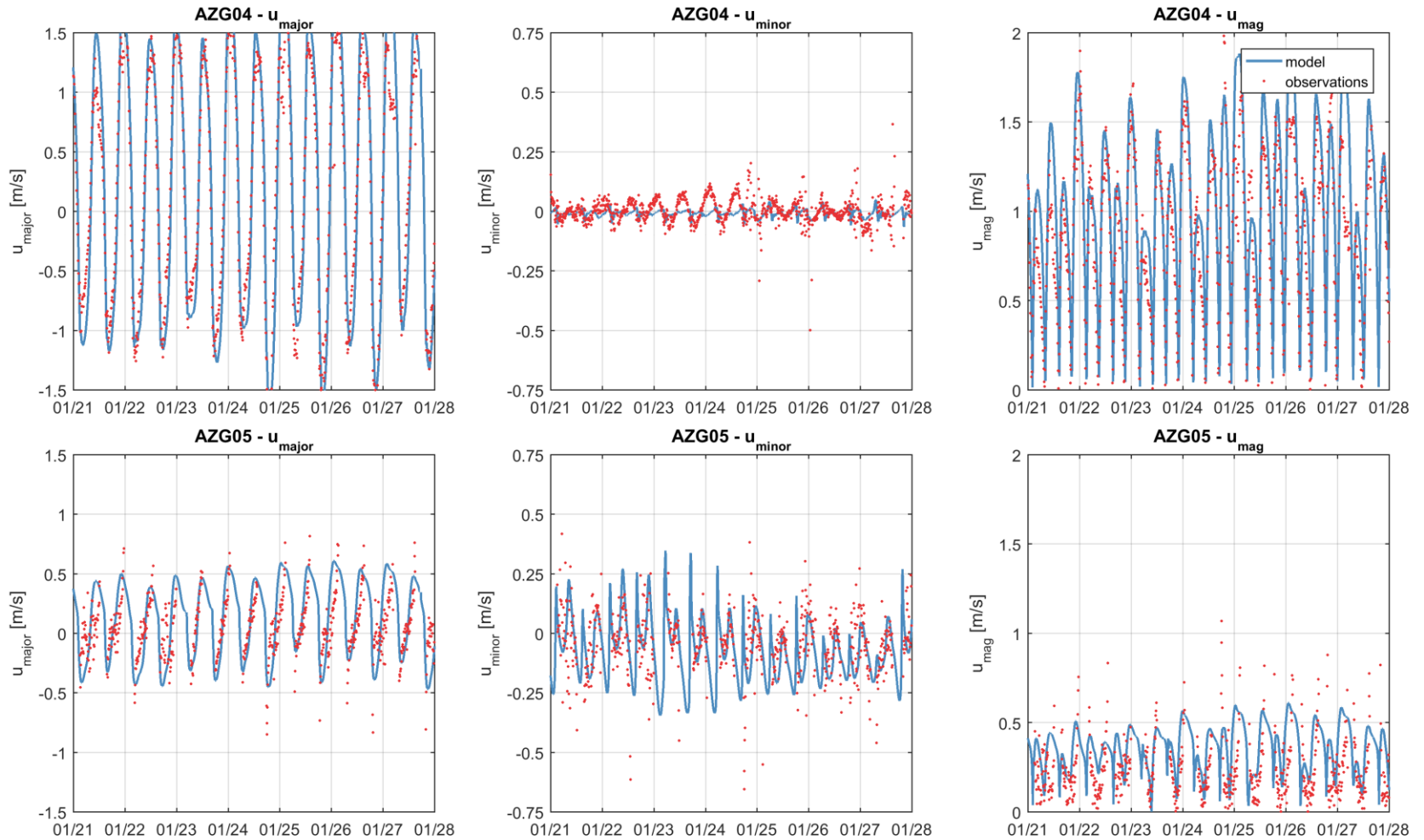
Figure 5.4   Time series of flow velocities in m/s as observed (red) and computed (blue) for the validation period in 2008. Left panels are velocities in the major axis (determined by tidal analysis of M2). Middle panels are minor axis (again determined by tidal analysis of M2). The right panel is the depth-averaged flow velocity magnitude.

### 5.3.3 Velocities 2011 (SBW: inlet)

The CGII-TA model reproduces the depth-averaged flow velocities during the validation period of 2011 well (Table 5.5 & Figure 5.5). The different RMSE's in flow velocity are in the order of 0.10 m/s. This means the accuracy is higher than other numerical modeling efforts (e.g. Deltares, 2009) and highger compared to the calibration period (Section 4.3.2). Moreover, there is no consistent bias in one of the axis or frame locations and the SCI reveals that the relative error is around 20%. On the other hand, the minor axis of AZG03 is reproduced less accurate (SCI around 70%).

The tidal ellipses of the various tidal components (Figure 5.6 and Figure 5.7) show a good agreement in the major and minor axis of the velocity. However, for AZG02 the modeled and observed minor axis deviates for the M2 and S2 tidal components. For AZG03 there is a small shift in the angle of the ellipse.

*Table 5.5  ADCP-derived depth-averaged flow velocity reproduction for 2011 divided into RMSE (first number), bias (second number) and SCI (third number) of the major and minor axis, x and y-axis and total magnitude and tidal magnitude (only magnitude from tide). Values are in [m/s]. Major and minor axes are based on the computed M2 orientation.*

| Different axis | AZG02 | AZG03 |
|---|---|---|
| Major | 0.12 / 0.01 / 0.19 | 0.12 / 0 / 0.14 |
| Minor | 0.03 / 0 / 0.68 | 0.02 / -0.01 / 0.72 |
| x-axis | 0.07 / -0.01 / 0.35 | 0.13 / 0.02 / 0.4 |
| y-axis | 0.1 / 0.01 / 0.18 | 0.12 / 0.01 / 0.14 |
| magnitude | 0.11 / 0.08 / 0.19 | 0.12 / 0.01 / 0.13 |
| tidal magnitude | 0.09 / 0.07 / 0.17 | 0.08 / 0 / 0.1 |
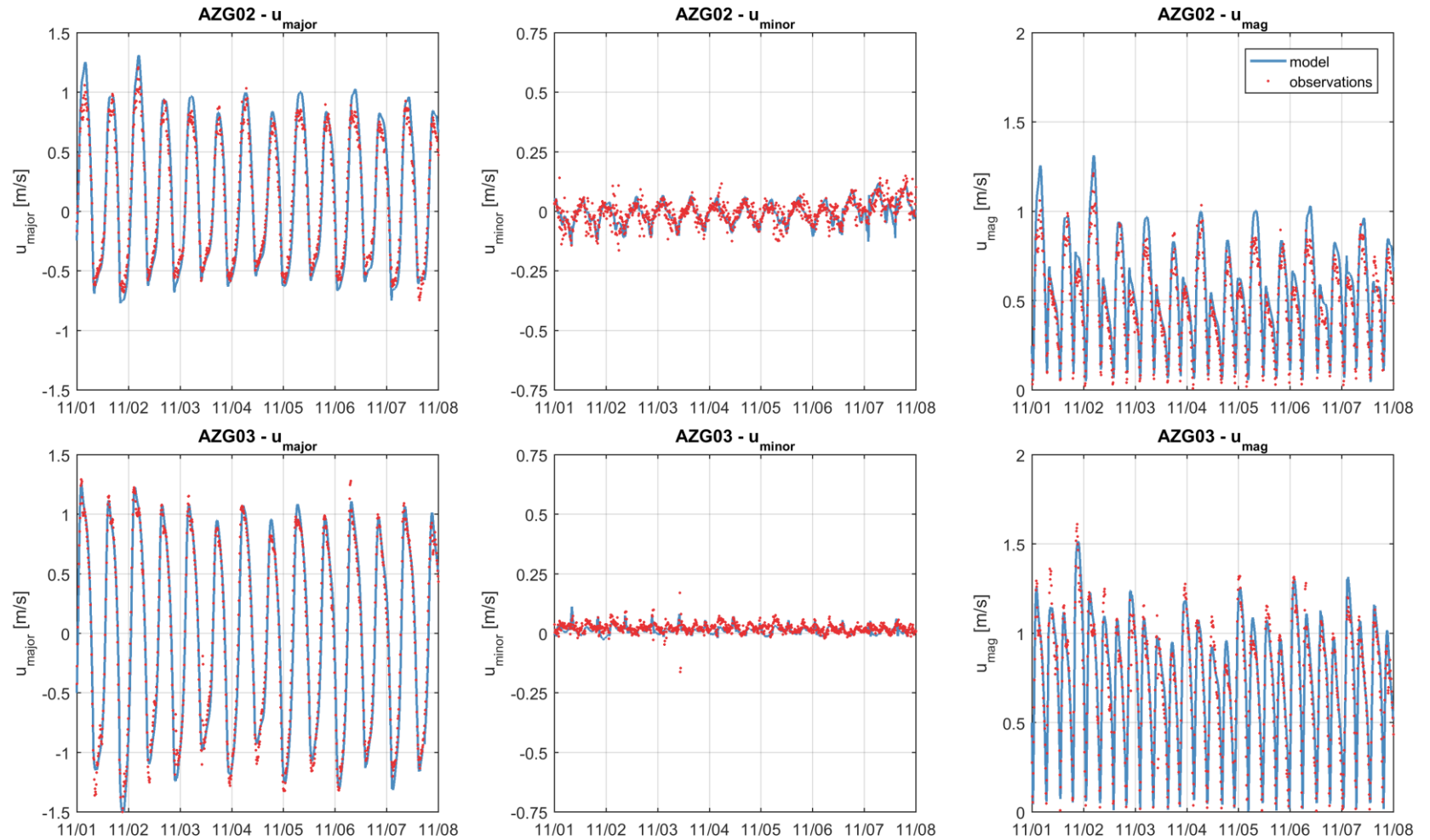
*Figure 5.5   Time series of flow velocities in m/s as observed (red) and computed (blue) for the validation period in 2011. Left panels are velocities in the major axis (determined by tidal analysis of M2). Middle panels are minor axis (again determined by tidal analysis of M2). The right panel is the depth-averaged flow velocity magnitude.*
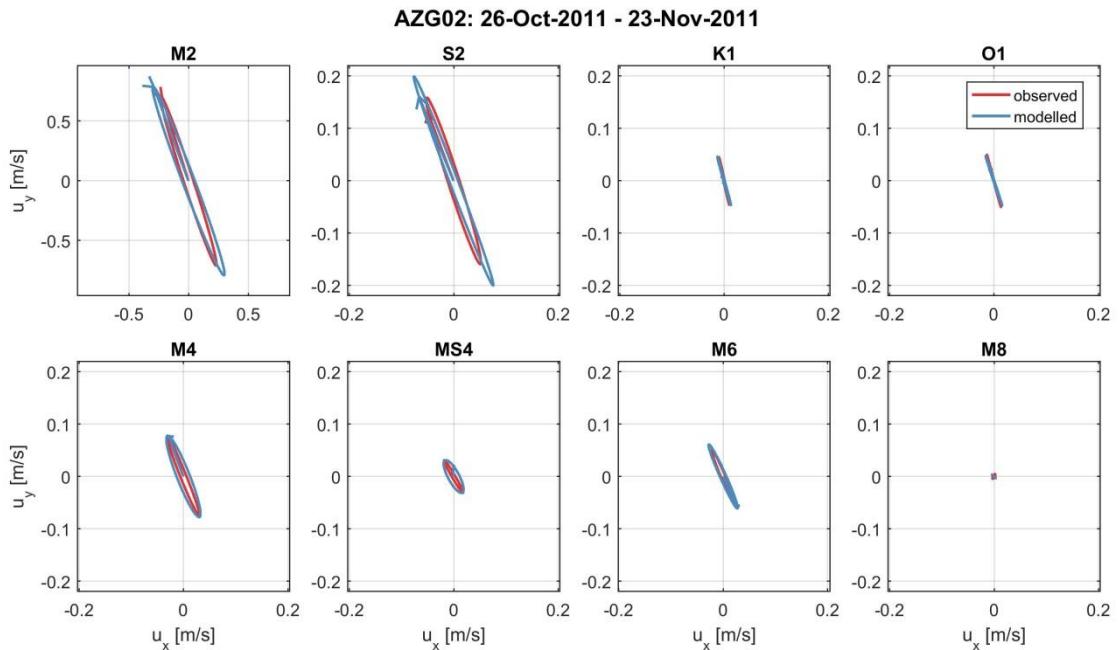
*Figure 5.6   Tidal ellipses for ADCP-AZG03 of the 8 most important tidal constituents as observed (red) and modeled (blue). Note: M2 has a different axis than other panels!*
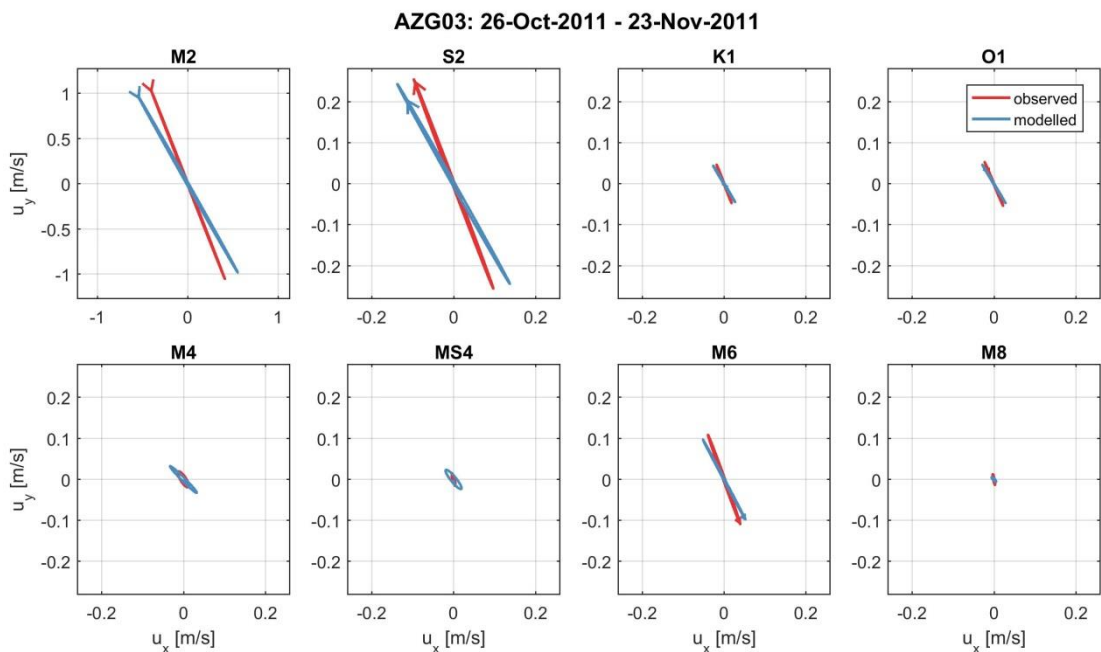


*Figure 5.7   Tidal ellipses for ADCP-AZG03 of the 8 most important tidal constituents as observed (red) and modeled (blue). Note: M2 has a different axis than other panels!*

5.3.4    Velocities 2017 (DVA; lower shoreface Ameland)
The CGII-TA model reproduces the depth-averaged flow velocities during the validation period of 2017 quite well (Table 5.5 & Figure 5.8). The different RMSE's in flow velocity are in the order of 0.10 m/s and there is no consistent bias in one of the axis or frame locations. On top of that, the SCI of the magnitude reveals that the relative error is smaller than 25%. These values show that the absolute and relative errors for the second CGII campaign (November 2017) are smaller than for the first campaign and are somewhat larger than the errors for the 2011 SBW period. The difference of the reproduction of the various campaigns might be due to the difference in the hydrodynamic environment for two measurement campaigns. For example; the velocities measured in 2011 were located within Ameland Inlet while velocities validated here are located at the lower shoreface of the Ameland ebb delta (Figure 2.1).

When looking in detail at the time series of Figure 5.8, one can observe some irregularity in the signal (e.g. minor axis of DVA-F4). It is not clear what the reason for this noise in the signal is but this might be due to storm effects.

In Figure 5.9 the tidal ellipses of the measurements and model are plotted on the model bathymetry. This figure shows that the amplitudes of the modelled and observed ellipses correspond well but that there is a shift in direction. The reason for this shift is elaborated in Appendix E.

*Table 5.6    ADCP-derived depth-averaged flow velocity reproduction for November 2017 divided into RMSE (first number), bias (second number) and SCI (third number) of the major and minor axis, x and y-axis and total magnitude and tidal magnitude (only magnitude from tide). Values are in [m/s]. Major and minor axes are based on the computed M2 orientation. This means the orientation of the major and minor axis can be different for the observed and measured data.*

| Different axis | DVA-F1 | DVA-F3 | DVA-F4 |
|---|---|---|---|
| Major | 0.09 / 0.01 / 0.19 | 0.14 / 0.03 / 0.27 | 0.14 / 0.06 / 0.29 |
| Minor | 0.03 / 0 / 0.63 | 0.07 / 0.01 / 0.62 | 0.09 / 0.01 / 0.57 |
| x-axis | 0.1 / -0.01 / 0.23 | 0.14 / -0.03 / 0.28 | 0.16 / -0.06 / 0.33 |
| y-axis | 0.15 / 0.01 / 1.02 | 0.11 / 0.02 / 0.7 | 0.15 / 0.07 / 0.69 |
| magnitude | 0.09 / 0.01 / 0.18 | 0.13 / -0.03 / 0.23 | 0.12 / -0.04 / 0.24 |
| tidal magnitude | 0.09 / 0.02 / 0.19 | 0.08 / 0 / 0.17 | 0.05 / 0.01 / 0.13 |
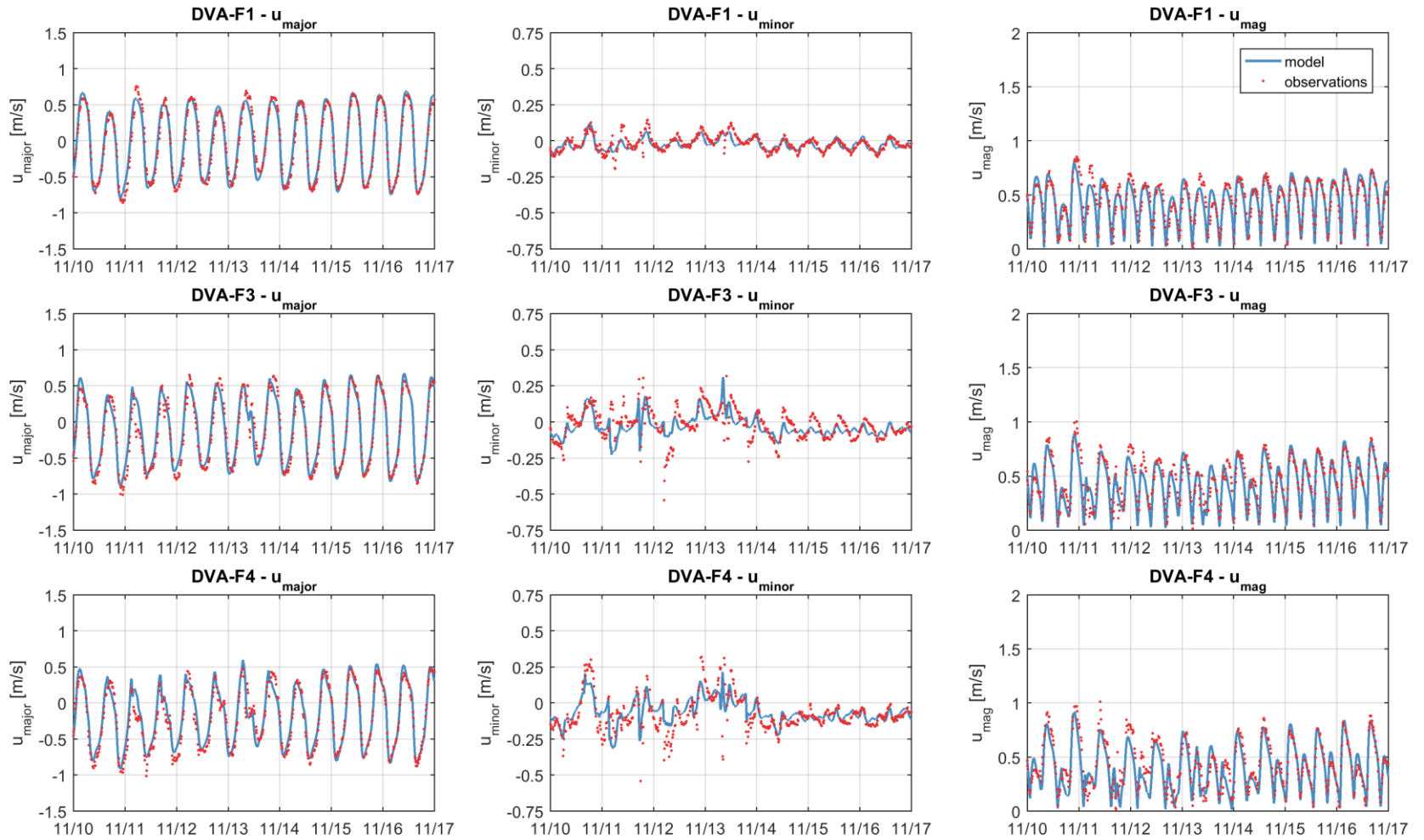
*Figure 5.8   Time series of flow velocities in m/s as observed (red) and computed (blue) for the validation period in 2017. Left panels are velocities in the major axis (determined by tidal analysis of M2). Middle panels are minor axis (again determined by tidal analysis of M2). The right panel is the depth-averaged flow velocity magnitude.*
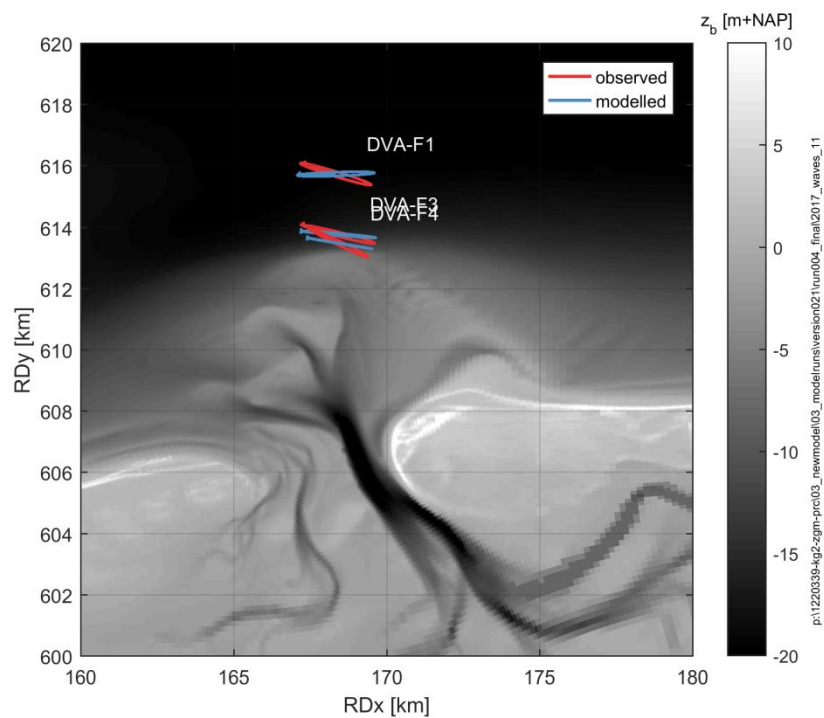
*Figure 5.9 Ellipse of the M2 tidal signal as observed (red) and modeled (blue) for the November 2017 period plotted on top of the model bathymetry.*

5.3.5    Velocities; 2018 January (DVT1, lower shoreface Terschelling)
The error of the reproduction of depth-averaged flow velocities during the validation period January 2018 (Table 5.7 and Figure 5.11) is similar to the calibration period (RMSE in the order pf 0.15 m/s; see §4.3.2). Yet, the performance of the model evaluated along the y-axis is poor (SCI larger than 1), but the flow magnitude is reproduced well. This is an indication that the modelled and measured direction do not compare well. This is visualized in Figure 5.10 as the ellipse of the flow presented on the model bathymetry.

The general pattern of the main flow direction along a longshore uniform closed coastal system is in the longshore direction. The tidal ellipses (Figure 5.10) based on the measured flow deviate from this general pattern, i.e. the major axes are more cross-shore orientated. Therefore, the deviations of the M2 tidal ellipse of the measurements suggest that the cause of these deviations is related to data processing. An error in the correction of the data on the basis of the compass directions is then the most plausible explanation. In Appendix E the effect of data processing on the directions in the measurements is elaborated.

Table 5.7  *ADCP-derived depth-averaged flow velocity reproduction for January 2018 divided into RMSE (first number), bias (second number) and SCI (third number) of the major and minor axis, x and y-axis and total magnitude and tidal magnitude (only magnitude from tide). Values are in [m/s]. Major and minor axes are based on the computed M2 orientation.*

| Different axis | DVT1-F1 | DVT1-F3 | DVT1-F4 |
|---|---|---|---|
| Major | 0.14 / 0.08 / 0.27 | 0.12 / 0.05 / 0.25 | 0.11 / 0.04 / 0.25 |
| Minor | 0.04 / 0.02 / 0.85 | 0.03 / 0 / 0.91 | 0.02 / 0 / 0.83 |
| x-axis | 0.14 / -0.09 / 0.28 | 0.12 / -0.05 / 0.26 | 0.11 / -0.04 / 0.26 |
| y-axis | 0.14 / 0.01 / 2.99 | 0.19 / 0.04 / 1.88 | 0.12 / 0.02 / 3.16 |
| magnitude | 0.13 / -0.02 / 0.25 | 0.11 / -0.03 / 0.24 | 0.11 / -0.01 / 0.24 |
| tidal magnitude | 0.05 / 0 / 0.12 | 0.06 / -0.01 / 0.15 | 0.06 / 0.01 / 0.14 |
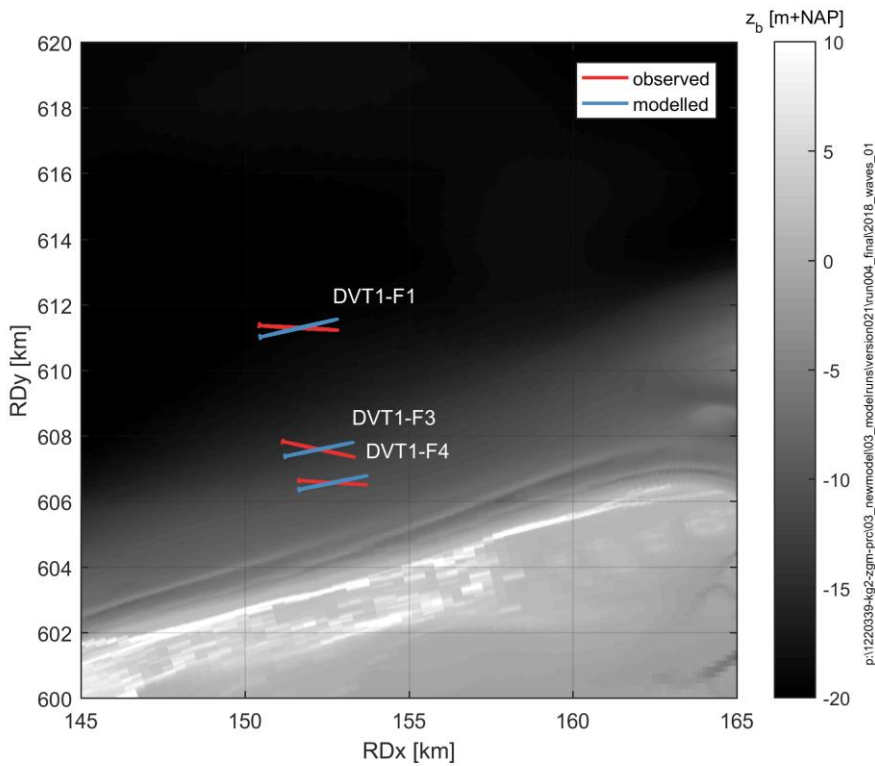


*Figure 5.10 Ellipse of the M2 tidal signal as observed (red) and modeled (blue) for the January 2018 period plotted on top of the model bathymetry.*
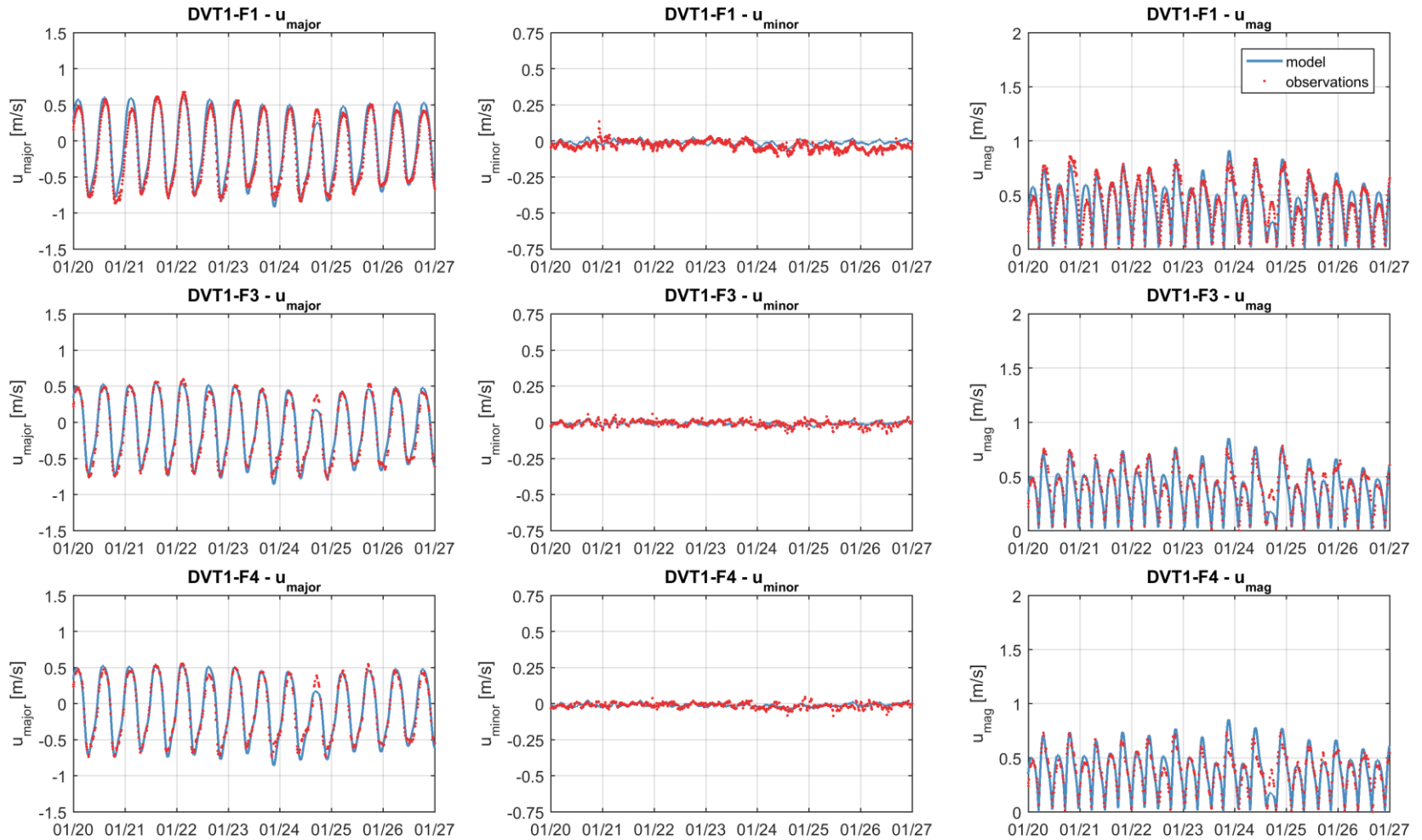
*Figure 5.11 Time series of flow velocities in m/s as observed (red) and computed (blue) for the validation period in January 2018. Left panels are velocities in the major axis (determined by tidal analysis of M2). Middle panels are minor axis (again determined by tidal analysis of M2). The right panel is the depth-averaged flow velocity magnitude.*

**Deltares**

5.3.6  Velocities; 2018 March (DVT2, lower shoreface Terschelling)

The CGII-TA model reproduces the depth-averaged flow velocities during the validation period March 2018 quite well (Table 5.8 and Figure 5.13). The RMSE-values in flow magnitude are in the order of 0.1 m/s and there is no consistent bias in one of the axis of the frame locations. Figure 5.13 does show, however, that the model is unable to capture the high energetic event during 17 and 18 March 2018. During this event there is a very strong flow in westward direction.

The SCI scores of the magnitude (Table 5.8) show values comparable to the other validation periods. There is, however, a very large SCI along the y-axis of frame 1. This is caused by a deviation in direction of approximately 10°, illustrated by the tidal ellipses of the M2 tidal signal in Figure 5.12. Because the model and the measurements align really well at frame 3, the major M2 tidal axis is assumed to align with the orientation of the coastline, and because this deviation is observed in other datasets (§5.3.5), it is assumed that this error between model and measurements is not due to a lack of model performance but due to data processing. The most plausible explanation for this deviation in the direction of the measurements is an error in (the calibration of) the compass heading (see Appendix E).

*Table 5.8  ADCP-derived depth-averaged flow velocity reproduction for March 2018 divided into RMSE (first number), bias (second number) and SCI (third number) of the major and minor axis, x and y-axis and total magnitude and tidal magnitude (only magnitude from tide). Values are in [m/s]. Major and minor axes are based on the computed M2 orientation.*

| Different axis | DVT2-F1 | DVT2-F3 |
|---|---|---|
| Major | 0.1 / 0 / 0.2 | 0.18 / 0.05 / 0.35 |
| Minor | 0.04 / 0 / 0.41 | 0.07 / 0 / 2.82 |
| x-axis | 0.1 / -0.01 / 0.21 | 0.17 / 0.05 / 0.34 |
| y-axis | 0.11 / -0.01 / 3.43 | 0.05 / 0.02 / 0.45 |
| magnitude | 0.09 / -0.01 / 0.19 | 0.16 / -0.05 / 0.32 |
| tidal magnitude | 0.03 / 0 / 0.06 | 0.03 / -0.02 / 0.07 |
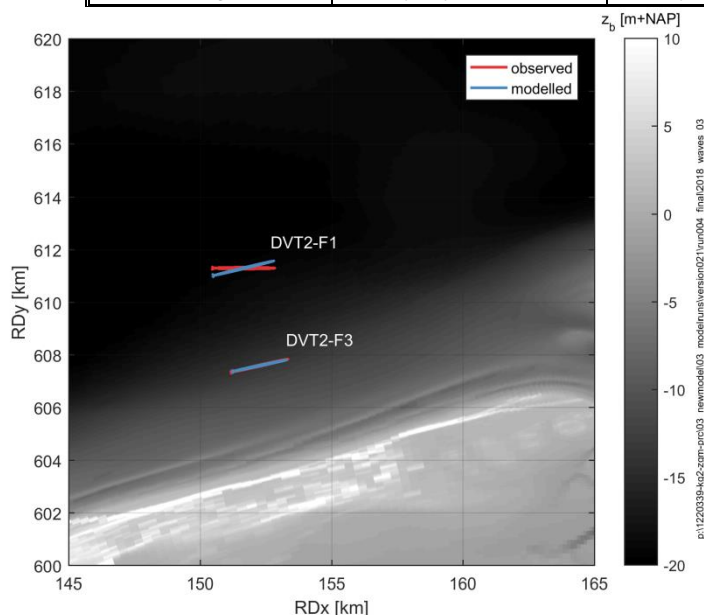


*Figure 5.12 Ellipse of the M2 tidal signal as observed (red) and modeled (blue) for the March 2018 period plotted on top of the model bathymetry.*
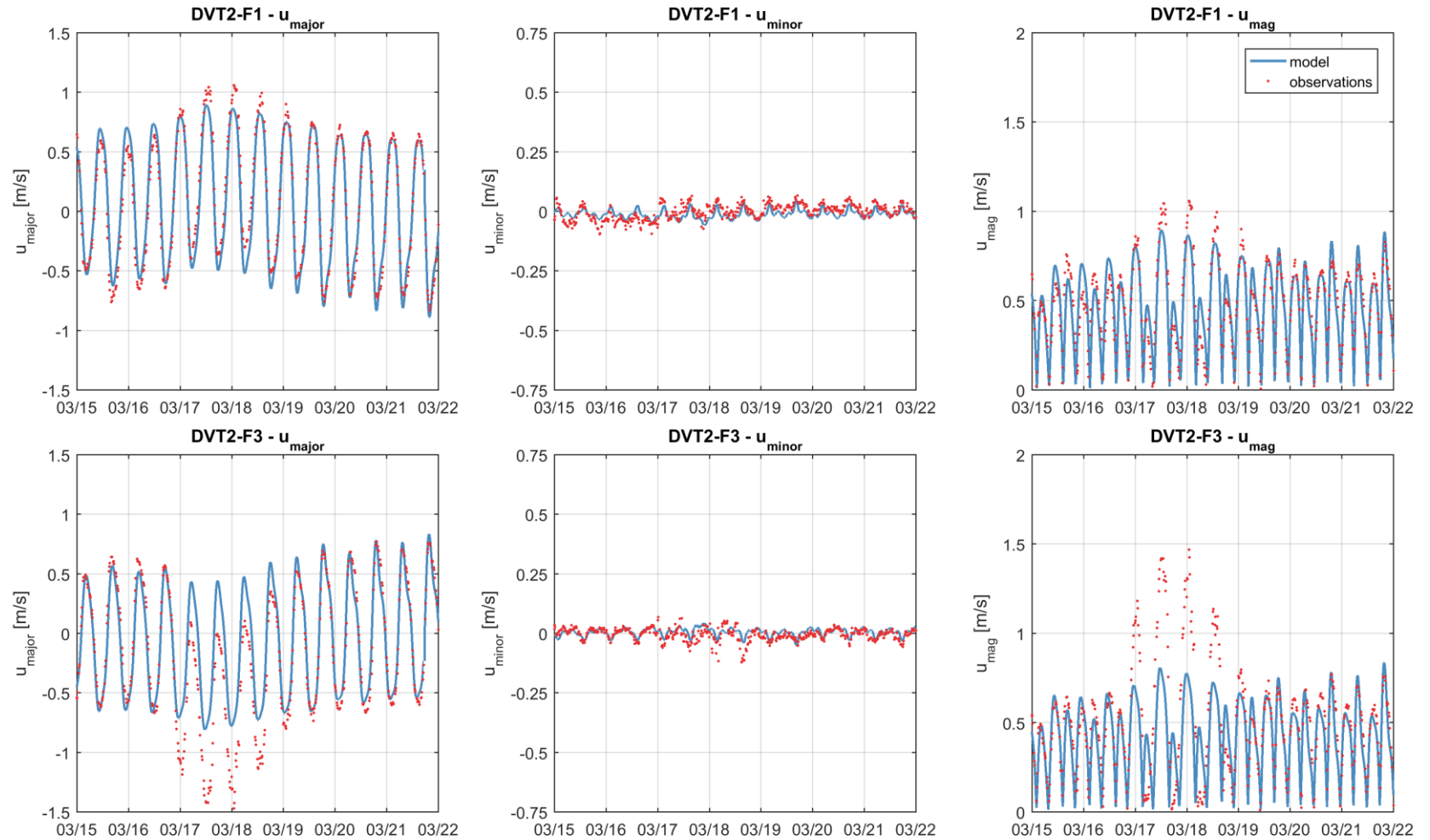
*Figure 5.13 Time series of flow velocities in m/s as observed (red) and computed (blue) for the validation period in March 2018. Left panels are velocities in the major axis (determined by tidal analysis of M2). Middle panels are minor axis (again determined by tidal analysis of M2). The right panel is the depth-averaged flow velocity magnitude.*

## 5.4 Waves

### 5.4.1 Accuracy 2011

The CGII-TA model reproduces the wave heights during the validation period of 2011 reasonably well (Figure 5.15 and Table 5.9). Wave heights offshore are reproduced with an RMSE of 0.07-0.28 m. For offshore stations, EIR, SON, AZB11 and AZB12 the errors are the lowest. Buoys in the inlet and the Wadden Sea basin have a larger absolute and relative error (SCI). Remarkable is the relative error of AZB22 and the fact that in the observations there is a clear tidal influence which is not modeled. Apparently, the water depth (and thus wave breaking) is not correctly reproduced by the model which could be related to an incorrect bathymetry in this morphological active area ('Bornrif bankje', see also Figure 2.1). Compared to the calibration periods the RMSE is in the same order (+/- 20 cm). However, for the calibration period, offshore wave heights were reproduced with higher accuracy. For stations in the Wadden Sea basin, the accuracy is similar. On top of that, the calibration period was known for its severe conditions (Hs > 6 m), while during the validation period wave heights were smaller (Hs < 2 m). Therefore the relative error (SCI) is larger for the validation period in 2011.

Wave periods are reproduced with an RMSE of 0.5-1.1 s (Figure 5.14 & Table 5.10). Similarly to the wave heights, for the offshore stations, the errors are the lowest (i.e. RMSE of 0.5 s) and the errors start to increase in the inlet and the Wadden Sea basin. The relative error varies between 10% offshore to almost 30% in the basin. Offshore there is no model bias (i.e. wave periods are in the same order) However, at AZB21 there is a positive bias of almost 0.4 s and at AZB32 there is a negative bias of almost 0.9 s. It is not clear why the model tends to have spatially varying over- and underestimation. Compared to the calibration periods, RMSE are similar to the calibration period.

Moreover, the wave directions were validated (Table 5.11). Figure 5.14 compares the observed and computed wave direction. The RMSE in wave direction is 30 - 35 degrees offshore and increases to 65 degrees at AZB41. Individual wave buoys have a bias between - 10 and +10 degrees (both under- and overestimation). Compared to the calibration periods, RMSE in wave direction is somewhat higher offshore but in the same order in the Wadden Sea basin.

*Table 5.9    Error statistics of wave heights ($H_{m0}$) in meters.*

| Stations | RMSE [m] | bias [m] | SCI [-] |
|---|---|---|---|
| Eierlandse Gat boei | 0.14 | 0.01 | 0.15 |
| Schiermonnikoog noord boei | 0.13 | 0.06 | 0.17 |
| Amelander Zeegat - Boei 1-1 | 0.16 | -0.02 | 0.19 |
| Amelander Zeegat - Boei 1-2 | 0.14 | -0.02 | 0.21 |
| Amelander Zeegat - Boei 2-1 | 0.16 | 0.08 | 0.31 |
| Amelander Zeegat - Boei 2-2 | 0.28 | 0.19 | 0.72 |
| Amelander Zeegat - Boei 3-1 | 0.16 | 0.13 | 0.68 |
| Amelander Zeegat - Boei 4-1 | 0.11 | 0.09 | 1.01 |
| Amelander Zeegat - Boei 5-1 | 0.09 | 0.07 | 1.36 |
| Amelander Zeegat - Boei 6-1 | 0.08 | 0.06 | 2.22 |
| Amelander Zeegat - Boei 3-2 | 0.15 | 0.11 | 0.72 |
| Amelander Zeegat - Boei 4-2 | 0.16 | 0.13 | 0.92 |
| Amelander Zeegat - Boei 5-2 | 0.09 | 0.06 | 0.67 |
| Amelander Zeegat - Boei 6-2 | 0.07 | 0.06 | 2.24 |

*Table 5.10   Error statistics of wave periods ($T_{m01}$) in seconds.*

| Statistical methods | RMSE [s] | bias [s] | SCI [-] |
|---|---|---|---|
| Amelander Zeegat - Boei 1-1 | 0.68 | -0.09 | 0.19 |
| Amelander Zeegat - Boei 1-2 | 0.98 | -0.12 | 0.28 |
| Amelander Zeegat - Boei 2-1 | 0.96 | -0.23 | 0.26 |
| Amelander Zeegat - Boei 2-2 | 1.34 | -0.51 | 0.34 |
| Amelander Zeegat - Boei 3-1 | 1.41 | -0.62 | 0.42 |
| Amelander Zeegat - Boei 3-2 | 1.08 | -0.38 | 0.34 |

*Table 5.11   Error statistics of wave direction (dir) in degrees.*

| Statistical methods | RMSE [degrees] | MAE [degrees] | Bias [degrees] |
|---|---|---|---|
| Eierlandse Gat boei | 27 | 17 | -2 |
| Schiermonnikoog noord boei | 29 | 17 | -2 |
| Amelander Zeegat - Boei 1-1 | 35 | 21 | 8 |
| Amelander Zeegat - Boei 2-1 | 40 | 26 | 8 |
| Amelander Zeegat - Boei 3-1 | 57 | 40 | -9 |
| Amelander Zeegat - Boei 4-1 | 64 | 42 | -14 |
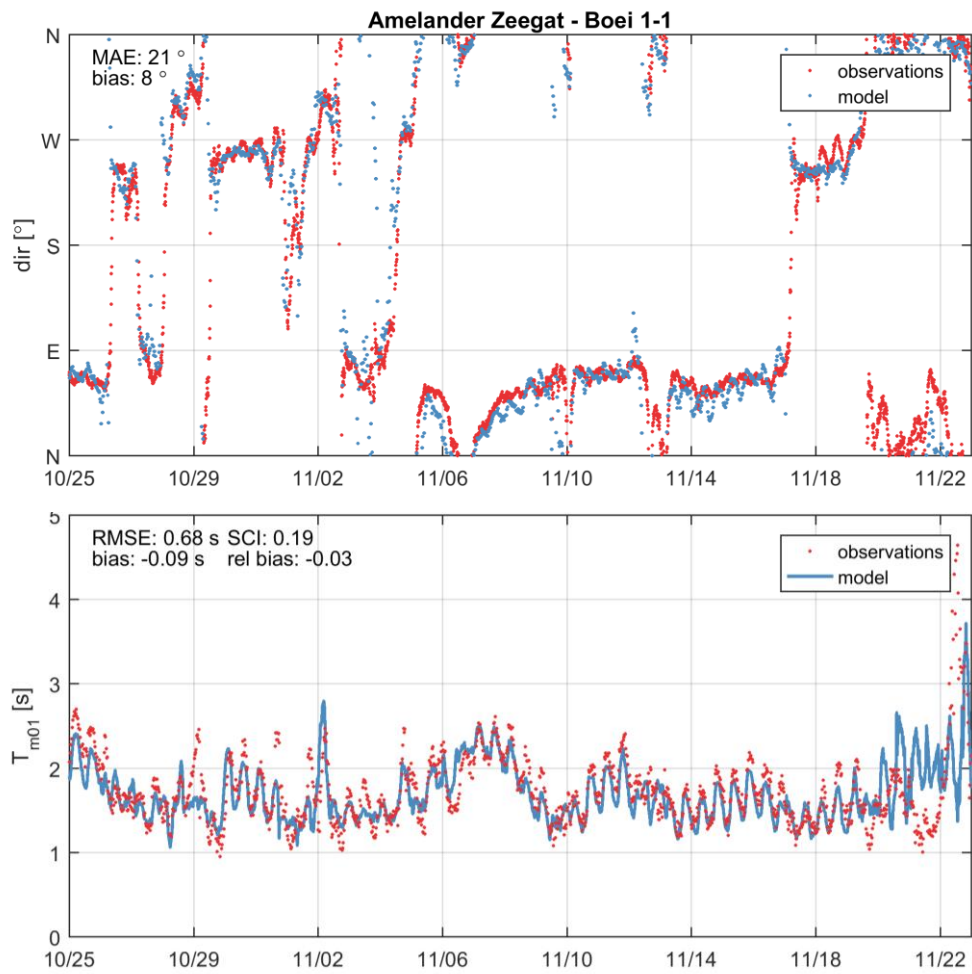
*Figure 5.14        Wave direction (dir – upper panel) and wave period ($T_{m01}$) in seconds (upper panel) and as observed (red) and computed (blue) for the validation period in 2011 at AZB11*
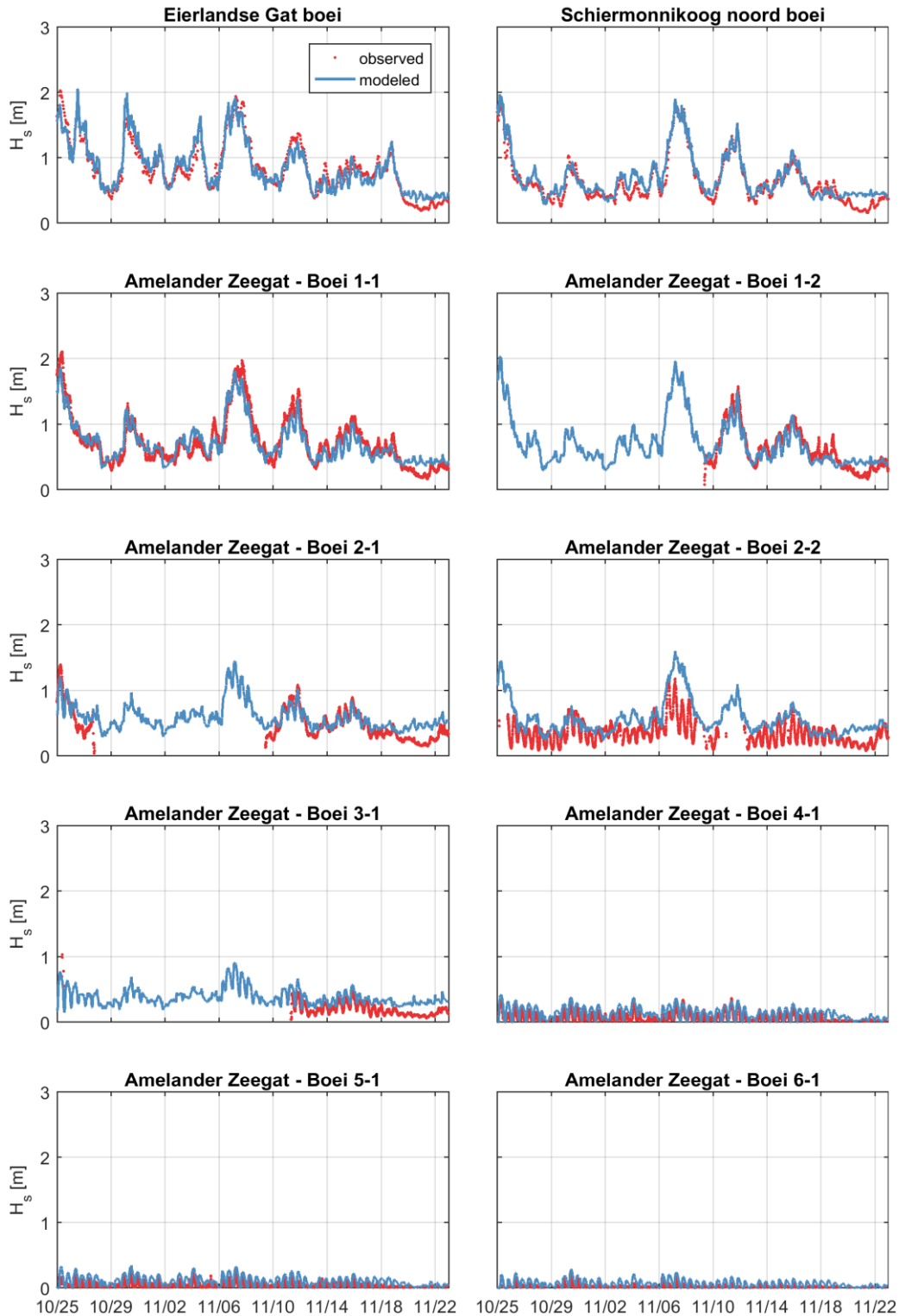
*Figure 5.15 Wave heights (H_{m0}) in meters as observed (red) and computed (blue) for the validation period in 2011.*

5.4.2    Accuracy 2008
The CGII-TA model reproduces the wave heights during the validation period of 2008 reasonably well (Table 5.12 & Table 5.13). Wave heights offshore are reproduced with an RMSE of 0.10-0.30 m. For offshore stations, EIR, SON, AZB11 and AZB12 the relative errors are the lowest (SCI of around 10%). Buoys in the inlet and the Wadden Sea basin have a larger absolute and relative error (SCI of around 30%). Compared to the calibration periods, RMSE are in the same order and similar to previous studies (e.g. Deltares, 2014).

Wave periods are reproduced with an RMSE of 0.6-1.2 s (Table 5.13 & Figure 5.16 – lower panel). Similarly to the wave heights, for the offshore stations, the errors are the lowest (i.e. RMSE of 0.6 s) and the errors start to increase in the inlet and the Wadden Sea basin. The relative error varies between 15% offshore to 30% in the basin. Compared to the calibration periods, RMSE are in the same order, but the error is higher compared to previous studies (e.g. Deltares, 2014).

Moreover, the wave directions were validated (Table 5.14 & Figure 5.16 – upper panel).The RMSE in wave direction is 10-15 degrees offshore and increases to 55 degrees at AZB41. Individual wave buoys have a bias with a maximum of 10 degrees (both under- and overestimation). Compared to the calibration periods, RMSE are in the same order, but the error is higher compared to previous studies (e.g. Deltares, 2014).

*Table 5.12   Error statistics of wave heights ($H_{m0}$) in meters.*

| Stations | RMSE [m] | bias [m] | SCI [-] |
|---|---|---|---|
| Eierlandse Gat boei | 0.31 | 0.21 | 0.12 |
| Schiermonnikoog noord boei | 0.20 | -0.08 | 0.10 |
| Amelander Zeegat - Boei 1-1 | 0.26 | -0.07 | 0.13 |
| Amelander Zeegat - Boei 1-2 | 0.29 | -0.15 | 0.15 |
| Amelander Zeegat - Boei 2-1 | 0.22 | -0.05 | 0.20 |
| Amelander Zeegat - Boei 2-2 | 0.22 | -0.07 | 0.19 |
| Amelander Zeegat - Boei 3-1 | 0.20 | -0.06 | 0.22 |
| Amelander Zeegat - Boei 4-1 | 0.11 | 0.08 | 0.39 |
| Amelander Zeegat - Boei 5-1 | 0.14 | 0.12 | 0.56 |
| Amelander Zeegat - Boei 6-1 | 0.14 | 0.12 | 0.72 |
| Amelander Zeegat - Boei 3-2 | 0.32 | 0.10 | 0.43 |
| Amelander Zeegat - Boei 4-2 | 0.15 | 0.09 | 0.35 |
| Amelander Zeegat - Boei 5-2 | 0.14 | 0.11 | 0.45 |
| Amelander Zeegat - Boei 6-2 | 0.11 | 0.08 | 0.66 |

*Table 5.13   Error statistics of wave periods ($T_{m01}$) in seconds.*

| Stations | RMSE [s] | bias [s] | SCI [-] |
|---|---|---|---|
| Amelander Zeegat - Boei 1-1 | 0.43 | -0.15 | 0.08 |
| Amelander Zeegat - Boei 1-2 | 0.47 | -0.21 | 0.09 |
| Amelander Zeegat - Boei 2-1 | 0.60 | -0.08 | 0.15 |
| Amelander Zeegat - Boei 2-2 | 0.98 | 0.34 | 0.22 |
| Amelander Zeegat - Boei 3-1 | 1.42 | -0.97 | 0.34 |
| Amelander Zeegat - Boei 3-2 | 1.11 | -0.47 | 0.30 |

*Table 5.14        Error statistics of wave direction (dir) in degrees.*

| Statistical methods | RMSE [degrees] | MAE [degrees] | Bias [degrees] |
|---|---|---|---|
| Eierlandse Gat boei | 10 | 7 | 1 |
| Schiermonnikoog noord boei | 13 | 10 | -3 |
| Amelander Zeegat - Boei 1-1 | 15 | 10 | 1 |
| Amelander Zeegat - Boei 2-1 | 21 | 13 | -2 |
| Amelander Zeegat - Boei 3-1 | 44 | 28 | -6 |
| Amelander Zeegat - Boei 4-1 | 55 | 38 | -13 |
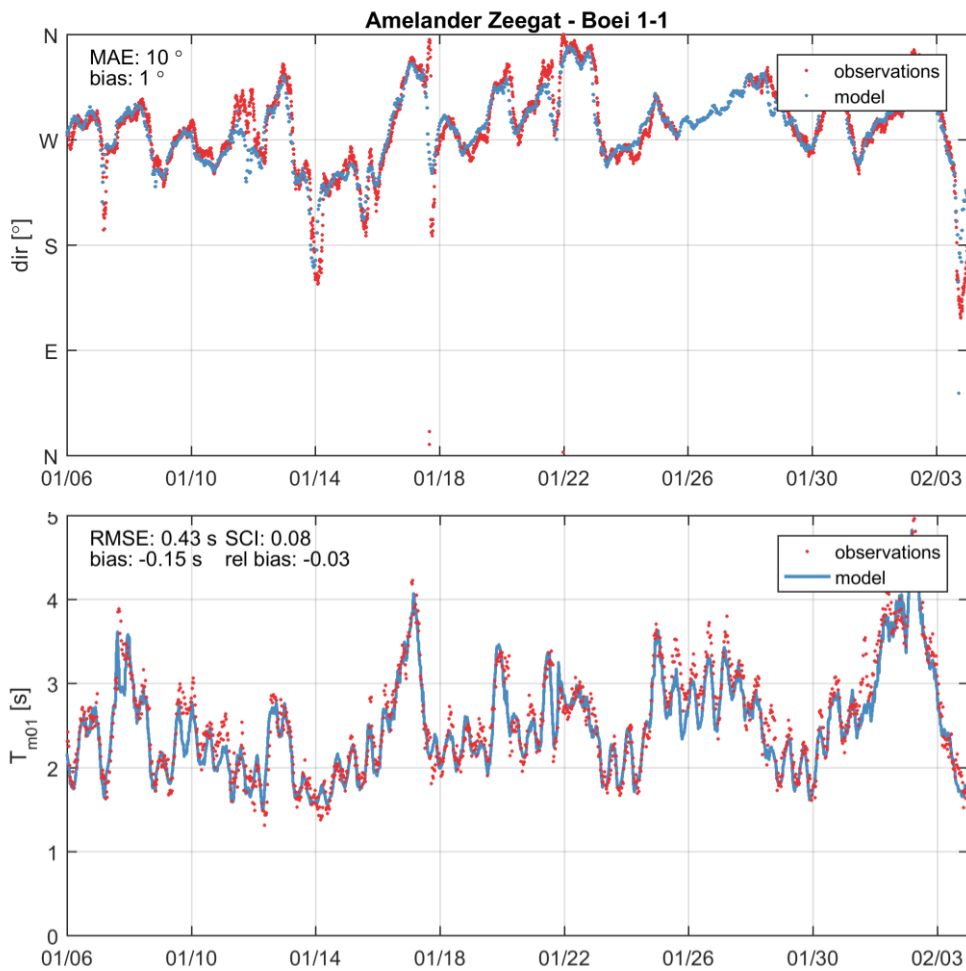


*Figure 5.16 Wave direction (dir – upper panel) and wave period ($T_{m01}$ – lower panel) in seconds (lower panel) and as observed (red) and computed (blue) for the validation period in 2008 at AZB11*
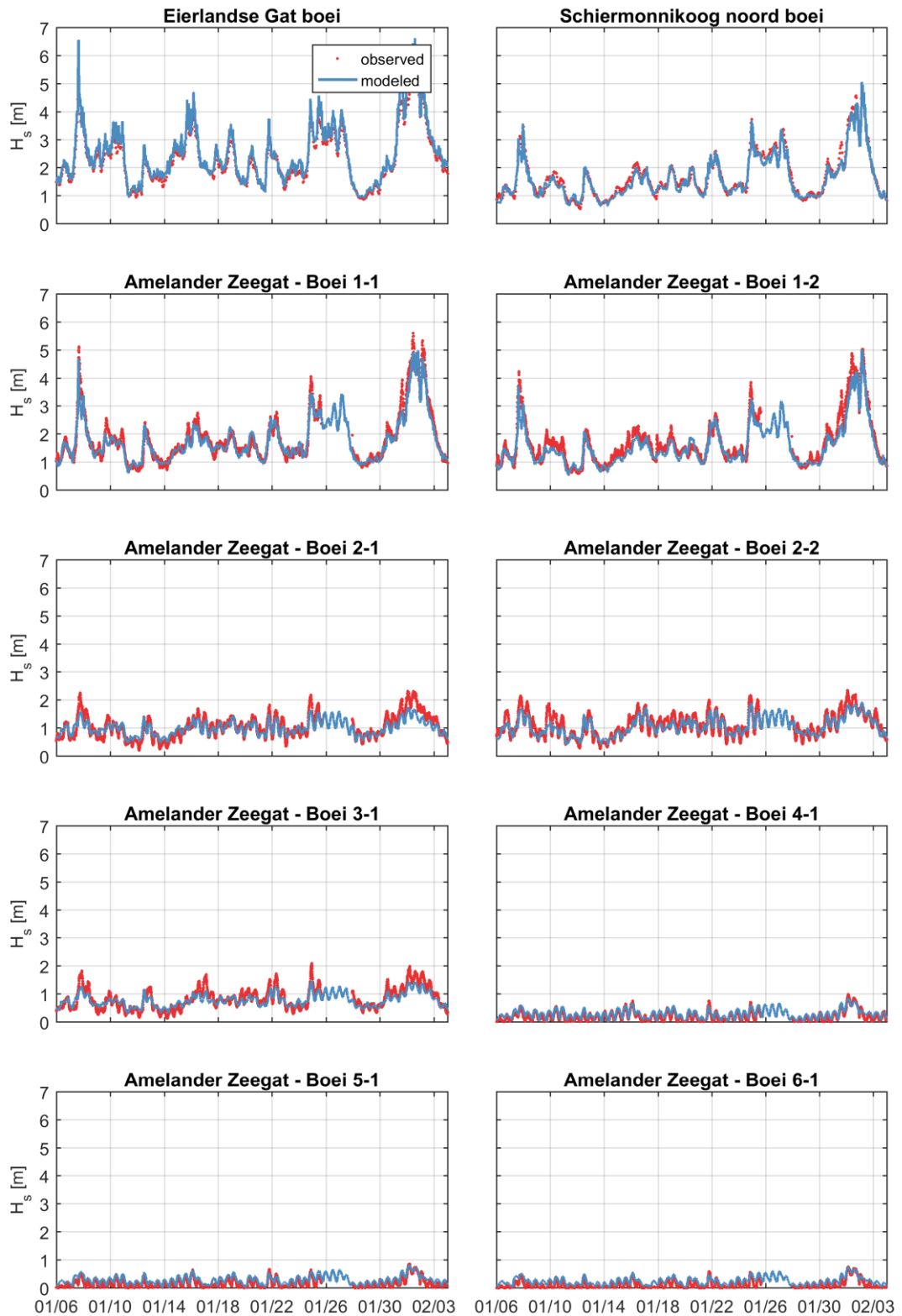
*Figure 5.17 Wave heights (Hm0) in meters as observed (red) and computed (blue) for the validation period in 2008*

### 5.4.3 Spatial patterns

The described model setup of the CGII-TA model with increased wave heights from the boundary in combination (calibration step 1) with default wave breaking with BKD (calibration step 2) results in the spatially-varying wave heights of Figure 5.18. Higher wave heights are computed further offshore. At the inlet, waves start the break. This is reproduced both by the model as the data.
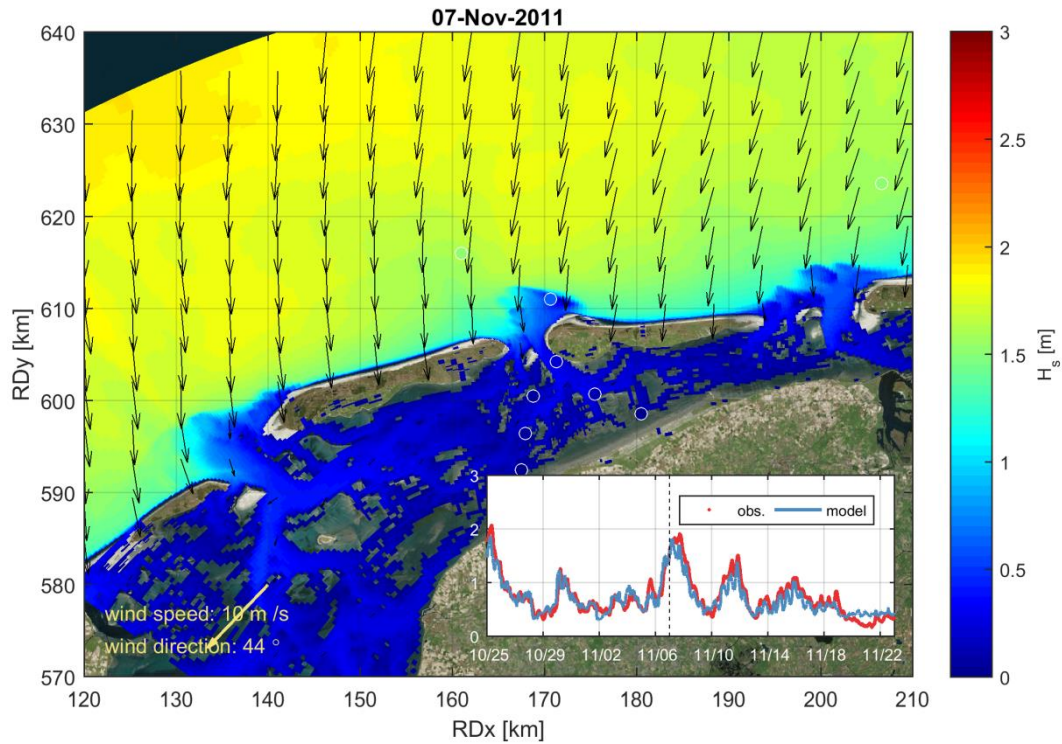


*Figure 5.18    Snapshot of the wave heights during the peak of the storm in September 2017. The heat map is the computed wave heights. The circles are the observed wave heights. Time series are wave heights (computed and observed) at AZB11.*

## 5.5 Conclusions

The CGII-TA model was validated for its reproduction of water levels in 2011 and 2008 and the discharge through the compared well to values from literature. The model was validated on an extensive set of velocity measurements in 2008, 2011, November 2017 (lower shoreface Ameland ebb delta) and January and March 2018 (lower shoreface Terschelling). The wave model was validated with wave measurements in the years 2011 and 2008.

- Water levels near the inlet are reproduced with an RMSE of less than 10 cm. This error is mainly related to the error made in the NTR and somewhat higher than the calibration period. This is in the same order as previous modelling efforts (e.g. Deltares, 2009a; Zijl et al., 2013)
- Velocities are reproduced with an RMSE in the order of 10-15 cm/s and the SCI is generally lower than 20-25%. This accuracy is similar to or higher (~5 cm/s) than the calibration period. The direction of the modelled flow does often not compare well to the measurements. This is, however, most likely due to an error in the measurements caused by errors in compass calibration.
- The tidal prism is in line with the values found in literature. The accuracy is in the same order as previous studies (e.g. Deltares, 2009a)
- Wave heights, periods and directions are reproduced respectively with an RMSE of less than 20 cm, 1.0 s and 35 degrees. This is similar compared to the calibration period and in the same order as previous studies (e.g. Deltares, 2010; Deltares, 2014)

The results of the model calibration and validation exercises are in agreement with previous model studies in the Ameland Inlet (e.g. Deltares, 2009a; Deltares, 2010; Zijl et al., 2013; Deltares, 2014), which was the objective. The good performance of the model gives confidence that the model can used as an instrument to study sand transport at the lower shoreface of Terschelling and Ameland and at Ameland inlet (see objective in Section 1.2). Therefore, the model can be considered appropriate for scenario simulation in the next modelling phases of the Coastal Genesis II project.

# 6 Discussion

### 6.1.1 Model schematization
In this study, a new hydrodynamic model was set-up, calibrated and validated with the focus to study sand transport on the lower shoreface and sand exchange through Amerland inlet. With the future application of the model in mind, we chose a model domain that starts in +/- 25 m water depth (25 km offshore), covers three inlets, has a model resolution focused on the surfzone, runs in depth-averaged (2DH) mode and includes waves (see Section 1.2 & 1.3 for the objective and model strategy).

Due to the limited spatial extent of the model domain, it is not possible to improve the accuracy of the offshore water level (i.e. tide + NTR / surge) within the model domain. Based on observations it was possible to improve the tidal reproduction by calibrating tidal amplitudes and phases. However, this cannot be done for the (offshore) NTR component of the water level, since the NTR is an irregular signal and varies from location-to-location. Therefore, the model always had a minimum error offshore in water levels of 6-8 cm. A possibility to improve the offshore generation of water levels is to apply a larger numerical domain. For example, including a larger part of the North Sea makes it possible to calibrate the large-scale wind-driven set-up. However, with the application of the model in mind, it did not seem feasible to increase the model domain. Moreover, by nesting water levels from an overall large-scale model it is possible to include wind-driven surge and therefore this is deemed not a limitation for the application in mind. Furthermore, it is believed that a water level RMSE of less than 10 cm is sufficient for a model aimed to compute sand transport. This is supported by the fact that the water level reproduction is comparable to that by the DCSMv6ZUNOv4 model of Zijl et al. (2013), a dedicated water level forecasting model.

The choice of the application of a depth-averaged model (instead of a 3D model) means that time-dependent baroclinic pressure gradients (e.g. due to the freshwater) are not resolved by the model. Also, the vertical undertow profile due to wave-breaking is not resolved. The importance of these currents for sand transport can only numerically be investigated using a 3D model. This will result in an expected increase of the computational demand by approximately a factor 2. However, a 3D model will not necessarily improve the accuracy of the long-term morphodynamic predictions due to other model uncertainties (e.g. in sediment transport).

Moreover, the resolution of the CGII-TA model in the Wadden Sea basin is not sufficient to fully capture the hydrodynamic processes in the small channels of the Wadden Sea basin. For example, the channel near Holwerd is less than 100 m while the model resolution in this area is 150x300 m. This explains why the tidal amplitude is underestimated at Holwerd. However, the resolution of the model is not a bottleneck in the application, because instantaneous and cumulative discharges through Ameland Inlet are well reproduced.

### 6.1.2 Calibration
Hydrodynamic calibration was carried out on water levels, discharge measurements, velocity measurements in the inlet and velocity on the watershed (Aquadopp). Each dataset resulted in an optimal set of calibration coefficients which are not the same for other datasets. On top of that, calibration coefficients could be varied in time (e.g. during a storm other coefficients can be used than during daily conditions). In this study, discharge measurements resulted in higher calibration coefficients than velocity measurements at the watershed. Eventually, we

choose to apply calibration coefficients of 0.5, 0.5 and 0.0 for respectively ripples, mega-ripples and dunes. These were the optimal values found for the velocity measurements in the inlet while still gave fairly similar results for the other measurements. For the calibration of this model, we aimed to have the most generic derivation for the roughness predictor because of the wide model application. However, this means that depending on the goal of the model application, different calibration coefficients could be used. Therefore, when the model will be used for a different application than the one in mind for this study (e.g. water level assessment during storms), other coefficients could be more suitable.

### 6.1.3 Discharge measurements

The modeled and measured discharges and volumes during the Coastal Genesis II measurement campaign compared well. However, for the instantaneous discharge, the moment of a reversal from flood to ebb directed discharge did not always exactly coincide with the measurements. On top of that, the distribution of the discharge did not match with the measurements. Generally, the flow velocities at the western transect (AQVPO in Figure 4.8) seems to be underestimated. It is not clear what the reason for this underestimation is. However, the impact of this underestimation is limited since the bulk of the discharge flows via the eastern transect (RWSII in Figure 4.8; Borndiep). Furthermore, the computed tidal prism agreed well with the values found in the literature.

### 6.1.4 Aquadopp measurements

The inclusion of three inlets in the model domain seems to have a positive effect on the ability of the model to simulate the exchange of water through the Ameland Inlet and the watershed. The instantaneous discharge and the tidal prism modeled and observed in the field align well. In particular, when the watershed would have been closed it would not be possible to have a net in- or outflow of water (i.e. ebb or flood dominance).

However, during the storm of 13 September 2017, the modeled depth-averaged velocities on the watershed were underestimated by the model. Several sensitivity simulations confirmed that either more momentum transfer from wind to the water column is needed (e.g. by increasing the wind speed) or that less bottom friction should be applied. Here, we chose to focus on the overall reproduction of the model. Decreasing friction coefficients resulted in a better reproduction of depth-averaged flow velocities on the watershed during the peak of the storm. However, these settings did for example not yield to an accurate reproduction of the cumulative discharge through Ameland Inlet.

# 7 Conclusions

## 7.1 Conclusions

The Coastal Genesis 2.0 (GCII, or Kustgenese 2.0) project is carried out to improve our knowledge for supporting the long-term coastal maintenance strategy and policy. In this report, we present the model set-up, hydrodynamic calibration and validation of the Terschelling-Ameland Kustgenese 2 model (CGII-TA model). This is the first step towards a model to predict sand transport at the Terschelling and Ameland lower shoreface and morphodynamics of the Ameland Inlet.

Overall, the model performs well in terms of computed water levels, flow velocities, discharges, wave heights, wave periods and wave direction. After calibration of the tidal constituents and bottom friction via the Van Rijn roughness predictor, the RMSE of the water level is less than 10 cm. The error is mainly related to the RMSE made in the non-tidal residual (NTR / surge). Depth-averaged flow velocities are reproduced with an RMSE of 10 to 15 cm/s, both in the calibration and validation periods. Moreover, the tidal prism is in line with the observations performed during the CGII campaign (MAE = 10 M $m^3$ or less than 2% of the tidal prism) and with observations found in the literature. Computational time is between 2-3 days for a full year without waves (1:150) or one month with waves (1:10).

Waves were calibrated by increasing the measured energy density that is applied at the model boundary with 10-30% in order to compensate for dissipation. The default wave breaking coefficients of the BKD formulation are used. Validation showed that wave heights and periods are reproduced respectively with an RMSE of less than 20 cm, 1.0 s and 20 degrees.

The CGII-TA model is suitable as base model for sediment transport modeling and in line with objectives defined in Section 1.2. In particular, the presented errors in water levels, flow velocities and waves are in the same order as other numerical modeling efforts (e.g. Deltares, 2009a; Deltares, 2010; Zijl et al., 2013; Deltares, 2014) while maintaining feasible computational time.).

## 7.2 Recommendations

The large flow velocities (>1 m/s) during the storm on 13 September 2017 are underestimated by the model. In order to accurately simulate wind-driven flow at the watershed, local wind measurements are needed. Therefore, it is recommended for future velocity measurements at the Wadden Sea basin to also include a local meteorological observation.

The model is calibrated on the offshore wave height by improving the energy in the variance density spectrum. However, wave breaking is simulated with default coefficients of the BKD formulation. Minor changes in the calibration coefficients did have some effect on the accuracy of the wave heights produced by the model when going from offshore to nearshore. However, it must be noted that it is not known whether a higher accuracy could be obtained when larger changes in calibration coefficients will be used or if a different wave breaking formulation is applied. It is therefore recommended to further analyze the effect of wave breaking in the model in order to improve the accuracy.

Offshore undertow related to wave breaking and density-driven currents are potential sand transport mechanisms. These are not (well) captured in the current 2DH, depth-averaged

CGII-TA model, which assumes is logarithmic vertical velocity profile. Therefore, it is recommended to investigate the vertical velocity profiles and the importance for net sand transport based on the KG2 field data and a 3D version of the CGII-TA model.

# 8 References

Aqua Vision. (2008). *Project Sterkte en Belasting Waterkeringen (SBW).*

Aqua Vision. (2012). *Verwerking ADCP data Amelander Zeegat Stormseizoen 2011 / 2012.*

Booij, N., Ris, R. C., & Holthuijsen, L. H. (1999). A third-generation wave model for coastal regions. I- Model description and validation. *Journal of Geophysical Research*, *104*, 7649–7666. http://doi.org/10.1029/98jc02622

Dee, D. P., Uppala, S. M., Simmons, A. J., Berrisford, P., Poli, P., Kobayashi, S., … Vitart, F. (2011). The ERA-Interim reanalysis: Configuration and performance of the data assimilation system. *Quarterly Journal of the Royal Meteorological Society*, *137*(656), 553–597. http://doi.org/10.1002/qj.828

Deltaprogramma. (2015). *Werk aan de delta. De beslissingen om Nederland veilig en leefbaar te maken.*

Deltares. (2009a). *SBW Wadden Sea: water level modelling. Calibration hydrodynamic model. Phase 2.*

Deltares. (2009b). *SBW Wadden Sea , water level modelling. Study on improvement of wind input. Phase 1.*

Deltares. (2010). *Wave propagation under influence of currents.*

Deltares. (2011). Morphological modelling of bar dynamics with Delft3D, (July 2015).

Deltares. (2014). *SWAN hindcasts Wadden Sea, December 2013: Tidal inlet of Ameland and eastern Wadden Sea.*

Deltares. (2017a). *Bench-mark morphodynamic model Ameland Inlet - Kustgenese 2.0 (ZG-C2)* (Vol. 0).

Deltares. (2017b). *Kustgenese 2.0; available measurements and bathymetric data at Ameland inlet, The Netherlands.*

Deltares. (2018). *Data report Kustgenese 2.0 measurements.*

Kalnay, E., Kanamitsu, M., Kistler, R., Collins, W., Deaven, D., Gandin, L., … Joseph, D. (1996). The NCEP/NCAR 40-year reanalysis project. *Bulletin of the American Meteorological Society.* http://doi.org/10.1175/1520-0477(1996)077<0437:TNYRP>2.0.CO;2

Lesser, G. R., Roelvink, J. A., van Kester, J. a. T. M., & Stelling, G. S. (2004). Development and validation of a three-dimensional morphological model. *Coastal Engineering*, *51*(8–9), 883–915. http://doi.org/10.1016/j.coastaleng.2004.07.014

Pawlowicz, R., Beardsley, B., & Lentz, S. (2002). Classical tidal harmonic analysis including error estimates in MATLAB using TDE. *Computers and Geosciences*, *28*(8), 929–937. http://doi.org/10.1016/S0098-3004(02)00013-4

Salmon, J. (2011). Re-scaling the Battjes-Janssen model for depth- induced wave-breaking, (November). http://doi.org/10.13140/2.1.2525.9842

Sutherland, J., Peet, a. H., & Soulsby, R. L. (2004). Evaluating the performance of morphological models. *Coastal Engineering*, *51*(8–9), 917–939. http://doi.org/10.1016/j.coastaleng.2004.07.015

Teske, R. (2013). Tidal inlet channel stability in long term process based modelling. *MSc Thesis*, (July).

van der Werf, J., Grasmeijer, B., Hendriks, E., van der Spek, A., & Vermaas, T. (2017). *Literature study Dutch lower shoreface*.

Van Der Westhuysen, A. J. (2010). Modeling of depth-induced wave breaking under finite depth wave growth conditions. *Journal of Geophysical Research: Oceans*, *115*(1), 1–19. http://doi.org/10.1029/2009JC005433

Van Der Westhuysen, A. J., Zijlema, M., & Battjes, J. (2007). Nonlinear saturation-based whitecapping dissipation in SWAN for deep and shallow water. *Coastal Engineering*.

Van Rijn, L. C. (2007). Unified View of Sediment Transport by Currents and Waves: part I and II. *Journal of Hydraulic Engineering*, (June), 649–667.

Vatvani, D., Zweers, N. C., Ormondt, M. Van, Smale, A. J., Vries, H. De, Makin, V. K., & Bilt, D. (2012). Storm surge and wave simulations in the Gulf of Mexico using a consistent drag relation for atmospheric and storm surge models, 2399–2410. http://doi.org/10.5194/nhess-12-2399-2012

Zijl, F., Verlaan, M., & Gerritsen, H. (2013). Improved water-level forecasting for the Northwest European Shelf and North Sea through direct modelling of tide, surge and non-linear interaction. *Ocean Dynamics*, *63*(7), 823–847. http://doi.org/10.1007/s10236-013-0624-2.

# A   Skill scores

In order to evaluate the outcome of hydrodynamic and morphodynamic models, an objective evaluation method is needed. According to Sutherland et al. (2004), a performance can be assessed by calculating the bias and accuracy. In the following paragraphs, all the different equations used in this report are presented.

## A.1   Bias and Relative bias

The bias is the difference in the central tendencies of the computed values ($X_i$) and the observations ($Y_i$). Both the bias and the relative bias are used and can be computed with the equation below. Bias and relative bias are used for both hydrodynamic and morphological models in order to analyze the systematic error. A positive bias means that the water or bed level is higher in the computed data set than the measurements. The bias can be concluded with:

$$Bias = \frac{1}{N}\sum_{i=1}^{N}(Y_i - X_i) \tag{1.1}$$

where $N$ is the number of data points. The relative bias is calculated by dividing the bias with the mean of the observations.

## A.2   Accuracy

Accuracy can be seen as the average size of the difference between a set of computed values (X) and the observations (Y). A commonly used measure for accuracy is the root-mean-square difference (RMSE) which can be calculated with the equation below.

$$RMSE = \sqrt{\frac{1}{N}\sum_{i=1}^{N}(Y_i - X_i)^2} \tag{1.2}$$

The uRMSE is calculated by calculating the RMSE as the equation above, but by substracting the bias first. Scatter index (SCI) is calculated by dividing RMSE with the mean of the observations. It presents the percentage of RMSE difference with respect to mean observation or it gives the percentage of the error.

Another indicator for the accuracy is the mean absolute error (MAE) which can be calculated with the equation below. The MAE has a clear interpretation.

$$MAE = \frac{1}{N}\sum_{i=1}^{N}(Y_i - X_i) \tag{1.3}$$

## A.3   Tidal analysis

The results from a tidal analysis are analyzed directly per tidal constituents' amplitude and phase (e.g. 1 cm difference between M2 amplitude observed and modeled). Moreover, the vector difference (VD) is computed and is defined as:

$$VD = \sqrt{\left(H_m\cos(G_m) - H_o\cos(G_o)\right)^2 + \left(H_m\sin(G_m) - H_o\sin(G_o)\right)^2} \tag{1.4}$$

in which $H_m$, $H_o$, $G_m$, $G_o$ are the modeled (m) and observed (o) amplitudes (H) and phases (G). The VD is an error measure per constituent and combines the error in amplitude and phase. These errors can also be quadratically summed (Root-Summed-Square, RSS) overall constituents, resulting in the RSS VD.

# B Validation of the NCEP, ERA-interim and HIRLAM atmospheric models

Three atmospheric models were validated against observational data of wind speed, direction and atmospheric pressure in the proximity of the Wadden Sea (Figure B.1); 8 stations: De Kooij, Nieuwe Beerta, Huibertgat, Groningen, Lauwersoog, Leeuwareden, Stavoren, Terschelling Noordzee). Model results for the entire year of 2007 indicate that, generally, NCEP results in higher errors and biases in both the wind speed as the atmospheric pressure (Table 8.1, Table 8.2 and Figure B.2). The differences between ERA-interim and HIRLAM are small and can mainly be seen in the reproduction in atmospheric pressure. For example, the atmospheric pressure is underestimated with 31 Pa compared to an overestimation of ERA-interim 13 Pa. HIRLAM has a more accurate wind reproduction. The full overview of skill scores for the wind speed magnitude and atmospheric pressure is presented in Table 8.1 and Table 8.2.
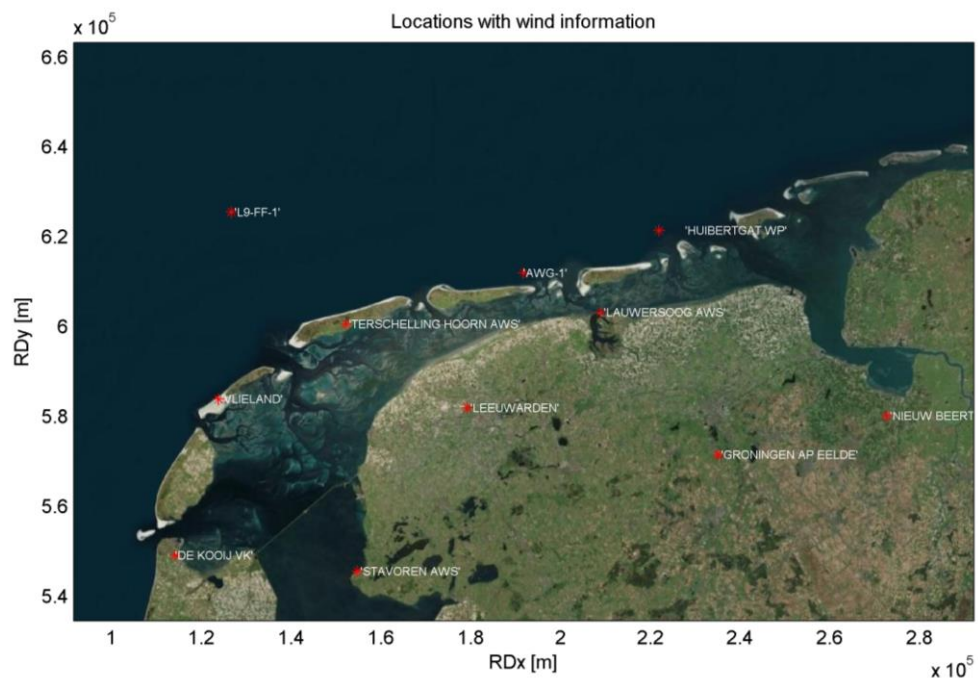


*Figure B.1  Location of KNMI meteorological measurement stations in the Wadden Sea area.*

We choose to apply HIRLAM, while it is less accurate in simulated pressure it has a more accurate reproduction of the wind speed. For hydrodynamic modeling purposes, wind is arguably more important.  Moreover, HIRLAM has a higher spatial resolution. We choose not to apply a single measured wind and pressure due to strong spatial variability during storm conditions. For example, during the storm of September 13[th,] 2017 variations in wind speed magnitude of about 10 m/s occurred (Figure B.3        )

*Table 8.1    Mean skill scores in the reproduction of atmospheric pressure for 8 stations in the proximity of the Wadden Sea*

| Error statistics | HIRLAM | ERAi | NCEP |
|---|---|---|---|
| RMSE (Pa) | 65 | 61 | 89 |
| Bias (Pa) | -31 | 13 | -41 |
| uRMSE (Pa) | 57 | 58 | 76 |

*Table 8.2    Mean skill scores in the reproduction of wind speed magnitude for 8 stations in the proximity of the Wadden Sea.*

| Error statistics | HIRLAM | ERAi | NCEP |
|---|---|---|---|
| RMSE (m/s) | 1.5 | 1.7 | 1.9 |
| Bias (m/s) | 0.1 | -0.2 | 0.9 |
| uRMSE (m/s) | 1.3 | 1.4 | 1.6 |

Error in wind magnitude (u_mag)

Error in northerly wind 10m above surface (v_10)

Error in easterly wind 10m above surface (u_10)

Error in atmospheric pressure at mean sea level (MSLP)
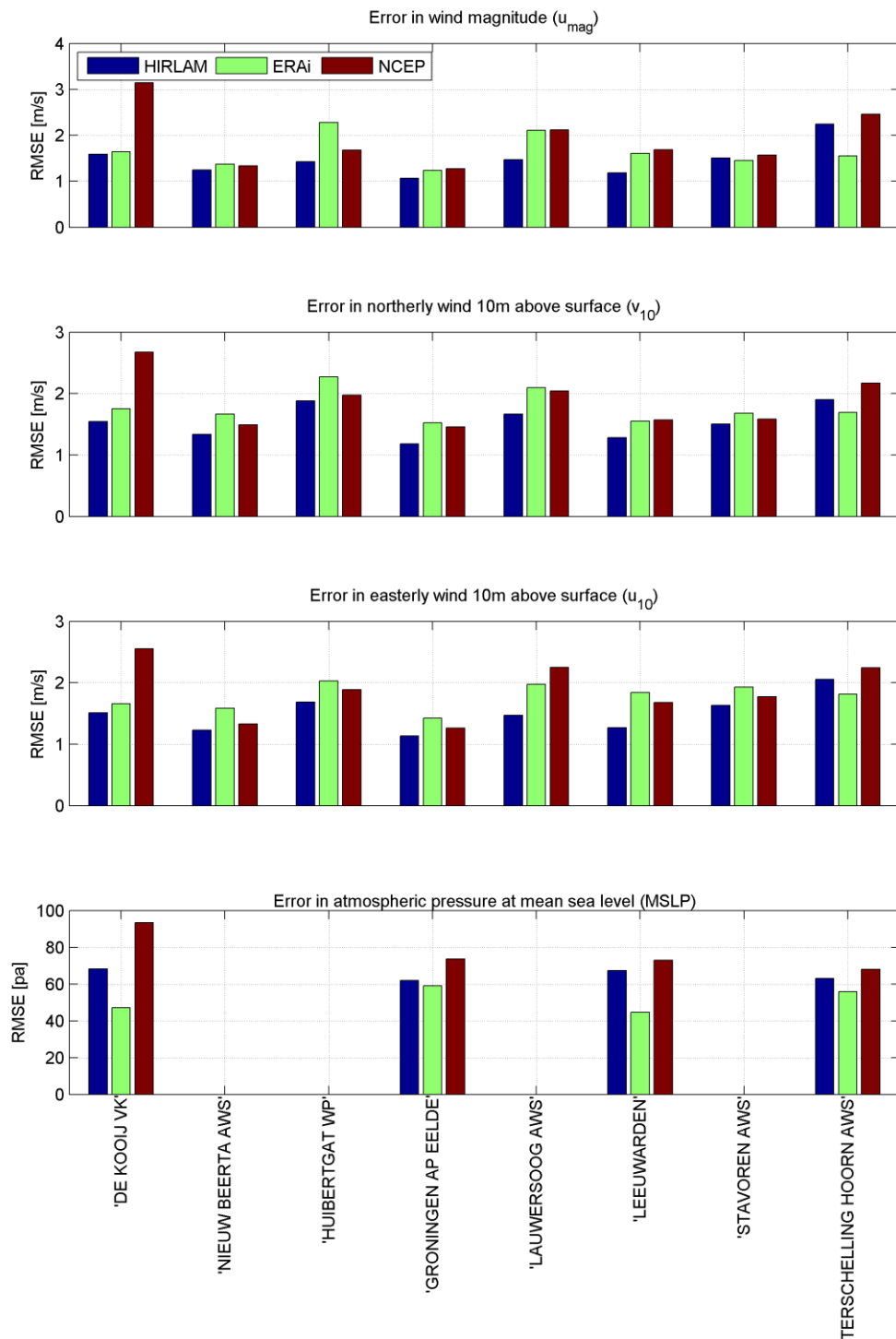
*Figure B.2   Overview of the error in wind speed magnitude (upper panel), northerly wind (second panel), easterly wind (third panel) and atmospheric pressure (lower panel). Different bar charts represent different atmospheric reanalysis models.*
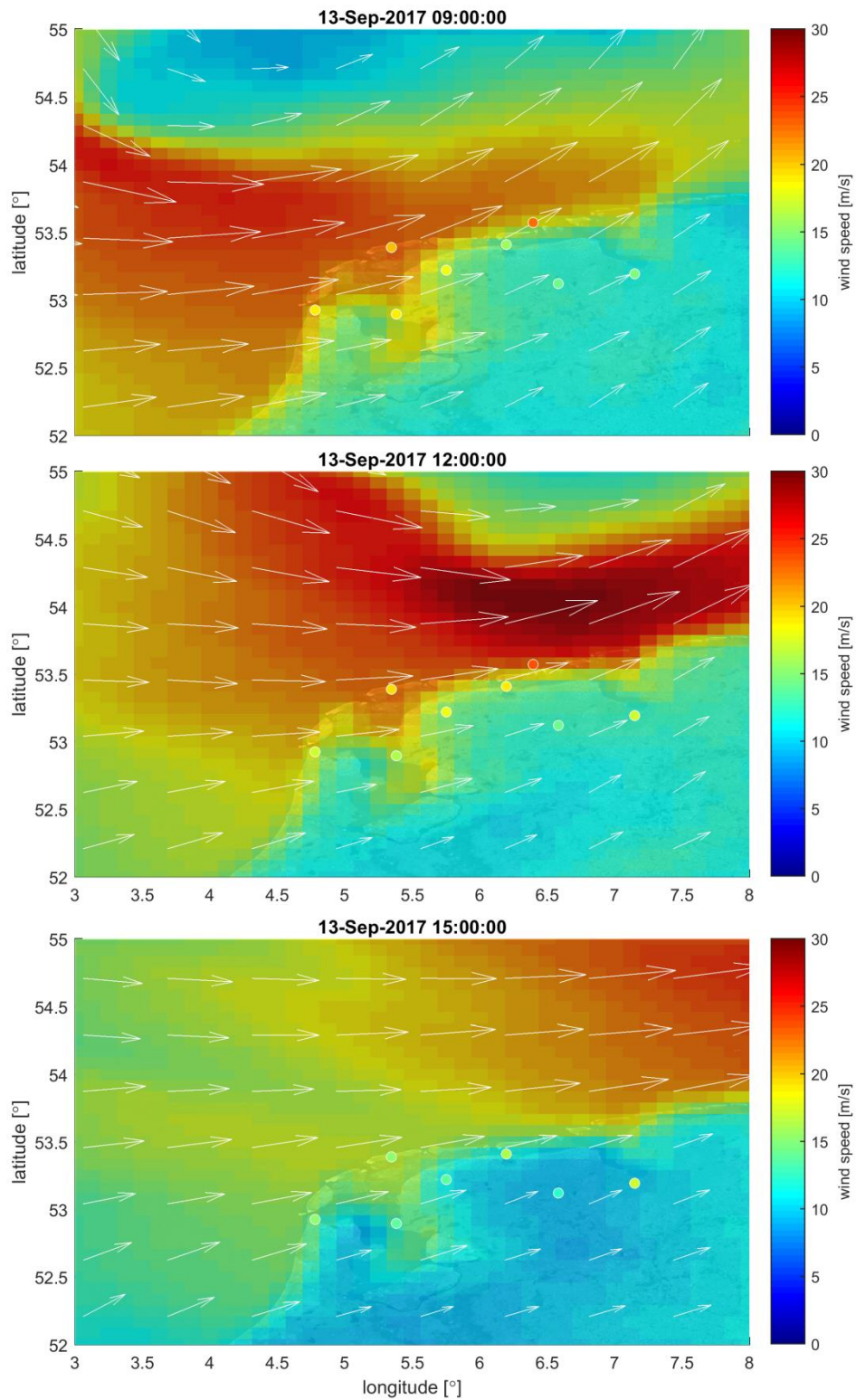
*Figure B.3   Snapshot of the wind speed magnitude as computed by HIRLAM (field) and measured (dots with a white outer circle) for September 13[th,] 2017 at 09:00 (upper panel), 12:00 (middle panel) and 15:00 (lower panel).*

# C   Validation of the DCSMv6ZUNOv4 model

The DCSMv6ZUNOv4 model (Zijl et al., 2013) was validated against observational data of water levels in the proximity of the Wadden Sea (Figure 2.2). Model results for the entire year of 2017 indicate that the model is capable of reproducing the tidal and total water levels. The root-summed-square vector difference (RSS VD) is on average 5.4 cm and the RMSE of the total water levels is 10.1 cm. The full overview of skill scores for the total water level and vector difference of the tide is presented in Table C.1

*Table C.1   Overview of the accuracy in terms of RMSE and RSS VD  of the DCSMv6ZUNOv4 model in reproducing water levels for the entire year of 2017 for the stations in the Wadden Sea*

| Stations | RMSE [cm] | RSS VD [cm] |
|---|---|---|
| Delfzijl | 12.3 | 4.4 |
| Den Helder | 7.9 | 3.2 |
| Den Oever buiten | 10.1 | 4.4 |
| Eemshaven | 10.9 | 4.9 |
| Harlingen | 9.1 | 6.2 |
| Holwerd | 19.5 | 13.9 |
| Huibertgat | 11.2 | 4.7 |
| Kornwerderzand buiten | 8.7 | 3.9 |
| Lauwersoog | 11.9 | 4.7 |
| Nes | 10.9 | 5.6 |
| Oudeschild | 8.1 | 4.1 |
| Schiermonnikoog | 11.7 | 7.7 |
| Terschelling Noordzee | 7.1 | 4.7 |
| Vlieland haven | 8.0 | 3.9 |
| West-Terschelling | 7.8 | 5.1 |
| Wierumergronden | 7.1 | 4.8 |
| **Average** | **10.1** | **5.4** |

# D   Sensitivity tests calibration period velocity on watershed

## D.1   Lower friction
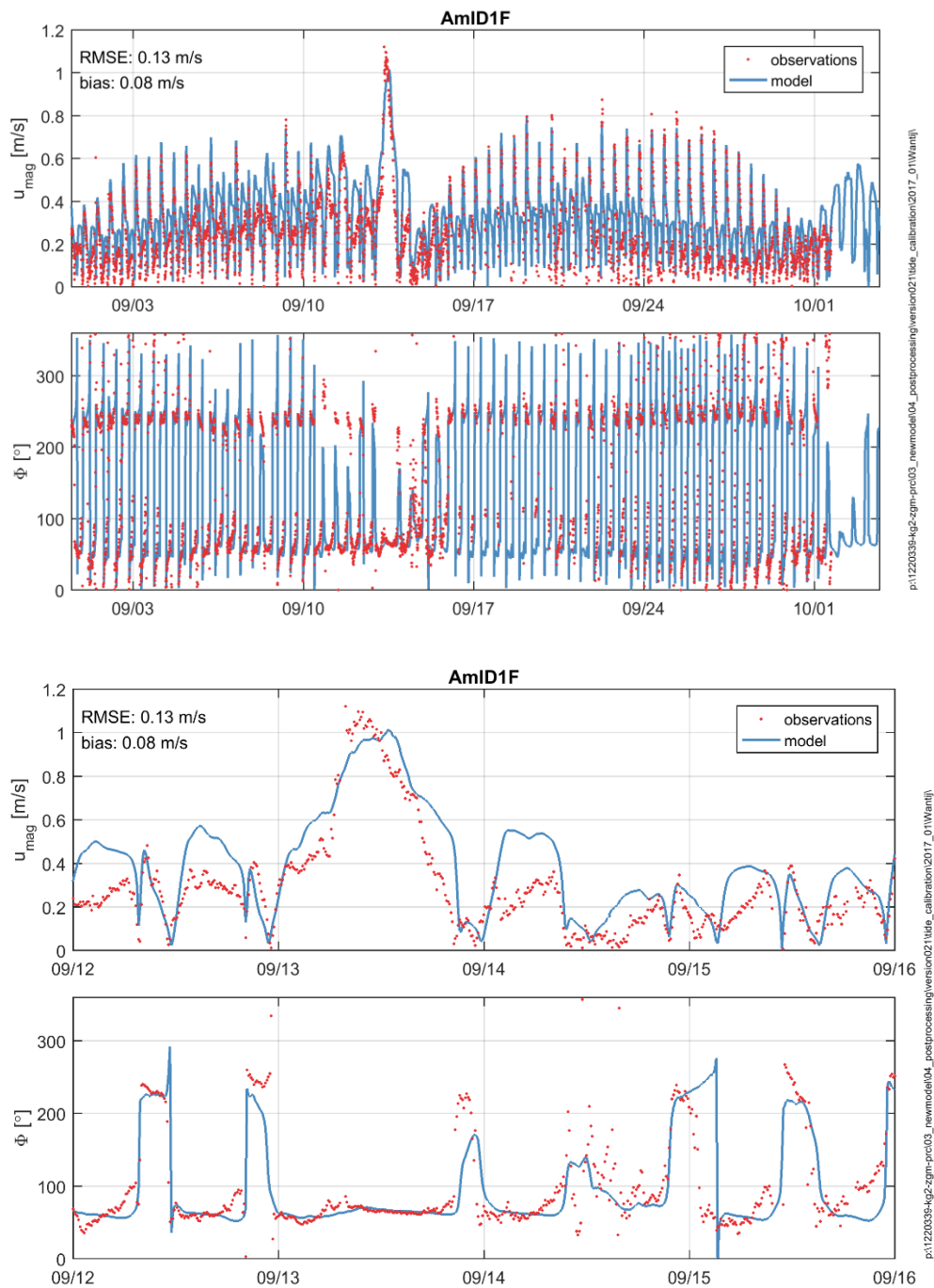


*Figure D.1   Time series of modeled (blue) and measured (red) magnitude (top) and direction (bottom) at Aquadopp location AmID1 at the watershed. Modelled values are based on the CGII-TA model with coefficient 0.1 for ripples and mega-ripples and no dunes in combination with HIRLAM winds.*

## D.2 ERA-interim winds
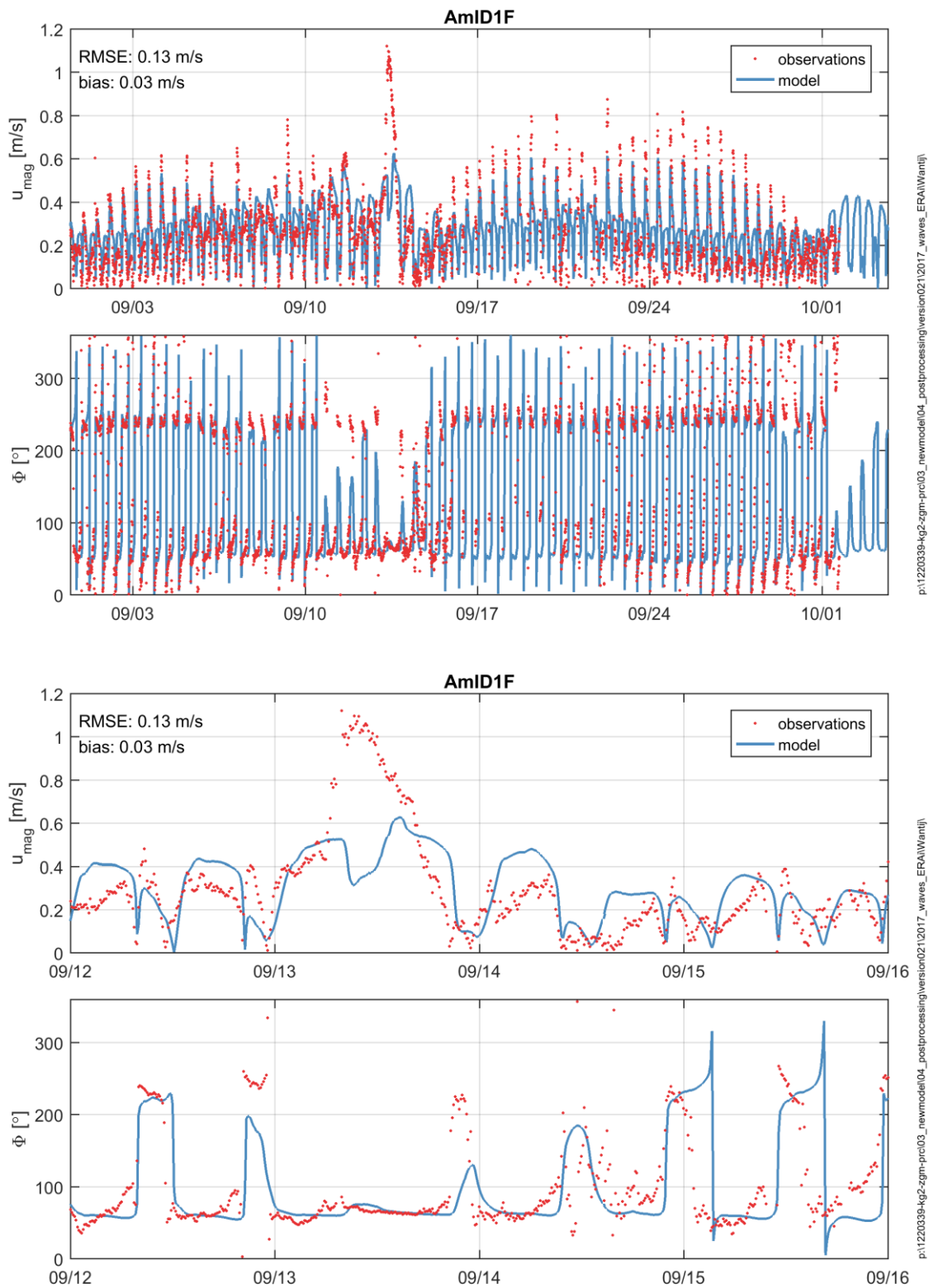


*Figure D.2 Time series of modeled (blue) and measured (red) magnitude (top) and direction (bottom) at Aquadopp location AmID1 at the watershed. Modelled values are based on the CGII-TA model with coefficient 0.5 for ripples and mega-ripples and no dunes in combination with ERA-interim winds.*

## D.3    Wind observed at Huibertgat
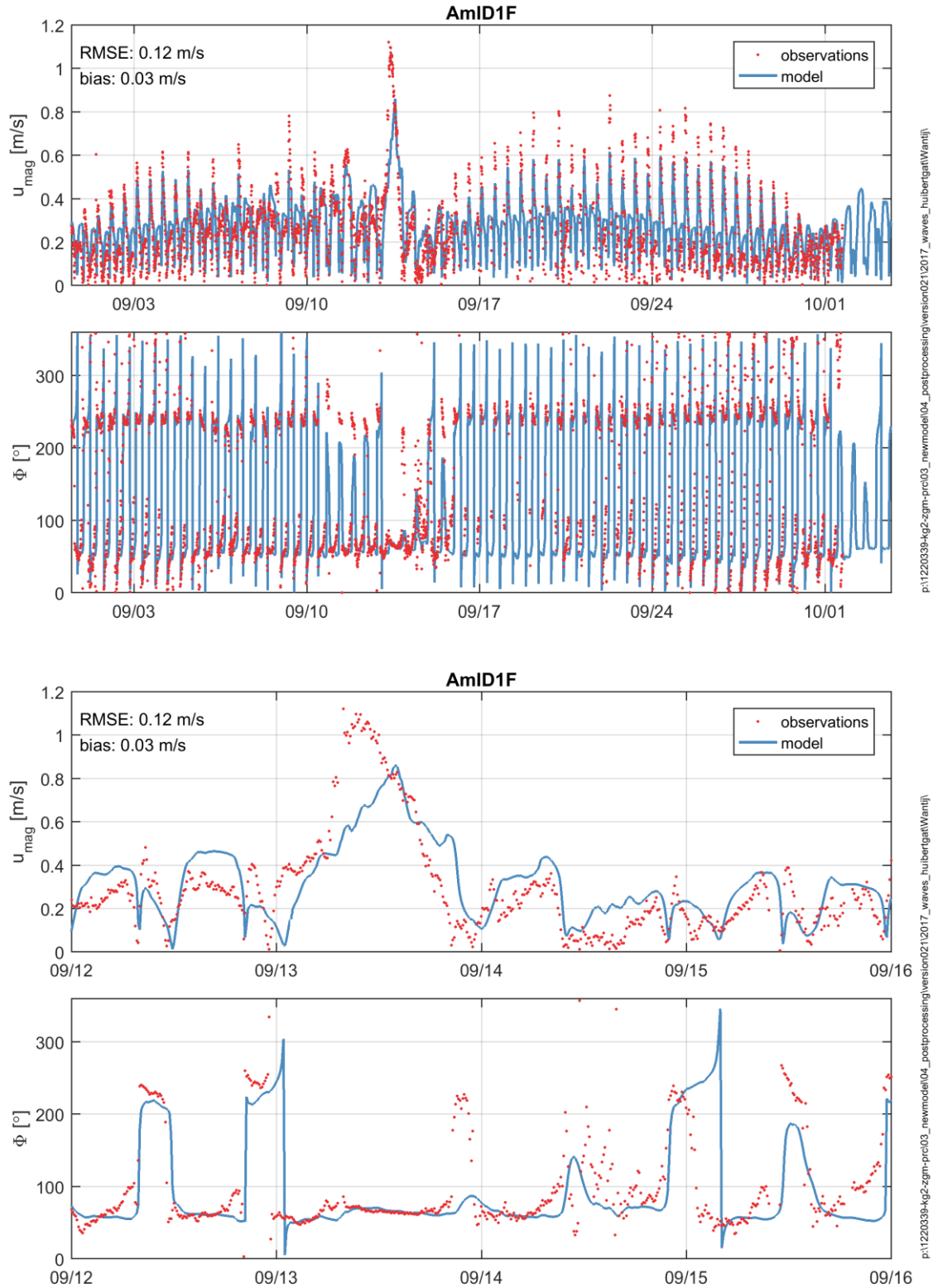


Figure D.3   *Time series of modeled (blue) and measured (red) magnitude (top) and direction (bottom) at Aquadopp*
*location AmID1 at the watershed. Modelled values are based on the CGII-TA model with coefficient 0.5 for*
*ripples and mega-ripples and no dunes in combination with wind observed at Huibertgat.*

# E   Directional deviation in CGII ADCP data

The calibration (Chapter 4) and validation (Chapter 5) of the CGII Terschelling-Ameland model with measured flows during the Coastal Genesis II measurement campaigns shows that there is a distinct mismatch between the modelled and measured flow directions for some of the datasets. This mismatch is best illustrated by the M2 tidal ellipse from model and measurements for the January 2018 campaign (Figure E.1, left). The two most plausible causes for this mismatch between model and measurements are:

1.  The resolution of the wave model; the size of the grid cells is not sufficient to capture local bathymetric variations and consequently relevant processes (e.g. wave breaking) are not modelled well
2.  There is an error in the directions of the measurements.

To test the first hypothesis the nested wave model (see Figure 3.1) is extended in western direction to cover the locations of the measurement frames of January 2018 (DVT1) campaign. It does not cover these locations in the original model as the model is set-up for the Ameland Inlet. The result of this sensitivity test is expressed as the tidal ellipse of the M2 signal as well (Figure E.1, right). The results show that the mismatch between model and measurement is still present even if the resolution of the wave model is doubled.
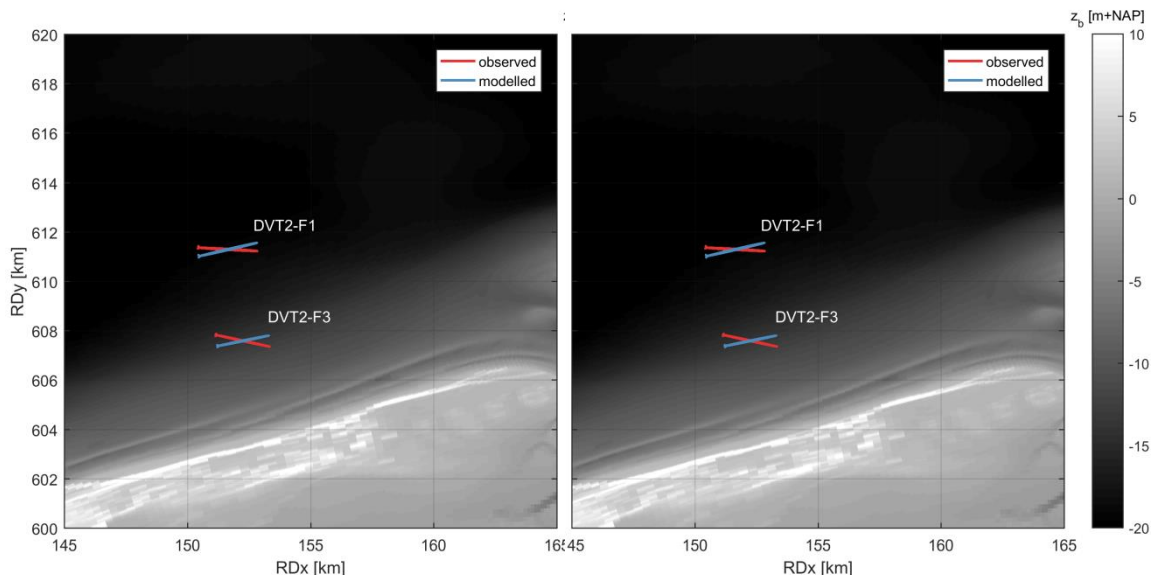


*Figure E.1   Modelled (blue) and measured (red) tidal ellipse of the M2 tidal signal for the original model (left) and the model with an westward extend nested wave model (right).*

To evaluate the effect of the data processing steps, tidal ellipses of the M2 tidal signals are created for all the frames of all CG II campaigns. In Figure E.2 the ellipses of the depth averaged velocity are shown for a depth averaging method in which a logarithmic profile is fitted to the data, a method in which the arithmetic mean of all bins containing data are used, and a method that uses the measurement at 37% water depth as the depth averaged velocity (see Deltares, 2018 for a full description of depth-averaging methods). The figure shows that -

although there are minor differences between the tidal ellipses of the different methods - there is no directional shift as indicated in Figure E.1.
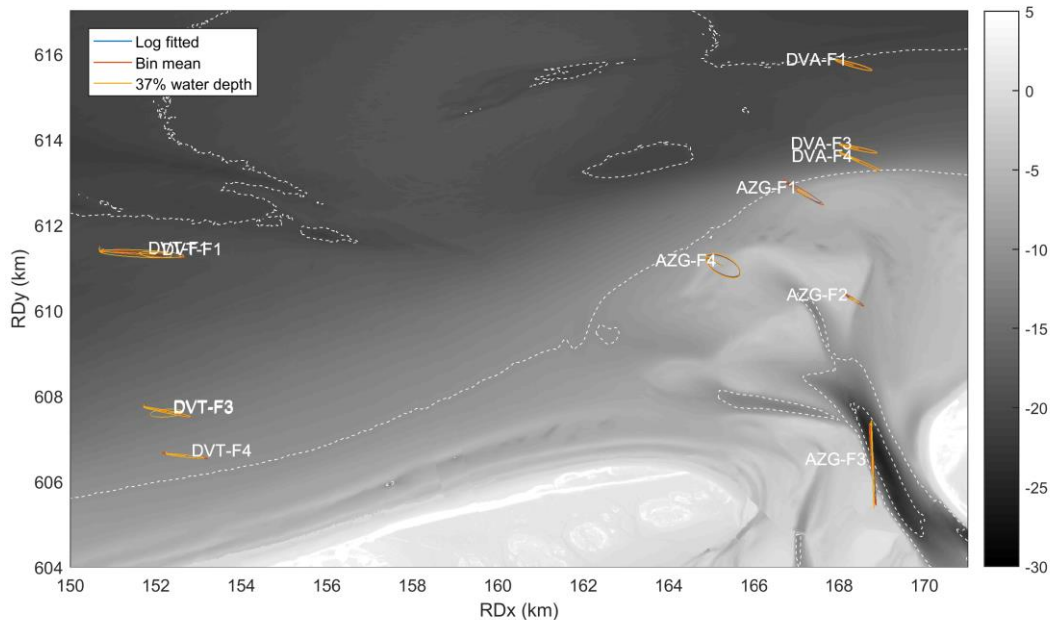


*Figure E.2  Ellipses of the M2 tidal signal for all frames and all CGII campaigns for the depth averaged currents acquired via fitting of a logarithmic profile (red) and the mean of all bins containing data (blue). Tidal ellipses are projected on the 2018 bathymetry.*

In Figure E.3 the tidal ellipses of the measurements from the September 2017 (AZG) campaign are shown. Here, the tidal ellipses are based on data before and after the frame was serviced. The ellipses show that there can be a major change in direction before and after the servicing. The ellips based on the data before servicing is better oriented with the direction of the channel and consequently corrsponds better to the numerical model.

In Figure E.4 the tidal ellipses are shown for the same location (DVT-F3) but subdivided in the data in January and March 2018 (separate campaigns). This figure shows that there can be a major change in direction as well and that the tidal ellipses are not similar. The reason that the tidal ellipses are not similar is indicated by the timesries of the eastward en northward velocity components in Figure E.5      . The figure shows that during the January compaign the U and V components are out of phase, and that during the March 2018 campaign the components are in phase (peaks and troughs occur simultaneously).

From these results it can be concluded that there are differences in main flow direction between similar datasets of the CG II campaigns. These differences are not due to the methods of depth averaging but probably are caused in a processing step prior to depth averaging (presumably the directional corrections). These differences in direction have effect on the comparison of the model and the measurements.
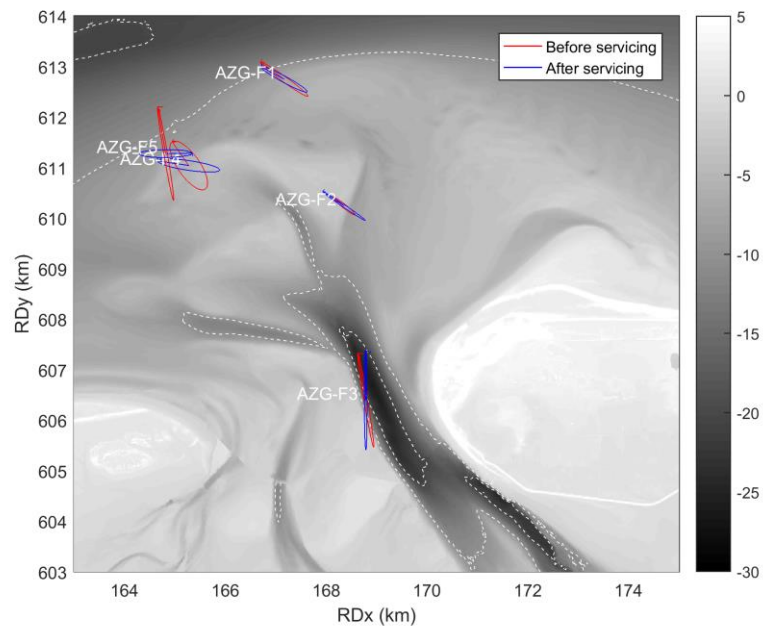
*Figure E.3 Ellipses of the M2 tidal signal for the September 2017 (AZG) campaign, subdivided in data before (red) and after (blue) the frames were serviced.*
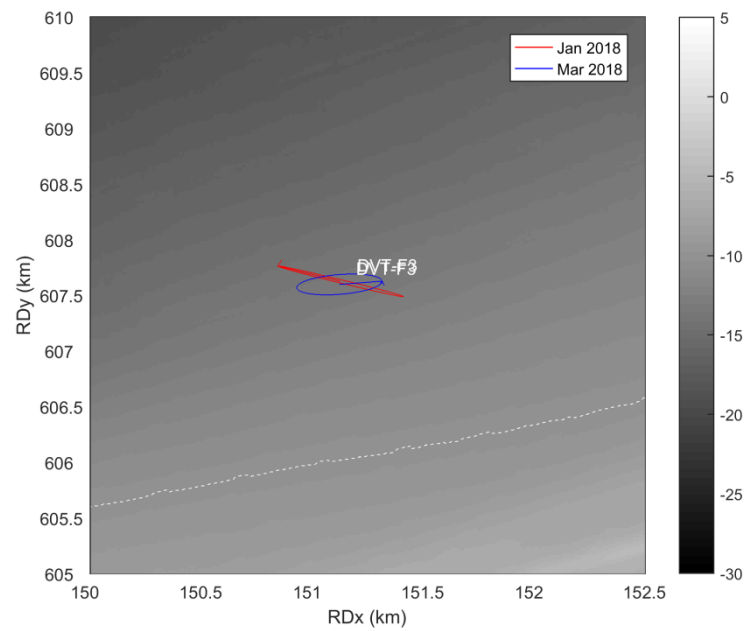


*Figure E.4 Ellipses of the M2 tidal signal for the September 2017 (AZG) campaign, subdivided in data before (red) and after (blue) the frames were serviced.*
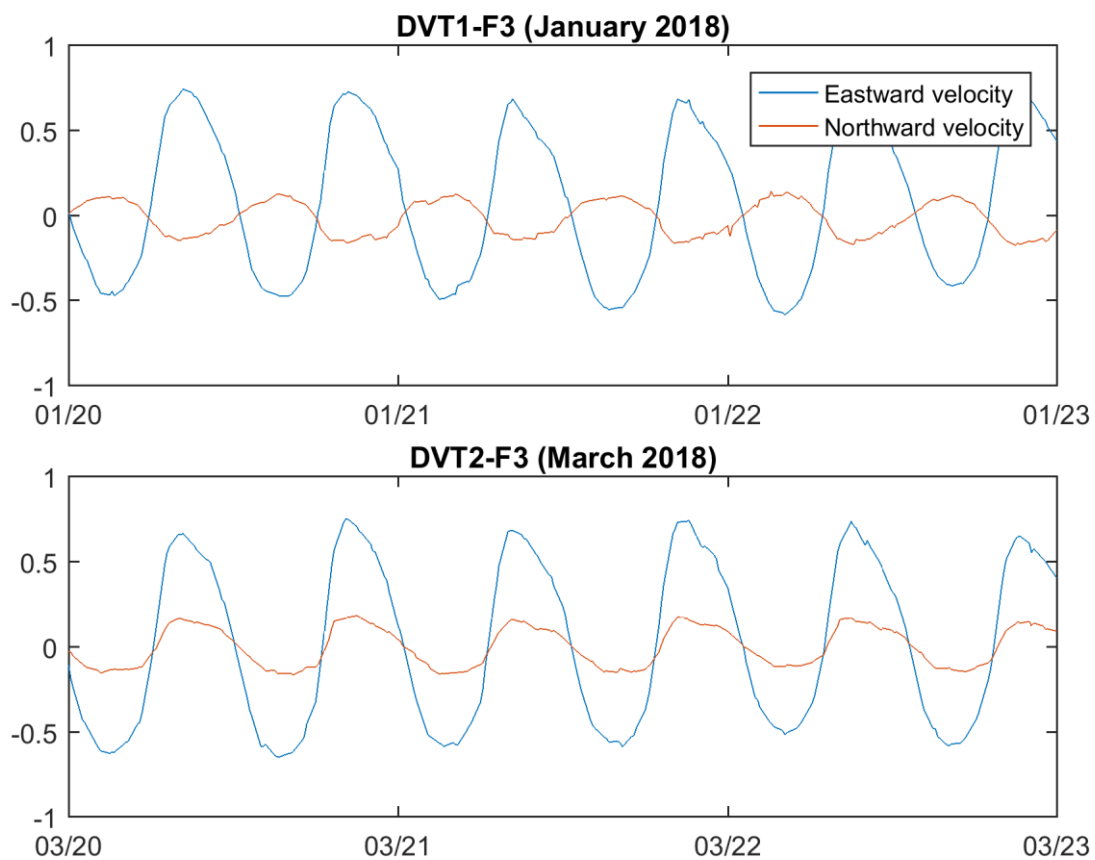
*Figure E.5   Timeseries of the eastward (blue) en northward (red) components of the depth averaged velocity at frame 3 during the January 2018 (top) and March 2018 (bottom) CGII campaigns at Terschelling*